



NOTICE

AVIS

The quality of this microform is heavily dependent upon the quality of the original thesis submitted for microfilming. Every effort has been made to ensure the highest quality of reproduction possible.

If pages are missing, contact the university which granted the degree.

Some pages may have indistinct print especially if the original pages were typed with a poor typewriter ribbon or if the university sent us an inferior photocopy.

Previously copyrighted materials (journal articles, published tests, etc.) are not filmed.

Reproduction in full or in part of this microform is governed by the Canadian Copyright Act, R S C 1970, c. C-30

La qualité de cette microforme dépend grandement de la qualité de la thèse soumise au microfilmage. Nous avons fait tout pour assurer une qualité supérieure de reproduction.

Si il manque des pages, veuillez communiquer avec l'université qui a conféré le grade.

La qualité d'impression de certaines pages peut laisser à désirer, surtout si les pages originales ont été dactylographiées à l'aide d'un ruban usé ou si l'université nous a fait parvenir une photocopie de qualité inférieure.

Les documents qui font déjà l'objet d'un droit d'auteur (articles de revue, tests publiés, etc.) ne sont pas microfilmés.

La reproduction, même partielle, de cette microforme est soumise à la Loi canadienne sur le droit d'auteur, SRC 1970, c. C-30.

THE DETERMINATION OF THE THICKNESS
AND COMPOSITION OF BINARY ALLOY,
THIN FILMS USING A
SCANNING ELECTRON MICROSCOPE

by

Douglas James Wilson

B.Sc., University of Victoria, 1984

A THESIS SUBMITTED IN PARTIAL FULFILLMENT
~~OF THE REQUIREMENTS FOR THE DEGREE OF~~
MASTER OF SCIENCE
in the Department
of
Physics

© Douglas James Wilson 1987

SIMON FRASER UNIVERSITY

July 1987

All rights reserved. This thesis may not be
reproduced in whole or in part, by photocopy
or other means, without permission of the author.

Permission has been granted to the National Library of Canada to microfilm this thesis and to lend or sell copies of the film.

The author (copyright owner) has reserved other publication rights, and neither the thesis nor extensive extracts from it may be printed or otherwise reproduced without his/her written permission.

L'autorisation a été accordée à la Bibliothèque nationale du Canada de microfilmer cette thèse et de prêter ou de vendre des exemplaires du film.

L'auteur (titulaire du droit d'auteur) se réserve les autres droits de publication; ni la thèse ni de longs extraits de celle-ci ne doivent être imprimés ou autrement reproduits sans son autorisation écrite.

ISBN 0-315-42619-5

APPROVAL

Name: Douglas James Wilson

Degree: Master of Science

Title of Thesis: The Determination of Thickness and Composition
of Binary Alloy, Thin Films using a Scanning
Electron Microscope.

Examining Committee:

Chairperson: E.D. Crozier

A.E. Curzon
Senior Supervisor

R.F. Frindt

G. Kirznow

S. Gyax
External Examiner
Professor
Department of Physics
Simon Fraser University

Date Approved: July 3, 1987

PARTIAL COPYRIGHT LICENSE

I hereby grant to Simon Fraser University the right to lend my thesis, project or extended essay (the title of which is shown below) to users of the Simon Fraser University Library, and to make partial or single copies only for such users or in response to a request from the library of any other university, or other educational institution, on its own behalf or for one of its users. I further agree that permission for multiple copying of this work for scholarly purposes may be granted by me or the Dean of Graduate Studies. It is understood that copying or publication of this work for financial gain shall not be allowed without my written permission.

Title of Thesis/Project/Extended Essay

The Determination of the Thickness and Composition

of Binary-Alloy, Thin Films using a Scanning

Electron Microscope

Author:

(signature)

Douglas James WILSON

(name)

Aug 10 1987

(date)

ABSTRACT

A method has been developed to measure the composition and thickness of thin films of binary alloys. It makes use of a scanning electron microscope operating with a Robinson detector for back-scattered electrons. The contrast between a given film and an adjacent uncoated reference substrate depends on the energy of the incident electron beam. This dependence has been measured and used to determine both thickness and composition.

In order to test the method the binary copper-tungsten system was investigated. Samples of copper-tungsten thin films were sputter deposited on silicon wafers in a variety of compositions and thicknesses. Each sample was characterized by standard techniques as well as by the new method and the results were compared. Theoretical calculations of backscatter coefficients were also obtained using Monte Carlo simulations and an analytical mathematical model.

Atomic composition ratios of the films were determined to within $\pm 5\%$ with the new method for films of mass thickness greater than $40 \mu\text{g}/\text{cm}^2$. Greatest accuracy was obtained using a calibration curve derived in the experiment. Thickness could be determined to within $\pm 3\%$ using a calibration curve as well, while theoretical results showed good agreement indicating that the calibration curves should be applicable to experimental systems of atomic numbers between that of copper ($Z=29$) and tungsten ($Z=74$).

ACKNOWLEDGMENTS

I wish to thank my supervisor Dr. A. Curzon for his guidance and assistance in the preparation of this thesis. I would also like to thank Dr. O. Rajora for his help with the scanning electron microscope. Thanks go to M. Matsen for his work on the Monte Carlo simulation program used in this thesis, to Dr. R. Frindt for allowing me the use of his IBM PC in the production of this manuscript, and to B. Goldstein, M. Gee, and my wife Baljit for their patience. Gratitude also goes to the Challenge work-study program of the Canadian government and Simon Fraser University Physics Department both of which funded this work in part.

TABLE OF CONTENTS

Approval Page	ii
Abstract	iii
Acknowledgements	iv
Table of Contents	v
List of Tables	ix
List of Figures	x
1 INTRODUCTION	1
1.1 Historical Background	2
1.2 Other Thickness Determination Methods	4
1.3 The Curzon-Rajora Thickness Measurement Method	10
1.4 Extension of the Curzon-Rajora Method to Binary Alloys	12
2 EXPERIMENTAL METHOD	16
2.1 Sample Preparation	16
2.1.1 Materials Chosen	16
2.1.2 Deposition Method	18
2.1.3 Sample Preparation	23
2.2 Sample Characterization	27
2.2.1 Composition Determination	27
2.2.2 Thickness Determination	29
2.3 Backscattered Electron Detector	31
2.3.1 Detector Used	31
2.3.2 Sample Holder Configuration	33

2.3.3	Backscatter Reference Material	35
2.4	Quantitative Contrast Measurement in the SEM	36
2.4.1	On-Screen Measurement	38
2.4.2	Computerized Contrast Measurement	38
2.5	Variation of the Parameters Used	42
2.5.1	Variation with Electron Beam Energy	42
2.5.2	Other Parameters Varied	43
3	THEORETICAL RESULTS	45
3.1	Analytical Models of Electron Backscattering	46
3.1.1	Background to Analytical Models	46
3.1.2	An Analytical Model for This Experiment	49
3.1.3	Error and Uncertainty for Analytical Calculations	52
3.2	Monte Carlo Simulations	54
3.2.1	Background to Monte Carlo Simulations	54
3.2.2	Monte Carlo model chosen for this Work	55
3.2.3	Error and Uncertainty in Monte Carlo Simulations	58
3.3	Results from the Analytical and Monte Carlo Calculations	59
3.3.1	Discussion of Results	59
3.3.2	Differences in Both Models from the Experiment	67

4.1	Results from the Independent Characterization of Samples	73
4.1.1	Composition Determinations	73
4.1.2	Thickness Determinations	75
4.2	Contrast Results from the SEM	79
4.2.1	Contrast Results for Samples	79
4.2.2	Comparison with Theoretical Results	85
4.2.3	Accuracy of Contrast Measurements	86
4.2.4	Sources of Random Uncertainties	91
4.3	Composition Determination	93
4.3.1	Composition Determination Method	93
4.3.2	Accuracy of Composition Determination	95
4.4	B.S.E. Contrast Thickness Determination	99
4.4.1	Intercept Method	99
4.4.2	Accuracy of this Method	101
4.5	Applicability of the Method	103
5	CONCLUSIONS	106
5.1	Summary of Experiment	106
5.2	Topics for Further Work	107
5.2.1	Variation of Incident Beam Angle	108
5.2.2	Improvements in Theoretical Models	108
5.2.3	Improving Signal Current	109
5.2.4	Measurement of Very Thin Films	109
5.2.5	Thickness Determination in Rough Films	110

5.2.6 Measurement of Films of Arbitrary

Composition	111
APPENDIX A	112
APPENDIX B	122
APPENDIX C	134
LIST OF REFERENCES	146

LIST OF TABLES

Table I	40
Table II	72
Table III	74
Table IV	75
Table V	76
Table VI	90
Table VII	95

LIST OF FIGURES

Figure 1	Schematic of Vacuum System	20
Figure 2	Schematic of a Planar Magnetron Sputter Gun	21
Figure 3	Schematic of Detector and Sample Holder	32
Figure 4	Contrast Image Obtained in the SEM	37
Figure 5	Theoretical Results for Pure Copper	60
Figure 6	Theoretical Results for 25% Tungsten, 75% Copper	61
Figure 7	Theoretical Results for 50% Tungsten, 50% Copper	62
Figure 8	Theoretical Results for 75% Tungsten, 25% Copper	63
Figure 9	Theoretical Results for Pure Tungsten	64
Figure 10	Monte Carlo Results for Thick Samples	66
Figure 11	Angular Distribution of Backscattered Electrons	68
Figure 12	Energy Distribution of Backscattered Electrons	70
Figure 13	Calibration Graph for the Thickness Monitor	77
Figure 14	Experimental Contrast Results for Sputter Run 9	80
Figure 15	Experimental Contrast Results for Sputter Run 24	81
Figure 16	Experimental Contrast Results for Sputter Run 15	82
Figure 17	Experimental Contrast Results for Sputter Run 22	83
Figure 18	Experimental Contrast Results for Sputter Run 11	84
Figure 19	Composition Calibration Curve	94
Figure 20	Experimental Contrast Results for Bulk Silicon	98
Figure 21	Experimental Thickness Calibration Curve	100
Figure A1	Computer Correction of Slopes in Linescan Images	116
Figure B1	Idealized Electron Path in the Everhart Model	125

1. INTRODUCTION

The central topic of this thesis is the extension of the backscattered electron thickness measurement technique to samples of binary alloys. The thesis is divided into five sections. Section 1 covers the need for more advanced techniques for thickness measurements and a brief comparison of the different methods now in use. Section 2 consists of a discussion of the experiments performed to extend the current thickness determination method using backscattered electrons and verify its usefulness.

Many theories have been developed to describe the backscatter coefficients seen experimentally and some of these have been combined to give an analytical model of the experimental results. This and Monte Carlo computer simulations are described in section 3. Section 4 consists of the results of the independent methods of composition and thickness determinations compared to results from this new measurement method, and discusses overall accuracy and applicability.

The conclusions in section 5 consist of two parts. A summary of the experiment and its results is given in the first part and possibilities for further development and experimentation are covered in the last part.

1.1 Historical Background

Quantitative thickness and composition determination of thin films on thick substrates is a technologically important and challenging problem. Its importance stems in part from the rapid increase of thin film uses in many industries, and from general interest in their properties by scientists. Thin films (for the purposes of this thesis defined as being less than one micron thick) have been used for many years as coatings for reflectors, mirrors, and for decorative finishes on small objects such as jewellery, but have gained increasing prominence in the production of solid state electronics, especially in microelectronics [1].

Determining the thickness of thin films has been of commercial interest whenever precious metals have been deposited, or when durability of the films has been required. Many of the physical properties of materials in thin film form are different to that material's bulk properties. These thickness dependent properties are of great interest to scientists and have found application in a variety of technologies.

The wide variety of thickness dependent optical properties displayed by thin films have long been known and often sought after. Anti-reflection coatings and beam splitting reflectors, for example, have transmission or reflection coefficients which

are highly dependent on the thickness of the films used. In the 1930's scientists working on vacuum evaporated thin film resistors discovered electrical and magnetic properties significantly different than those of bulk materials of similar composition [2]. More recently, thickness dependent changes in energy band structure and super-conductivity in thin films has attracted scientific interest, as have problems related to the deposition of extremely small structures of controlled resistivity to create microscopic transistors and circuits. Thus for much work which involves understanding the physical or electrical properties of deposited films, some knowledge of their thickness is essential.

The large number of thickness dependent properties of thin films have allowed many thickness measurement methods to be developed for different applications [3]. These methods can be divided into those which measure mass thickness T_M and those which measure dimensional thickness d . Dimensional thickness can be defined as the mean distance from the substrate surface to the upper surface of the deposited film. Mass thickness is defined as the mass of film material per unit area coated. For smooth uniform films (on smooth substrates) the dimensional thickness d can be determined from mass thickness T_M using the density of the thin film material ρ_f :

$$d = T_M / \rho_f \quad (1)$$

Though this conversion is simple in theory, the density of the thin film material is usually different than that of bulk material of the same composition (10-15% less for evaporated or sputtered films) due to film porosity and internal stresses, and ρ_f is often difficult to measure.

Dimensional thickness is useful for optical reflectance and absorption applications (where the wavelength is of the same order of magnitude as the thickness), whereas mass thickness is more important in transmission and absorption of particles and high energy photons. Often in the literature the term "thickness" is used for both d and M_f , and the type of thickness must be inferred from the type of measurement used.

1.2 Other Thickness Determination Methods

An ideal thickness determination method would be:

1. non-destructive to film or deposit,
2. independent of composition, size or shape of the coated object, or provide information to eliminate composition dependent effects,
3. useable either during deposition for thickness control or after deposition for independent determinations,
4. accurate over a wide range of thicknesses,
5. simple to use and require a minimum of specialized equipment and computing time to analyse,
6. standardless or require a minimum of standards and calibration.

In very controlled deposition environments such as laboratory vacuum evaporators, two popular methods for determination of mass thickness fulfil many of the above ideals. The method of direct weighing of the substrate before and after deposition has undergone great improvements in accuracy recently due to the advent of simple yet precise electrobalances accurate to a fraction of a microgram. Quartz oscillator thickness monitors have also undergone sufficient development to give resolution of $0.5 \mu\text{g}/\text{cm}^2$. Both of these methods were used as standard comparisons to characterize the samples deposited in the present work, so are discussed further in section 2.2.

However, no thickness determination methods have yet been devised which have all the ideal qualities listed above. A great number of methods have been developed over the years, but for comparison with the new method, discussion here will be limited to those which can be classified as non-destructive and capable of measurement after deposition has been completed.

Most* non-destructive post-deposition measurements involve particle or x-ray beams impinging on the sample with sufficient energy to pass through the film, and then measuring the resulting reflectance or x-ray emission. Of these, the technique of using

*Most, but not all, see for examples, Dudding who uses other electronic methods [4].

x-rays to excite x-ray fluorescence in substrate and film has undergone significant development and has found many commercial applications [5].

Accurate thickness measurements for films less than 0.003 cm thick has been demonstrated by measuring either the attenuation of the substrate x-rays by the thin film (when compared to an uncoated substrate) or by quantitative measurement of characteristic x-rays excited in the thin film. X-ray interactions with solids are highly wavelength dependent. Thus for thin alloy films on substrates quantitative theoretical results are difficult to calculate. Thus both methods require calibration curves derived from reference standards and a knowledge of composition of both the thin film and substrate materials.

The complexities of using x-rays to generate x-rays in the sample can be partially overcome by using an electron beam to generate them instead. Electrons are much more efficient at x-ray generation and do not penetrate the sample as far, thus reducing the interference from substrate fluorescence. Using electrons has the disadvantage of needing a high vacuum environment rather than the room pressure needed for x-ray work. However, when an electron microscope is used as the electron source, the resulting combination is a powerful research tool.

Because of the advantages electron beams have over x-rays

they are commonly used in composition analysis work in the field titled micro-beam analysis. Ability to focus electrons to areas less than a micron in diameter is often coupled with the ability to scan the beam in the SEM, so much of the micro-beam analysis done is with x-ray spectrometers attached to SEM sample chambers.

Thickness measurement using electron beam excited x-ray fluorescence has become quite popular as an outgrowth of electron micro-beam composition analysis. An unknown sample's thickness can be determined simultaneously with its composition even if the sample contains many different elements in both thin film and substrate. As the exciting beam of electrons does not penetrate as far as an equal energy x-ray beam, thickness measurements are limited to thinner samples.

Most SEMs and microbeam analysers have a maximum beam acceleration of 40-50 kilovolts. This limits the range of the electrons in the sample to the order of a micron and thus the maximum thickness measureable to somewhat less than this. The x-rays produced in the sample are usually collected and separated into their wavelength or energy spectrum and the peak heights of the characteristic K, L, and M fluorescence of each constituent in the sample is measured.

Unfortunately, the computation of composition and thickness of the sample from this spectrum, though simpler than from an

x-ray excited spectrum, is complicated by several factors. The volume in which x-rays are produced by the electron beam is highly dependent on the structure and constituents of the sample being analysed. These x-rays also generate secondary x-rays by x-ray fluorescence and are absorbed differentially by the sample as well. So although simple calculation schemes are available for special circumstances [6], in general modelling of each experimental system must be done by extensive computer simulation, or "Monte Carlo" methods [7].

The increasing popularity of the above method is in part due to the increasing availability of solid state energy dispersive x-ray analyzers. These detectors are readily adaptable to scanning electron microscopes, which combine the above advantages with the ability to image the spot being analysed, providing accurate placement of an extremely collimated beam. Considerable success has been achieved with steadily increasing precision being obtained [8] and the methods can be extended to films of 5 or more elements [9] assuming x-ray intensity peaks of the constituents of the film do not overlap with each other or with those of the substrate.

A simpler thickness measurement is in common use in transmission electron microscopy for free standing films of known composition. Total electron beam current passing through the sample I_s is measured using a Faraday cup placed below the sample. Total beam current I_{total} is then measured by moving

the sample out of the way, and the fraction η_t :

$$\eta_t = I_t / I_{\text{total}} \quad (2)$$

transmitted through the film is related exponentially to the thickness of the film. With calibration curves this method can give extremely accurate results for films of thickness up to the total penetration depth of the electrons.

The electron transmission method will not work on films supported on substrates, but if the Faraday cup is placed over the sample (as done by Hohn and Niedrig, 1972 [10]) the total backscatter current I_b can be measured. Roughly equal amounts of secondary electrons are also emitted by the sample but these are low energy and are typically rejected by placing a -50 Volt bias on the Faraday cup. The backscattered signal also has the advantage of being approximately independent of the crystal structure of the sample [11], which can affect transmission results.

The number of electrons backscattered by a given film has been observed to be linearly proportional to the thickness of the film for thicknesses up to half the total penetration distance of the electron beam for freestanding films. This linearity makes thickness computation simple and accurate for a large variety of materials. For films on substrates the backscatter coefficient η_b again varies linearly with thickness, but as the thickness tends to zero η_b tends to the value of η_s .

the backscatter coefficient of the substrate rather than zero obtained with an unsupported film. Thus thin films supported by substrates can have their thickness measured also, as long as the substrate material has a backscatter coefficient which is much lower or higher than that of the film.

1.3 The Curzon-Rajora Thickness Measurement Method

Unfortunately, Faraday cups are not very amenable to use in the Scanning Electron Microscope (SEM), in which the beam must be scanned fairly quickly giving low signal to noise ratios. Thus, large solid angle backscattered electron detectors, either of semiconductor or scintillator type, have been developed for backscattered electron imaging in SEM work [12, 13]. With these more sensitive detectors commercially available, a method for determining supported thin film thickness analogous to the Niedrig Faraday cup method has been developed by Curzon and Rajora in 1985 [14].

The semiconductor or scintillation detectors do not normally measure absolute current, thus the Curzon-Rajora method is a comparative method which uses a reference material (usually bulk material of the same composition) of known backscatter coefficient. The method may be illustrated by referring to observations of lead films on silicon. A piece of bulk lead was placed adjacent to the film and the SEM was operated in line scan mode in which the beam repeatedly scanned along a line on

the sample. The ratio of the backscatter signals from the silicon supported lead film and the adjacent reference bulk lead was measured and used to determine film thickness. This method retains advantages of the linearity of backscatter ratio for a wide range of thicknesses found in the Faraday cup method, and it has the advantage of not needing any specialized detectors or other equipment.

Applicability and accuracy of the Curzon-Rajora method are similar to those of the Faraday cup method. The electron beam must penetrate through the film in sufficient quantity to show some backscatter contrast difference, and this puts an upper limit on the thicknesses measured of about 400 nm. for copper in an SEM capable of acceleration potentials of 40 kilovolts. The minimum thickness measurable with this method is more complex and is dealt with at length in section 4.4, but for this experiment thicknesses of 0.040 milligrams per square centimeter (mg/cm^2) have been measured with good accuracy (this translates to approximately 21 nm for tungsten films and 45 nm for copper).

The overall accuracy of all backscattered electron thickness measurement methods is largely dependent on the sample's inherent contrasting Z values for the components of the thin film and substrate. For many applications in the semiconductor industry, where silicon or silicon dioxide are being coated by metals, this does not present a problem except for aluminum based alloys. Both the Niedrig and Curzon-Rajora methods work

well only for films whose composition is well known, usually this includes only pure elements and stoichiometric compounds.

In many practical situations thin films of alloys or non-stoichiometric compounds have superior properties to films of pure elements or stoichiometric compounds. The difficulties in controlling the proportions of these components are well known [15, 16]. Thus in many practical cases the elements present in a film are known but not their relative concentrations. Reliable composition analysis from x-ray fluorescence of thin supported films encounters the same difficulties as the x-ray fluorescence thickness measurements. That is, absorption and fluorescence effects of the film-substrate system are complex, and need to be modelled carefully with computer simulations or other mathematical techniques.

1.4 Extension of the Curzon-Rajora Thickness Measurement to Binary Alloys

Thus, this thesis presents an extension of the Curzon-Rajora backscattered electron method of thin film thickness measurement using the SEM for the case of binary alloys or mixtures of known elements in unknown relative concentration. Information about both thickness and composition is mixed together in the backscatter coefficient η_0 of the unknown sample with respect to some known bulk reference

material, so one of the measurement parameters must be varied to distinguish between Z contrast and thickness contrast.

Various parameters have already been studied in the literature. In 1976, K. Murata [17] looked at the angular distribution of backscattered electrons from thin films and noted that at normal incidence the amount of electrons scattered nearly normal to the surface was more characteristic of the substrate η_{bulk} and those scattered nearly parallel to the surface were (proportionally) more characteristic of the η_{bulk} of the film material.

Similarly, several investigators [18,19] have observed that if the sample is tilted with respect to the incoming beam, the majority of electron paths will be longer in the surface film than they were at normal incidence. This leads to an η_{bulk} related more to the thin film material as well, though due to the scatter broadening of the beam in the sample the relationship is not a straightforward one.

As early as 1957 Holliday and Sternglass [20] noted that at accelerating potentials (electron energies) below 5 kV. the depth of penetration of the electrons decreases to the point that films over $40 \mu\text{g}/\text{cm}^2$ thick will appear semi-infinitely thick, thus giving a value for η_{bulk} which can then be correlated to the bulk value for a reference sample of known atomic number.

The relationship between η_{bulk} and the atomic number Z of pure elements has been studied by many workers [21,22] for a variety of incident electron energies. They have verified that the majority of scattering of the impinging electrons is with the core orbital electrons of the solid (at kilovolt accelerating potentials). This implies that η_{bulk} is a monotonically increasing function of Z , so pure elements could be uniquely identified by this value. Alloys of two elements with atomic numbers Z_1 and Z_2 will have an η_{bulk} related to an effective atomic number Z_{eff} . Various equations for this relationship have been derived or proposed. Recently, a review and study by Herrman and Reimer [23] showed that even simple relationships give reasonable results.

Once composition of the alloy is derived, the thickness can be measured by similar methods to the original Curzon-Rajora method of using standard calibration curves from the element of atomic number Z closest to that of Z_{eff} . But to make this work more general, and because calibration curves are unavailable for many values of Z , other methods have been explored in sections 4.3.1 and 4.4.1.

The work of Holliday and Sternglass was on the penetration range of electrons in various materials [24], rather than on thickness measurements. They found the depth of penetration to be approximately independent of material for a given mass

thickness, thus suggesting that thickness could be measured by observing at what electron energy the η_{bulk} of the substrate first influences total η_b .

Fortunately, η_{bulk} for most materials was observed to be almost constant as the energy of the incident electrons E was varied, so the measurement of the onset of slope in the η_b with energy E graph was a clear indication of electron penetration (assuming the η_{bulk} of the substrate to be very different than that of the film material). This onset of penetration can be used to determine the thickness of an unknown sample, as will be explained in section 4.4.

2. EXPERIMENTAL METHOD

This section describes a series of experiments on a binary alloy system performed in an effort to extend the Curzon-Rajora thickness measurement method to alloys. Well characterized samples were needed to test the accuracy of the new method, and details of how these samples were deposited and characterized are given in sections 2.1 and 2.2. The underlying goal was to evolve a straightforward technique which could be routinely applied to other analytical work. The actual techniques used in measurement are described in section 2.3.

Finally, different parameters were varied to separate thickness and composition information, as discussed in section 1.4. Those efforts which did not contribute to the final method have been discussed only briefly in section 2.4, along with the final method.

2.1 Sample Preparation

2.1.1 Materials Chosen

The samples prepared consisted of many thin binary alloy films with carefully measured thickness and composition values throughout the range of interest. They were supported on smooth substrates. Copper and tungsten have many virtues which made them suitable for this study.

- 1) Copper and tungsten were chosen for the alloy components of this initial study due mainly to their wide separation of atomic numbers, 29 and 74 respectively, which displays the relevant details of data analysis clearly while helping to generalize the method to materials with Z values between those of copper and tungsten.
- 2) Both copper and tungsten produce very uniform, fairly tough and adherent films which show little surface structure even under the highest magnification of the SEM. Contrast due to surface features is an additional variable which was necessary to control. It is discussed further in section 2.3.
- 3) Copper also is one of the lowest atomic number base metals which is nonferrous. This is a desirable quality as we did not want any magnetic contrast to interfere with the experiment.
- 4) Tungsten was also chosen for its good sputtering characteristics, and copper sputters well also.
- 5) The Cu $K\alpha$ x-ray peak is adjacent to the W $L\alpha$ peak. This helps improve the accuracy of the x-ray fluorescence composition analysis.
- 6) Both materials form stable thin surface oxides, thus they do not oxidize into flakes in the same way as, for example, thallium does.
- 7) Copper and tungsten are not miscible in one another to more than a fraction of an atomic percent. Thus concentration fluctuations due to compound formation could be avoided.

It was considered desirable to avoid such fluctuations so as to minimize the complexity of the experimental results.

Substrates were chosen to be single crystal silicon wafers of the type normally used in integrated circuit manufacture. Though a semiconductor, Si does not charge significantly under the electron beam when in single crystal form, and the material has relevance to industrial applications for this thickness measurement method.

Atomic mixtures of the two elements were deposited by simultaneously sputtering targets with both tungsten and copper surfaces. This resulted in smooth and uniform metallic films of colour between that of copper and tungsten, but which were thermodynamically unstable, and deteriorated over a period of days to months. The deterioration rate depended on deposition and storage temperatures and was marked by a noticeable migration and grouping of the copper into islands, presumably both in and on the surface of the film. This process is discussed in detail in section 4.2.3 as it led to some anomalous backscatter contrast results.

2.1.2 Deposition Method

Sputter deposition was chosen after initial trials with evaporation techniques for two reasons;

1. Once equilibrium has been reached at the target surface, the numbers of each type of atom sputtered in an alloy

target or a target of two different metal surfaces is constant over a long period [25].

2. Sputtered films often show superior surface finish and adherence [26].

These properties combine to give the superior composition uniformity and film quality needed for the wide range of compositions and thicknesses used in the experiments.

The sputtering equipment used was a Basic Sputtering Corp. US' planar magnetron sputtering gun with an Energy Research Associates model PPS 7901 DC plasma power supply. This was placed in an NRC model 3114 high vacuum system, as shown in figure 1. The planar magnetron was of the single, concentric-pole, permanent-magnet type with the magnet placed such that the magnetic field lines radiate through the target (which is placed in front of the magnet as shown in figure 2) in a semi-toroidal manner. Plasma was generated by controlling the flow of prepurified Argon to between 6 and 12 SCCM (standard cubic centimeters per minute) with an MKS type 257 flow control system with associated electronic valves. Flow rate was measured with MKS flowmeters and the pressure was measured with an MKS type 310 pressure transducer. The system could be operated in either constant pressure mode or constant flow rate, to ensure a total Ar partial pressure in the bell jar of between .010 torr (a torr is equal to approximately 133.3 Pascals) to 1.00 torr held constant to within .001 torr in most circumstances.

Figure 1. Schematic of Sputtering System. Samples were sputter deposited in an NRC vacuum evaporator which has been modified for sputter deposition as shown. Substrates were mounted 6-8 at a time around the circular sample holder (shown here in perspective view), and rotated into position for coating using a geared shaft. A slot in the shield allows only one sample at a time to be exposed to the sputter gun. The quartz crystal thickness monitor is also exposed to the sputter gun through the same slot, and is used to monitor the deposition rate. The argon pressure necessary to sustain the sputtering plasma in the bell jar is controlled automatically by the MKS pressure controller and its associated pressure transducer and flowmeter/valve.

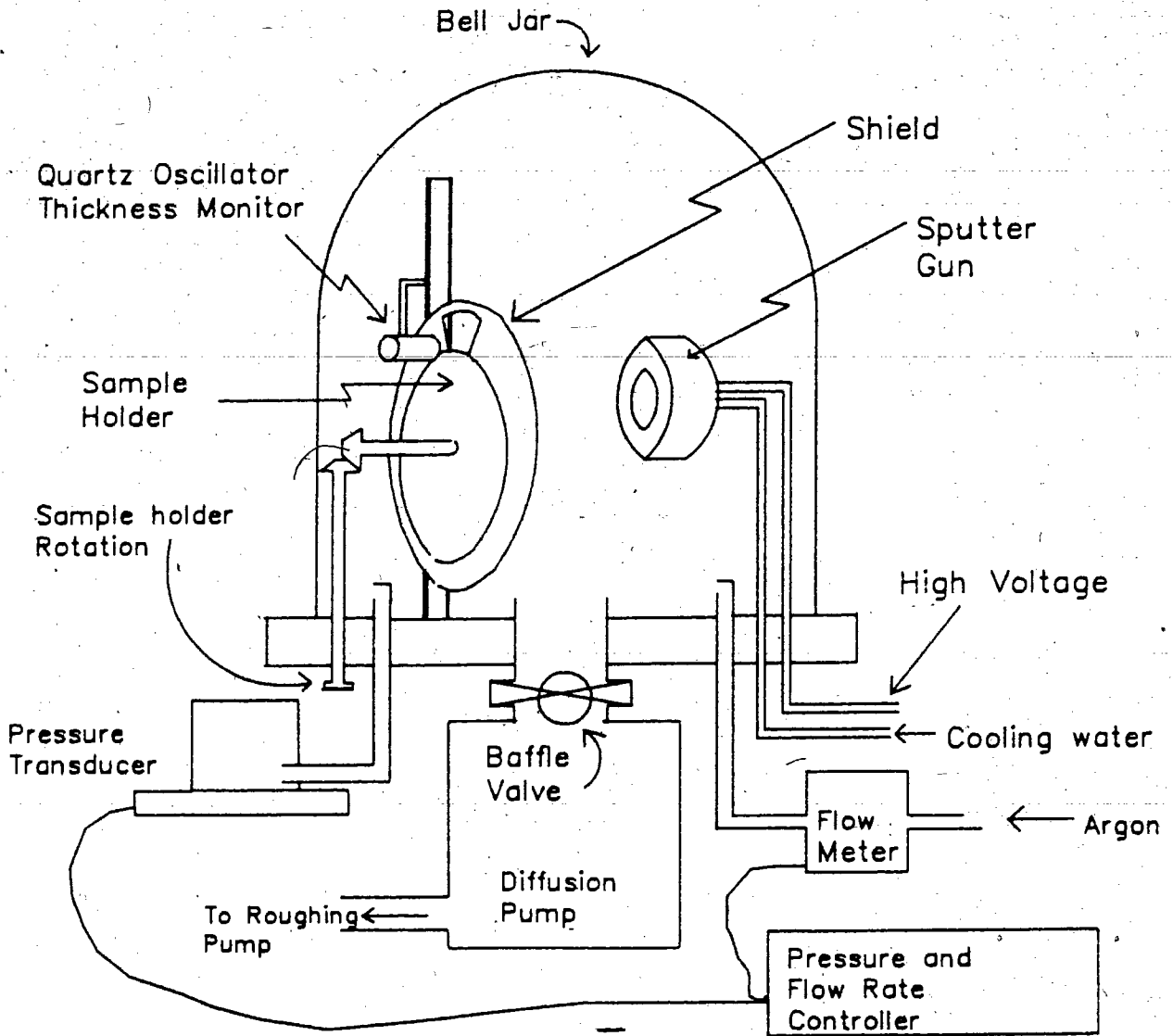
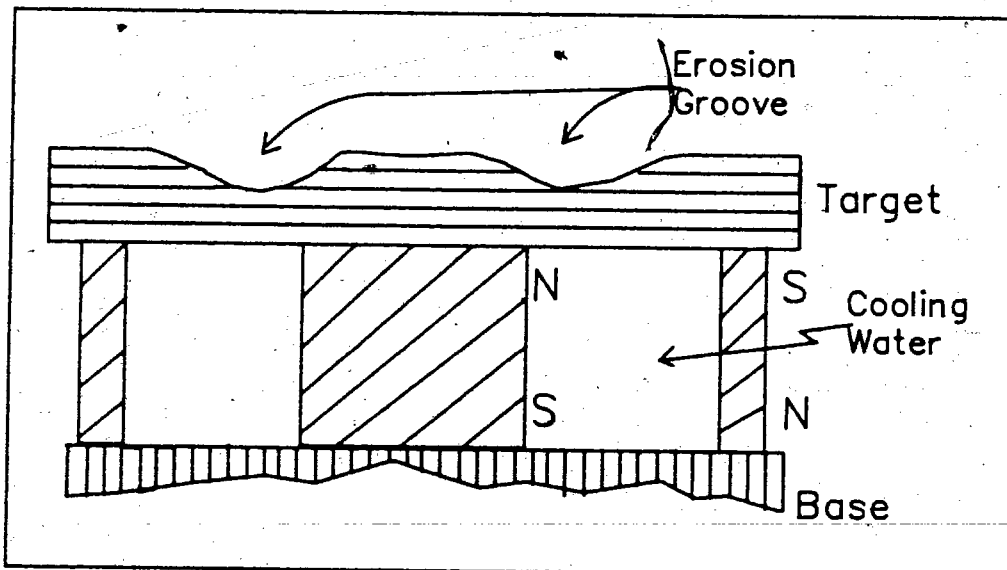
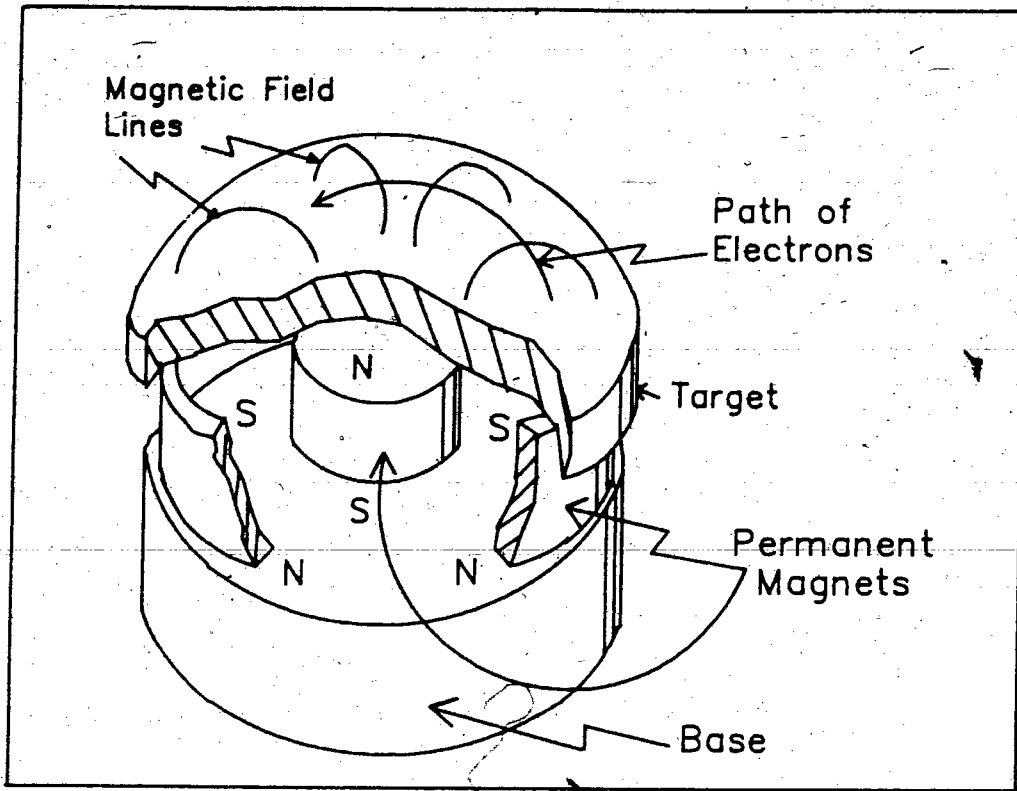


Figure 2. Schematic of a Planar Magnetron Sputter Gun. In figure 2a, a cut away view of a simplified sputter gun is shown, including the placement of the permanent magnets. The effect on the path of charged plasma above the target is also shown. In figure 2b, a cross section of the same sputter gun shows the resulting erosion pattern of the target by the charged particles and the spaces below the target for cooling water.



300 to 500 volts DC was applied between the target and grounded vacuum system and the ensuing argon plasma was concentrated by the magnetic field to a toroidal ring at the surface of the target. The Cu-W targets which were exposed to the plasma were composed of either copper plate with tungsten foil bonded to the surface or a tungsten foil and copper foil bonded to the surface of an aluminum support plate.

All target materials were checked for purity using x-ray fluorescence in the scanning electron microscope as described in the next section. Bonds between the different metals needed both thermal and electrical conductivity so colloidal Silver paste was used for most connections, and colloidal graphite was used where there was chance of accidental exposure to plasma during deposition.

The surface area of Cu and W exposed to the high plasma density toroid determined the proportion of each element sputtered off. However, the relative numbers of atoms sputtered off per incident argon atom (referred to as 'sputter yield') for the two elements are quite different. For example, for normally impinging argon at 500 eV kinetic energy the sputter yields for Cu and W have been measured to be 2.3 and .6 atoms per incident ion respectively [27]. This is due to the similarity in atomic mass of Cu and Ar atoms and the large discrepancy between those of Ar and W, so collisions of Ar^+ ions with Cu had much greater

chance of having a high momentum transfer single collision.

For our experiment these sputter yields can only be used as guidelines, because most of the Ar^+ ions do not impinge on the sputter gun target at normal incidence. In fact, the erosion pattern of the targets indicate that the plasma ions race around the toroid in a clockwise direction (figure 2b) so that the raised edges of the foils and inserts placed on the surface of the target across this 'racetrack' are exposed to fairly intense erosion. This fact also contributes to the determination of the composition of sputtered products and perhaps to a variation in composition with time over long periods as sharp edges in the target are worn down.

2.1.3 Sample Production

Long sputtering times (on the order of hours) were used to produce films of approximately 500 nm. thickness for each of the sputter target geometries. These films were sufficiently thick that in x-ray fluorescence composition analysis they would appear infinitely thick at all the available electron beam kinetic energies (0-40 kV). Thick films were normally sputtered first so that the other films then sputter deposited had compositions closest to that of the surface of the thick film in case there were any variation of sputter yields with time.

To provide a convenient size of substrate for further measurements, commercial grade high purity Si four inch diameter

wafers were scribed and broken into 1 cm. squares. This presented minimal difficulties as the wafers obtained had a [100] crystal orientation so tended to cleave in perpendicular directions. The crystal cleavage plane orientation was given by the manufacturer as a flat on one side of the wafer. Most wafers were extremely clean and were coated without further surface preparation, but some were cleansed in a chromic acid bath, followed by acetone and alcohol washes with a final quick rinse with distilled water and blow dry with dry air.

No effects upon thickness or uniformity of deposition were noted between the two surface preparations, though cleaned and not cleaned substrates were used in separate sputter runs to ensure uniform internal consistency. In all cases substrates were handled with steel tweezers both before and after coating to avoid contamination from finger prints.

Substrates were mounted 6 to 8 at a time on a circular rotating sample holder shown in figure 1, which was built to allow all samples for one target configuration to be sputter coated in one "run" i.e. without bringing to air and re-evacuating the apparatus for each sample. This was especially important in sputtering as residual air and water vapour ionizes in the plasma giving extremely reactive oxygen ions which form oxides in the deposited film, as discussed in section 4.1.3. Precautions taken against this were;

1. the vacuum system was left pumping overnight (or even over the weekend in some cases)
2. the system was pre-sputtering for 1/2 to 1 hour to getter any oxygen left over (and to bring the target into equilibrium)
3. high purity argon with low moisture content was used
4. sputtering rates were maintained as high as possible without over-heating target or substrate surfaces.

The target surface was water cooled from the back, but substrates relied almost exclusively on radiative heat loss, thus caution was needed for it was found that substrate overheating led to rapid sample deterioration as discussed in section 4.3.

Attempts were made to produce alloys with tungsten concentrations of 25, 50, and 75%. Control of composition was effected by varying the size and shape of the tungsten and copper surfaces exposed to the Ar plasma in a systematic manner. Variations from planned compositions are due to the variation in target erosion areas and the different sputter yields of copper and tungsten discussed in the previous section.

Mass thicknesses of approximately 25, 75, 150, 250, and usually 375 and 1000 $\mu\text{g}/\text{cm}^2$ were chosen to explore the limits of the applicability of this thickness determination method. Thickness was controlled by rotating the substrate into and out of position and recording the amount of deposited material with

the quartz oscillator thickness monitor as discussed in section 2.2.2. The results of these runs are explained in detail in the results section 4.1, and show a general evolution in the understanding of the sputtering mechanisms of what turned out to be a fairly complex system.

Many variables control the deposition in this sputtering environment so records of each run included information on overall evacuation times and ultimate vacuum achieved before the argon was added, argon flow rate and pressure, voltage and current applied to the sputter gun, and deposition rate as measured with the quartz oscillator thickness monitor and digital stopwatch. More qualitative observations included apparent cleanliness of the bell jar (as occasional pump oil backstreaming was noted) and colour, density, and shape of the plasma. All parameters could be maintained at constant levels within uncertainties for extended periods, even 12 hours in the case of sputter run 11 (pure tungsten deposited at slow rates).

As mentioned in section 2.1.1, sample deterioration with time was of concern whenever Cu-W alloys were deposited.

Measures introduced to minimize this deterioration included

- 1) keeping all samples in a vacuum dessicator at all times to prevent oxidation.
- 2) In sputter run 19, samples were immersed in liquid nitrogen immediately after deposition. This had to be abandoned as the nitrogen left surface deposits

upon evaporation in the SEM.

- 3) Finally, doing all backscatter contrast measurements the same day as the films were deposited. This procedure was introduced with good success after the measurement method had been sufficiently refined.

Even with these precautions, samples deteriorated, sometimes with surprising speed, but backscattered ratio measurements were expected to be quite insensitive to the internal crystal structure and mixed phase samples as long as structures are smaller than the backscattered electron generation volume [10]. This volume is typically greater than 500 nm. in diameter. Phases of this size should be clearly visible in the SEM image at high magnification, and observations in this area have been described in section 4.5. Thus more complex deposition methods such as deposition on liquid nitrogen cooled substrates or post-deposition coating with silica were not considered necessary.

2.2 Sample Characterization

2.2.1 Composition Determination

Compositions were determined for each sputter run by x-ray fluorescence in the scanning electron microscope. X-ray fluorescence spectra were taken with an EE&G Ortec energy dispersive x-ray spectrometer and analysed by their proprietary

'ZAP' standardless peak height corrections software on an EEDS II dedicated computer (also manufactured by the same company).

The program uses standardized empirical corrections for the three major variables affecting the quantity of x-rays given off by elements in a sample. Atomic number, or Z effects, x-ray absorption by all elements in the sample, and secondary x-ray fluorescence corrections are calculated in an iterative matrix formulation (thus the name ZAF, as changed to ZAP). These empirical corrections have been derived for thick samples with smooth surfaces. Thus for sputter runs 2 through 15 only the thick sample deposited specifically for analysis was analysed. Though analysis routines based on empirical formulae are prone to long term drifts in measuring parameters, our system is checked regularly for accuracy using stoichiometric compounds.

Further composition checks were done for the Cu-W systems in sputter runs 16 to 18, in which thin films were sputtered simultaneously onto glass slides which had been previously coated with a thin layer of rock salt (NaCl), by means of vacuum evaporation. These films were floated free from their substrates by immersion in distilled water, the film remaining on the surface of the water due to surface tension. Then they were mounted on perforated aluminum foil for ZAF x-ray analysis as well.

X-ray analysis from free standing films requires minimal ZAF corrections and can therefore be more accurate than when full ZAF corrections are needed. EE&G proprietary software to make these minimal corrections was also available. Another advantage is that background count levels are lower and there are no interfering substrate x-ray peaks. However, care was needed to ensure that all brass components in the SEM sample chamber were covered with Al foil to prevent extra Cu X-rays from being excited by tungsten $k\alpha$ x-rays or by stray electrons.

Composition determination also included some measure of sample homogeneity because, as mentioned previously, sample deterioration with time was a consideration throughout the work with Cu-W alloys. The method of measuring whether deterioration was advanced enough to affect other measurements consisted of visual checks with backscatter and secondary electron detectors under high magnification in the SEM. With both of these detectors, structures within the sample could be detected by change in backscatter ratio, and surface structure rearrangements or oxidations could be seen. Further discussion of work in these determinations is given in section 4.1.

2.2.2 Thickness Determination

The 1 cm^2 substrates were sufficiently large to be differentially weighed before and after deposition of the alloy on a Cahn Electrobalance with an accuracy of ± 0.2 micrograms ($\mu\text{g.}$). This gave relative accuracies of 8% to 0.2% for the

masses of the films ranging in mass from 25 to 1000 μg . An uncoated substrate was included in each sputter run to act as a mass control, to ensure that the calibration or counterweight of the electrobalance had not changed over the 2 to 5 days the substrates were in the sputtering apparatus.

Mass thickness was also measured during deposition with a Sloan vibrating crystal thickness monitor. The principle of operation for such monitors is that a quartz crystal plate (water cooled for thermal stability) is forced to vibrate at its natural harmonic frequency in the radio frequency range by the piezoelectric effect. This frequency is picked up through a transducer in the crystal holder and taken via coaxial cable outside the vacuum system to the monitor. The monitor generates an adjustable reference signal to compare with the incoming signal to generate a beat frequency indicating the difference in the two signals.

The crystal's natural harmonic frequency is a linear function of its mass over a frequency range of several hundred thousand hertz (Hz), its mass increasing as deposits accumulate on its surface. The change in frequency with mass deposited is sufficiently sensitive that for the thinnest films in this experiment the frequency changed by 1000 Hz. This change was measured to $\pm 1\%$, so this helped increase significantly the overall accuracy of thickness measurement for the thinner films as well as providing thickness control during deposition.

The relationship between decrease in frequency $|\Delta f|$ with mass deposited ΔD is an empirical one given by;

$$|\Delta f| = \frac{\rho_f \Delta D}{c_v} \quad (3)$$

where c_v is a calibration constant. The calibration constant was given by the manufacturers as being approximately equal to 2, however this was checked on every run by graphing the weight measurements versus $|\Delta f|$ as shown in section 4.1.2.

2.3 Backscattered Electron Detection

2.3.1 The Backscattered Electron Detector

For this study backscattered electron contrast measurements were done with a Robinson style scintillation detector. This detector came as a commercially available option on our ISI DS 130 SEM. It consists of a plate of scintillator plastic which sits over the sample holder and is attached via a light pipe to a photo-multiplier tube which resides outside the evacuated SEM sample chamber, as shown in figure 3. The scintillator plate is approximately 2.9 cm. wide and 6.0 cm. long with a copper ringed aperture in the center to transmit the electron beam. The fairly complex geometry of the scintillator plate was necessary because of the need to provide enough room in the sample chamber for other detectors and for sample movement, so is really a compromise solution in an attempt to cover as much solid angle as possible.

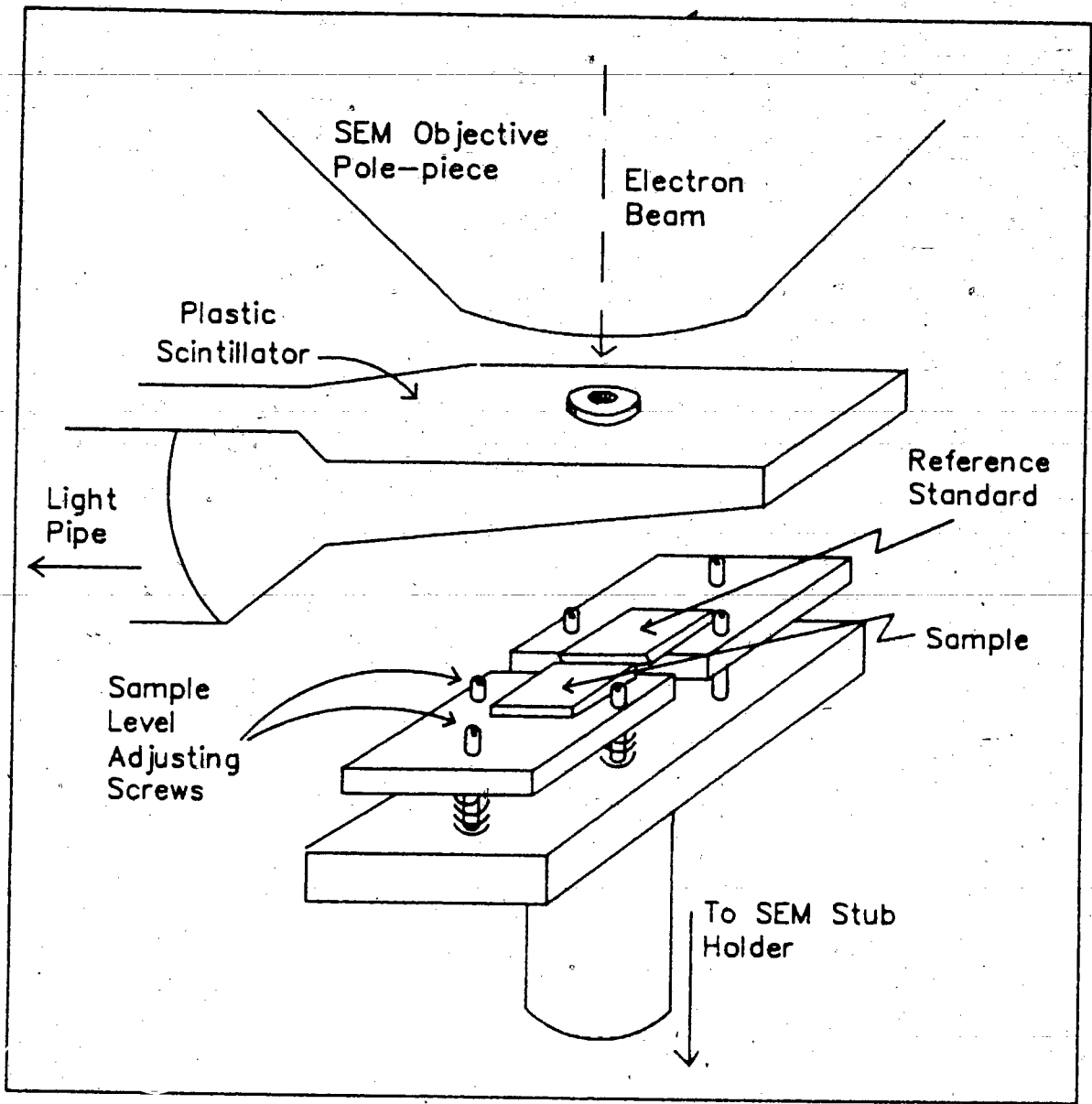


Figure 3 Schematic of the Detector and Sampleholder. This diagram has been drawn in perspective to show the shape of the Robinson backscattered electron detector used in the ISI DS 130 scanning electron microscope. The light pipe directs the scintillation light caused by the energetic backscattered electrons to a photomultiplier tube outside the sample chamber. The sample and reference substrates can be made coplanar on the sampleholder simply by turning the adjusting screws, as springs under the adjusting screws provide the needed counterforce.

With the sample approximately 2.7 cm. below the scintillator, the solid angle subtended by the plate for electrons escaping from the sample surface is roughly 1.0π steradians (str.). The solid angle of the aperture and surrounding ring is about 0.1π str. This is due to the necessity of scanning the beam over a wide area in low magnification imaging, but the detecting surface does form an annulus covering the angles of maximum backscatter intensity as measured by Hohn [28].

2.3.2 Sample Holder Configuration

Due to the assymetrical shape of the detector, the orientation of the sample with respect to the detector affects the resulting signal. This observation will be discussed further in section 2.4.2, but to minimize differences in sample substrate and reference substrate orientations a new sample holder was developed. Thin film sample and reference substrates were mounted immediately adjacent to one another on separate supports as shown in figure 3. The substrates, reference materials, and films were all placed in electrical contact with the sample holder using colloidal silver paste.

The support for the sample was mounted on 3 adjustable spring loaded screws, which allowed any sample to be adjusted parallel to and in the same plane as the reference substrate. This adjustment was accomplished most simply by using the specularly reflective nature of the sample surfaces. When observed at glancing angle, any adjustment to bring the sample

into the same plane as the reference was done such that the edge between them would be just visible from either side.

To adjust the surfaces to be coplanar, the images of a straight line (such as the overhead fluorescent lighting used in our laboratory) were made parallel and continuous across the two surfaces under all orientations. After some practice this method showed reproducibly parallel surfaces even under high magnification in the SEM. Important to the accuracy of the method was viewing images of distant objects rather than close ones, and viewing them at a variety of orientations and angles.

Once the samples were mounted and leveled, the sample holder was placed in the SEM such that the samples would be perpendicular to the electron beam column, and the specimen chamber was then evacuated. The first samples were tilted 90 degrees from horizontal while being viewed to determine if the leveling process had succeeded. The angle was measured directly off the stage, and variation over 1/2 degree was noted in the initial trials, even at high magnification. This was very important for the measurements of backscatter with incident beam angle, discussed in the next section, where angle was changed between normal to almost vertical for each sample.

2.3.3 Backscatter Reference Material

A study was carried out to determine the optimal reference material for electron contrast measurements. The final choice

after several different materials were tried was the thick pure W sample prepared in sputter run 11. It was measured against the W foil used as the sputter target several times to ensure equivalent reflectivity for all energies and angles. The advantage of using deposited material rather than the W foil was increased surface smoothness, the smoothness being equivalent to that of the other thin film samples to be measured.

Other materials tried included the silicon wafer material used as sample substrates, and tungsten foil used for sputter targets. The silicon wafer material had the advantages of ready availability, purity, uniformity, and highly polished front surface. However, after many measurements it became apparent that results using this material were not very repeatable at different magnifications. Further study revealed that at low magnifications the channeling pattern of the single crystal silicon (heretofore assumed to be negligible) played a role in the repeatability problem. The tungsten foil was available in .08 mm thickness with a semi-polished roller finish. This surface was rather rough for regular work, as its surface contrast could change results 1-3% (see section 4.4 for experimental work on this) depending upon magnification and angle.

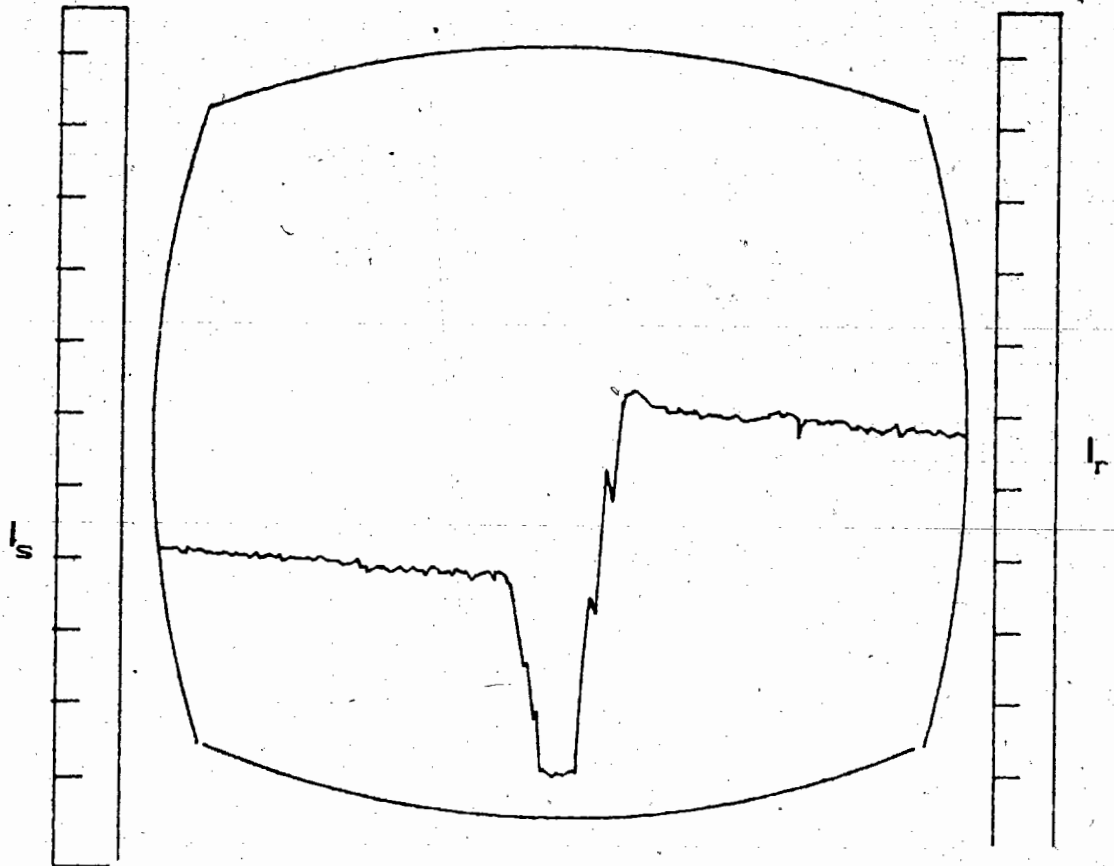
2.4 Quantitative Contrast Measurement in the SEM

Two methods were used to obtain quantitative contrast information from the backscattered electron signal. In both, a suitably smooth, clean surface was found using the SEM in regular imaging mode and placing both Backscatter Electron (BSE) and Secondary Electron (SE) produced images on the two screens. Moderate magnification of 20x to 100x was used to ensure sufficient overview of the sample to take average intensities of both thin film and reference. The sweep was then switched to linescan mode, in which the electron beam sweeps quickly and repeatedly over a single line across both thin film sample and the different reference material.

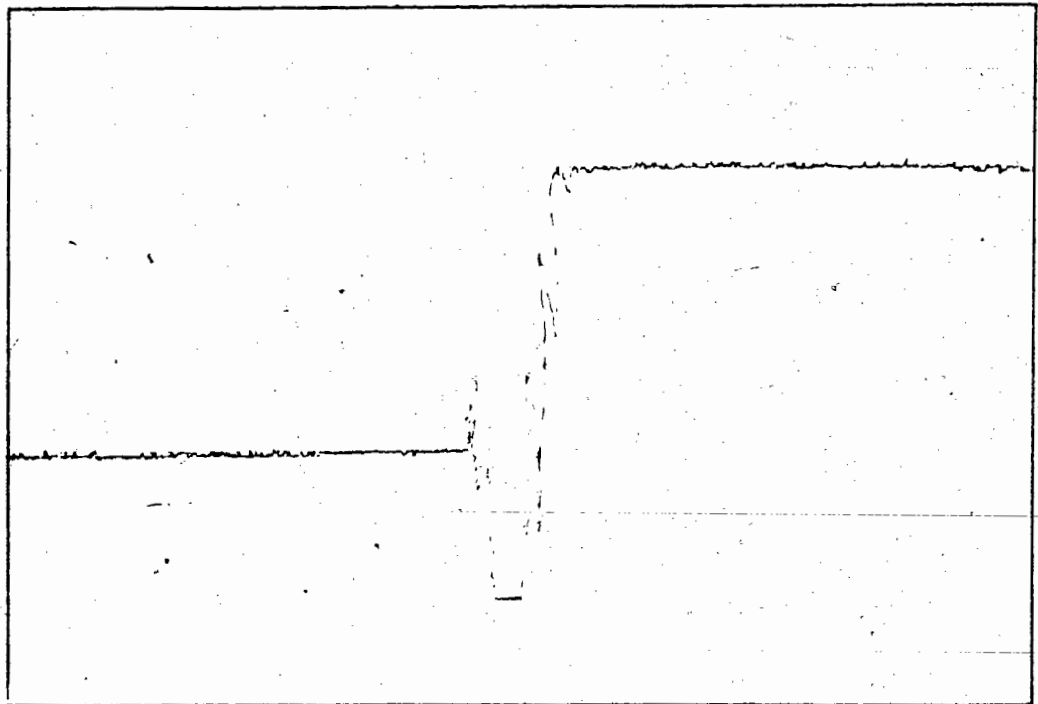
The signal was then switched to modulate the y deflection of the screen as a function of detected intensity, and the amplification adjusted such that intensities from both surfaces appeared as lines on the screen with a much lower line in between, as shown in figure 4. The low level signal is due to the small gap between reference standard and the sample. The beam diameter and intensity were normally at maximum (approximately 10^{-9} Amperes) to provide ample signal to the Robinson detector even at low beam accelerating potentials. The contrast was measured directly on the screen or by a computer method.

Figure 4. Contrast Images Obtained in the SEM. The upper drawing shows the screen of the scanning electron microscope with a typical linescan image on it. The height of the line on the screen indicates the signal level from the backscattered electron detector. As the beam of the SEM scans rapidly over the same line on the target, the image on the screen is constantly being refreshed at the same rate. Thus a continuous line, blurred by random noise, appears on the screen. The two scales taped on either side of the screen act as a reference to measure the difference in height between the signals from the sample (usually placed on the left, as shown here) and the tungsten reference. The lower picture shows the image that the EEDS II computer obtains after accumulating data from five, one second sweeps. Note that the noise is significantly reduced due to the longer data accumulation times possible with the computer.

SCHEMATIC OF THE SEM SCREEN, SHOWING A LINESCAN IMAGE



GRAPH OF THE SAME IMAGE OBTAINED FROM THE COMPUTER



- 4

2.4.1 On-Screen Contrast Measurement

Backscatter intensities were measured directly on the screen using a ruler and a grid taped to the edges of the screen. The background, or zero signal level of the y deflection unfortunately was found to change as a function of signal amplification, so the system had to be rezeroed whenever the amplification was changed.

Re-zeroing was done by turning the electron gun current down to stop beam emission, then repositioning the resulting zero level line to correspond to a round number of the taped on grid using the brightness level control. Often the beam current could be adjusted using the Wehnelt cap voltage of the electron gun to set the reference sample intensity to a convenient level as well, usually 10 cm. above zero level, thus letting the unknown sample reading be divided by a simple number to simplify relative intensity calculation and provide consistent screen parallax error.

2.4.2 Computerized Contrast Measurement

A somewhat more precise method was devised using the EEDS II computer and some associated image processing and control software (also proprietary to this same company). Once the linescan image had been obtained on the SEM screen by the methods discussed previously, a program was run to accumulate the linescan image in the 2048 channels of the multichannel analyzer normally associated with spectrum collection. The

program actually takes control of the scan of the SEM and a menu is given for a range of scan speed and size to be chosen. A linescan repeated 5 times at lowest magnification was normally chosen with scan speed of one sweep per second over a length of 1 to 3 mm.

There are 4 specialized firmware memories for 2048 channel images (or 8 1024 channel images) in the EEDS II computer, so once 3 different images were obtained the beam current was turned down and an image of the electronic background or dark signal level was taken and stored in the final image memory. This background level is controlled by the brightness level controls on the SEM and the computer interface analog to digital converter. This interface module has an LED display indicating whether the incoming signal (in this case from the same circuitry which controls the screen image) is of the appropriate magnitude for proper digital conversion by its amplifiers.

Both brightness and contrast controls on the SEM were adjusted to maintain the signal between upper and lower levels displayed on the interface module before any data were taken. If this was not done, the analog to digital converter would clip high signals or have an incorrect overall level, leading to mistaken contrast readings which appear superficially normal as the appearance of the image is not distorted very much.

To test for systematic errors and random measuring

uncertainty, many images of the same sample were taken at different settings of both contrast and brightness. Results are tabulated in table I for silicon versus tungsten at 20 keV (both samples thick) with on screen measurements tabulated as well for comparison. Results showed minimal differences as long as settings were kept from extreme values, but settings were left the same or changed only minimally throughout every actual measurement to maximize internal measuring consistency.

TABLE I

RANGE OF LEDS	ZERO ERROR	CONTRAST	FROM SCREEN
Extreme Overrange	none	.7474	.76
Moderate Overrange	none	.2285	.24
High-Within Range	none	.2205	.22
Mid-range	none	.2193	.22
Low-range	none	.2129	.22
Mid-range	low	.2095	.20
Mid-range	Extreme low	.1418	.15

A program was written in EE&G's BASIC-like programming language (called ORACL) to subtract the background image's counts, set up and illustrate (in different colours) the two regions of the image to be compared, and to calculate their contrast ratio. The program and an explanation of the

mathematics in it are given in appendix A. To maximize accuracy, the default settings in the program averaged the two signal levels over 500 channels each. The counts of the channels in each area were summed and divided by the number of channels to obtain an average level which smoothed the signal noise. However, it was soon noted that if the signal had an inherent slope, this method could lead to systematic errors.

Slopes were frequently visible in the image, which should be two straight horizontal lines on the screen as shown in figure 4. No slopes were noted in the images taken with the beam current turned down, indicating that the source of the sloping signal was not in the electronics of the data collection or image processing. The symptoms indicated more than one source to the problem and several steps were taken to minimize this.

- 1) The lowest practical magnifications were used to gain an average value of backscatter intensity and an accurate estimate of the slope.
- 2) Sample and reference had different slopes if not properly leveled on the sample holder, thus the care described previously in ensuring that they were coplanar.
- 3) Slopes appeared on solid samples as well as thin films, but to ensure that it was not a charging effect liberal applications of silver paste were used when attaching samples to the sample holder to ensure good electrical contact.

As the sloping signal was never completely eliminated, an option for the image analysis program was written which measured the slope of each side by taking two small areas at the extremes of the areas summed over, summing, and using these points to determine slope. As the same slope (within uncertainty) was seen in both sample and reference, the two slopes averaged, and corrections were calculated for the relative contrast using the method shown in Appendix A. The program was written to print out both slopes and the corrected and uncorrected values of the contrast ratio. The values for slopes ranged from 0 to 1% typically, and produced corrections of approximately 1%.

2.5 Variation of Parameters Measured

As mentioned in the introduction it was the goal of this experiment to measure both thickness and composition of thin films of known binary alloys. Thus for two unknowns two variables must be measured. One of these is BSE contrast with known solids. The choice of the second was determined by studying how the contrast changed with variation of one of the experimental parameters. Several parameters were possible, but the three most promising parameters were those ~~already~~ found in the literature, as reviewed in section 1.4.

2.5.1 Variation with Electron Beam Energy

Straight line graphs were obtained when contrast was plotted versus the reciprocal of the electron beam energy. As will be discussed in section 4.1, this made electron beam energy an appropriate variable to use in the straightforward separation of thickness information from composition information. In addition the energy may be lowered and raised quickly and accurately without changing the sample-detector geometry, thus energy was selected to be the second variable to be used in the determination of both thickness and composition.

2.5.2 Other Parameters Varied

The two other parameters mentioned in the introduction were also tested before choosing the final method. Variation of the angle at which the beam is incident on the surface of the sample was varied by tilting the whole sample stage. The Robinson detector was mounted on the side on which the majority of electrons were deflected when the sample was tilted, but remained stationary throughout. This meant that the solid angle subtended by the detector changed with angle as well, so results were complicated by this and became difficult to interpret.

The solid angle from which electrons were collected was varied by a simple technique. The Robinson detector could be partially withdrawn from the sample chamber normally to facilitate other measurements by the SEM. To vary the solid angle of the detector then was simply a matter of withdrawing

the detector far enough that it did not interfere with the incoming beam.

With the detector withdrawn all the way possible, only electrons from angles 70 to 90 degrees to the beam normal were collected. With the detector part way out, electrons from approximately 35 to 60 degrees from the beam could be detected, and with the detector in normal position, as mentioned previously, electrons from approximately 10 to 50 degrees were collected.

The reason these two methods were not pursued in favour of the variation of energy method is that information from composition and thickness of the unknown film being measured is not simple to separate. Also it was felt that both of these methods would require the use of thin film standards of similar composition to the unknowns. Both of these methods exceeded the scope of the immediate research but both have potential for further development, as discussed in section 5.2.

3 THEORETICAL RESULTS

Interactions between rapidly moving electrons and solid metals are complex in general, with many scattering mechanisms possible [29]. X-ray excitation, Auger processes, and electron-plasmon interactions all play roles along with the more familiar Rutherford elastic scattering. Scattering cross sections for the various interactions are often poorly defined experimentally, so rigorous formulations describing either the electron's path through a solid or its statistical probability of being scattered back out of the solid are not practical in general.

Mathematical models which have been developed to approximate the interactions fall into two main categories, analytical equations and Monte Carlo simulations. Both types have been adapted to model the results of this study. Various analytical expressions are described in section 3.1 as an attempt to obtain a closed form expression from semi-empirical relationships. Section 3.2 describes 'Monte Carlo' type computer simulations of an electron's path through the solid which, when done several thousand times by computer, gives the necessary statistical information about the fraction back-scattered. Results from analytical and statistical models are compared and summarized in section 3.3. They are discussed side by side in terms of results and approximations, in sections 3.3.1 and 3.3.2.

3.1 Analytical Models of Electron Backscattering

3.1.1 Background to Analytical Models

Efforts to model mathematically an electron beam's interactions with solids have been going on since beams of electrons have been experimentally realizable, with important pioneering work being done by J.J Thomson, Rutherford, Bethe, [30, 31, 32] and more recently by Nakhodkin et. al., Everhart, and Thummel [33, 34, 35]. Early theories concentrated on transmission of electrons through gases and very thin foils to study diffusion and electron collisions with single atoms. In the late 1920's and early 1930's Bethe [32] expanded the diffusion case to electrons passing through infinite solids. In addition, he derived a more exact formulation for the continuous energy loss observed as an electron passes through a solid based on quantum mechanics. Though sophisticated, the Bethe model was not solvable to determine backscatter coefficients in closed form, and neglected contributions from single event backscattering.

In 1960, Everhart [34] published a simple model to explain the total backscattering coefficients of solids. This model relied on the assumption that all electron backscattering could be modelled as electrons undergoing one large angle collision before escaping to the surface. The Rutherford single scattering formula [31] (see appendix B) was used to calculate the probability of backscatter into a given solid angle from an

infinitesimal thickness of the target. The probability of electron scatter into angles which took the electrons out of the target was integrated from the surface of the target to a characteristic depth $R/2$, subject to the condition of the electron having enough energy to reach the surface.

The characteristic range, R , of electrons in the target was calculated using the Thomson-Widdington continuous energy loss formula (which is a mathematically simpler, approximate form of the Bethe energy loss formula [32]). This range is one of the boundary conditions of the integration. The characteristic range was defined as the mean distance an electron can travel in the solid before its energy goes to zero. This simplified range is proportional to the square of the incident beam energy, and is discussed further in section 3.1.3 as this is a source of error when modelling energy dependent backscattering coefficients.

Given the simple analytical form of the electron range in the target, the probability of backscatter can be integrated in closed form, yielding a value for the backscatter coefficient. Quantitative yields calculated by this model were about 1/3 of the experimental values, but showed good correspondence with the experimentally observed trend of increased backscatter with increasing Z . In Everhart's paper a fitting factor was added to the formula to simulate multiple scattering, and this helped the model to fit experimental results for elements of $Z < 40$.

In 1961 Archard [36] used simplifying assumptions to expand the Everhart model to a two collision case, and found much better agreement with experiment without using Everhart's fitting parameter. Archard calculated backscattered electron coefficients for the high atomic number elements from a simplification of the diffusion theory of Bethe [32]. Archard's simplifying assumptions included the geometrical ideal that all electrons penetrate the target to a given distance, then scatter isotropically from that point. The electrons then followed the diffusion formula to make their way out of the sample. Because of these geometrical assumptions, the Archard model works well only for flat, semi-infinite bulk solids, with no closed form analytical solutions for more complicated geometries, such as our thin film system.

In the early 1970's Thummel [35] modified Archard's diffusion model by adding a probability distribution to the depth at which the incoming beam is scattered. This distribution increases with depth (as the electrons lose energy to the sample) as the beam passes through the sample, then decreases asymptotically to zero as more electrons are scattered or absorbed. The isotropic scatter to the surface can be integrated at each point along the way, to the depth where electrons no longer have sufficient energy to reach the surface again. This gives the depth dependence needed to apply the diffusion model to thin films. Thummel's model neglects single

scattering, so gives values somewhat lower than experimental if realistic probability distributions are used.

3.1.2 An Analytical Model for This Experiment

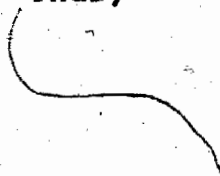
In 1981 Niedrig proposed a combined model [37] using the Thummel model with a modified probability distribution and the Everhart model without the Everhart fitting factor. Thus it is a more realistic simulation than previous work, as both single 'large angle' scattering and isotropic 'small angle scattering' diffusion contributions to the total backscattering coefficient η_b are accounted for. A detailed explanation of the mathematics of Niedrig's model has been given in appendix B, along with brief explanations of the Everhart and Thummel models from which it was derived. The combination of the two models is a fairly simple one. The Everhart model was added unmodified to a modified Thummel model, using Everhart's original (analytically derived) scattering constant rather than his fitting factor described in the previous section.

To make the added Thummel equation consistent with this, Niedrig added a diffusion constant multiplier k to the original Thummel model. The introduction of k was justified as a description of the fraction of electrons scattered by diffusion, and thus unavailable to be single scattered. Niedrig calculated k by setting the single scattering portion of the combined model to zero, and comparing results with a modified Thummel model which used a more realistic probability distribution than

Thummel's original work. The values of η_b calculated from this modified Thummel's model were approximately 2/3 of experimental values. Thus, the one third due to the Everhart model was added to this two thirds due to the modified Thummel model.

Values of η_b from the Niedrig model show good correlation with published experimental data [21, 37] for pure materials throughout the range of atomic numbers, though it does not use explicit fitting factors. This model works reasonably well for thin free standing films also, but the diffusion aspect requires an isotropic target, so the model has not been extended to supported thin films. The complications inherent in electron diffusion across boundaries in material is an area for further work.

Thus to adapt Niedrig's model to our experimental system, two modifications were necessary. The first was to change variables from those of pure materials to effective values for an alloy of given composition, and the second was to include the effects of having the thin film sample supported on a substrate of known composition.

- 1) To obtain effective values for Z and A for alloys, a simple average value was taken according to the relative proportions of atoms present in the solid. Thus;
- 

$$Z_{\text{eff.}} = a_1 Z_1 + a_2 Z_2 \quad (4a)$$

$$A_{\text{eff.}} = a_1 A_1 + a_2 A_2 \quad (4b)$$

where a_1 and a_2 are the relative fractions of atomic species 1 and 2. This approximation gave good results for random mixed alloys, though somewhat more complicated methods have been worked out [23, 38] for compounds and heterogeneous mixtures.

- 2) To account for the backscattering of electrons by the substrate which supports the thin film we utilized a simple empirical relation derived by DeNee and others [39, 40]. They observed that the backscatter ratio of the film-substrate system combination η_b is similar to that of a free standing film η_{thin} but varies between the substrate η_s and the bulk value η_{bulk} rather than from zero. Thus;

$$\eta_b = \eta_s + \frac{\eta_{\text{thin}}}{\eta_{\text{bulk}}} \left[1 - \frac{\eta_s}{\eta_{\text{bulk}}} \right] \quad (5)$$

Values for η_{thin} can be supplied by the Niedrig formula, as can values for η_{bulk} and η_s .

To calculate values for η_{bulk} , η_s , and η_{thin} using the Niedrig analytical expression, values for Niedrig's diffusion coefficient k were needed for each effective atomic number, as k

is a function of Z_{eff} . The formula for solving for k is discussed in appendix B. It was necessary to solve for k numerically, so the computer program written in BASIC to do this is also included in appendix B. Another program included in appendix B was written to calculate η_{bulk} and η_{thin} , plug them into DeNee's formula, and derive η_b for our experimental system.

3.1.3 Error and Uncertainty for Analytical Calculations

The major source of error in Niedrig's analytical model is the neglect of the backscattering contribution from multiple 'large angle' Rutherford type collisions. This approximation appeared to have led to many of the differences between this model and experiment, as discussed in section 3.3 below. Though the model showed good correspondence with bulk backscatter coefficients, this does not indicate that it is the true picture of real electron-solid interactions. The majority of elastically scattered electrons undergo more than one elastic collision. Therefore the division of electrons into single backscattered and diffusion backscattered is somewhat artificial.

There are also several "constants" in the formulation which are subject to experimental error or which are not truly constant as a function of the experimental variables. An example of such a constant is the electron range, which depends on the electron energy. Though such parameters are sources of

systematic error in the model, more accurate formulations were not included as this would complicate the model significantly, and is a topic for further research.

The model uses an E^2 dependence on range in the range-energy relationship which is valid at energies above 100 keV. However, at lower energies the exponent becomes dependent on incident beam energy as well, changing from 2 at 100 keV down to approximately 1.5 at 5 keV. This has been shown both theoretically by Bethe [32] and experimentally by several others [34, 41]. This error makes the theoretical model give values of η which are too low at lower values of incident energy and too high at high incident energy.

The empirical constant in the range-energy relationship (referred to as Terrill's constant [34]) been measured by Cosslett and Thomas [41] to be a function of incident beam energy as well. The effects of an energy dependent Terrill's constant were studied for the Everhart model by Kalef-Ezra, Horowitz, and Mack [42]. They included an approximate relation for the energy dependence based on an empirically fit curve and studied the resulting energy dependence of calculated back-scatter coefficients for low Z elements. Results showed reasonable agreement with published experimental data, indicating that with further work, similar improvements could be made in the Niedrig model.

Sources of random uncertainty are few in the analytical model. Most constants used are well known, such as the value of electronic charge e , and Avogadro's number N_a . The only experimentally measured constant was Terrill's constant of effective electron penetration.

3.2 Monte Carlo Simulation

3.2.1 Background to Monte Carlo Simulations

Monte Carlo simulations use an entirely different set of approximations from those of analytical models, resulting in a more versatile approach to the calculation of backscatter coefficients. The method had been developed for nuclear physics applications but was applied to the backscatter of 10-50 keV electrons by Bishop [43], Shimizu and Murata [44], and was used in analysing samples by Kyser and Murata [45] in 1974 on thickness determination using X-ray peak heights. These simulations used the elastic scattering formula of Rutherford to simulate an electron's interaction with a solid, but allowed the electron to undergo multiple elastic collisions in suitably randomized directions using computer simulation.

The computer program follows the progress of a simulated electron until it either makes its way out of the solid (either by passing through or coming back from the direction whence it came) or loses enough energy to be 'absorbed' at thermal energies. The computer program then starts over with a new

electron starting at the surface of the solid, eventually simulating a sufficient number of electrons to compile significant statistics.

An advantage of the Monte Carlo method is that it can simulate the complicated geometries of actual samples quite simply. This is because the computer program keeps track of the coordinates of a simulated electron's path through the solid during the simulation. Boundaries between different materials and the outer surface of the sample can be expressed in these coordinates and supplied to the computer program as well, so when an electron passes beyond given coordinates it is told to respond to the parameters of a different material (or be counted as having escaped in the case of the outer surface). Thus in the case of copper-tungsten on silicon the computer uses the silicon parameters for scattering calculations once an electron penetrates the thin film and enters the substrate.

Although the simulations of an individual electron's path through a solid might seem to imply a detailed knowledge of the individual interactions which take place, results from simulations which use average parameter values show results remarkably consistent with experiment. This has been amply shown in the literature on the subject, see especially [46].

3.2.2 Monte Carlo Model Chosen for this Work

The model chosen for this experiment is that of the

National Bureau of Standards (N.B.S.), as published in [47].

There are three important approximations in the N.B.S. model:

- 1) an electron passing through the solid undergoes elastic scattering collisions only in accordance with a modified Rutherford scattering equation.
- 2) Electrons lose energy continuously as they pass through the solid according to a formula derived by Bethe [32].
- 3) Intervals between collisions are governed by a mean free path equation suitably randomized.

A summary of the mathematics of this model is given in appendix C, but the physical implications of each of these approximations are discussed below.

The 'elastic scattering only' approximation ignores the other scattering processes mentioned in section 3.0, but for electrons with kinetic energies greater than about 10 keV, elastic scattering is expected to dominate over other processes [29]. The majority of electrons backscattered have energies within 30% of incident (see figure 12 in section 3.3.2) so that for simulations with incident electron energy 15 keV or above, the approximation is a good one. In this study, simulations were carried out down to 5 kV, so the effects of this approximation are discussed further in the next section.

In the N.B.S. model, the Rutherford scattering formula has been modified to include relativistic effects of the electrons and an atomic screening factor after Mott [48]. Relativistic

effects are generally negligible below about 20 kV. and the atomic screening factor describes the effect of orbital charges of the electrostatic field of the nucleus. If electrons only underwent elastic collisions, they would never lose energy. The simplest approximation to make the Monte Carlo model work is to assume a continuous energy loss to the surrounding solid. The expression derived by Bethe [32] has been found to be quite accurate experimentally, and is based on the solid being modelled as an electromagnetic continuum.

Finally, the rate at which collisions occur in a given solid is given by the collision cross-section. This cross-section can be derived from the modified Rutherford scattering formula if the number of atoms per cubic centimeter is given. This can be found from the density and atomic number A of the material. Because the value obtained in this manner is a mean path length, the Monte Carlo simulation uses an exponential randomization around this mean.

To adapt the N.B.S. model to our experimental system the program was modified to include a 'depth' parameter to indicate the thickness of the film. If a simulated electron's coordinates passed beyond this depth the parameters were changed for those of silicon. Also parameters such as atomic number and mass were needed, and as in the analytical model, these were calculated using simple average values as shown in equations 4a and 4b. Although there are many improvements on the N.B.S.

model cited in the literature [46,49], this model has gained wide acceptance over the last ten years and as such is a useful reference to the experimental results.

3.2.3 Error and Uncertainty in Monte Carlo Simulations

The main source of error arising from the above approximations is that values obtained for lower energy simulations will be less accurate. This leads to values for η which are too high for low energy. This effect was indeed noted in the results section 3.3. Other sources of error include the approximations used in the Rutherford scattering formula and Bethe energy loss formula, which both have very approximate semi-empirical portions. The Rutherford formula has the empirical atomic screening correction and the Bethe formula has been modified with a fitting factor.

Random uncertainty is inherent in the Monte Carlo method, as all results are statistical compilations of individual simulations. To estimate this uncertainty, Poisson distributions were used, but it is important to note that the distribution applies to the number of electrons backscattered, not the total number simulated. Thus, uncertainty can be given by;

$$S = \sqrt{n} \quad (6)$$

where n is the number of electrons backscattered from a given sample and S is the approximate uncertainty. For a typical

measurement 1000 electrons were simulated and backscattering ratios ranged from .17 to .62, giving uncertainties of $\pm 7\%$ and $\pm 4\%$ respectively. For more important measurements (such as for bulk values of Cu or W) over 5000 electrons were simulated to give uncertainties less than $\pm 2\%$ relative.

3.3 Results of Analytical and Monte Carlo Calculations

3.3.1 Discussion of Results

The results from the analytical model and the Monte Carlo simulations are shown in figures 5 through 9 for the full range of compositions and electron beam energies used in the experiment. Plots were tried on regular linear and log-log plots, but the linear-inverse energy plotting seems to give the best fit and allows straight line sections (horizontal and inclined) to be drawn through the important regions of the graphs.

Both analytical calculations and Monte Carlo simulations give absolute values for the backscatter proportion η_b for an element of atomic number Z_{eff} and atomic weight A_{eff} . The experiment, however, gives the relative proportion of electrons escaping from the thin film on substrate to those escaping from the solid reference (in this case tungsten) η_b/η_{W} . Thus to simulate experimental results, all results were divided by the appropriate bulk tungsten backscatter coefficient.

Figures 5-9 Theoretical Results. All theoretical results were obtained and plotted in a similar manner. The upper graphs show results from the analytical model of section 3.1.2, and the lower graphs show results from the Monte Carlo simulations of section 3.2.2. The same mass thicknesses were used in each graph and were plotted using the same symbols for each graph. The results for $.028 \text{ mg/cm}^2$ thick samples have been plotted as squares, crosses indicate results for $.084 \text{ mg/cm}^2$ thick samples, diamonds were used for samples $.168 \text{ mg/cm}^2$ thick, and triangles represent results for $.280 \text{ mg/cm}^2$ thick samples. Compositions are in atomic percents of copper and tungsten. All backscatter results have been plotted relative to those for thick tungsten to simulate experimental conditions. Results were plotted as the inverse of the incident electron beam kinetic energy, also in agreement with experimental conditions.

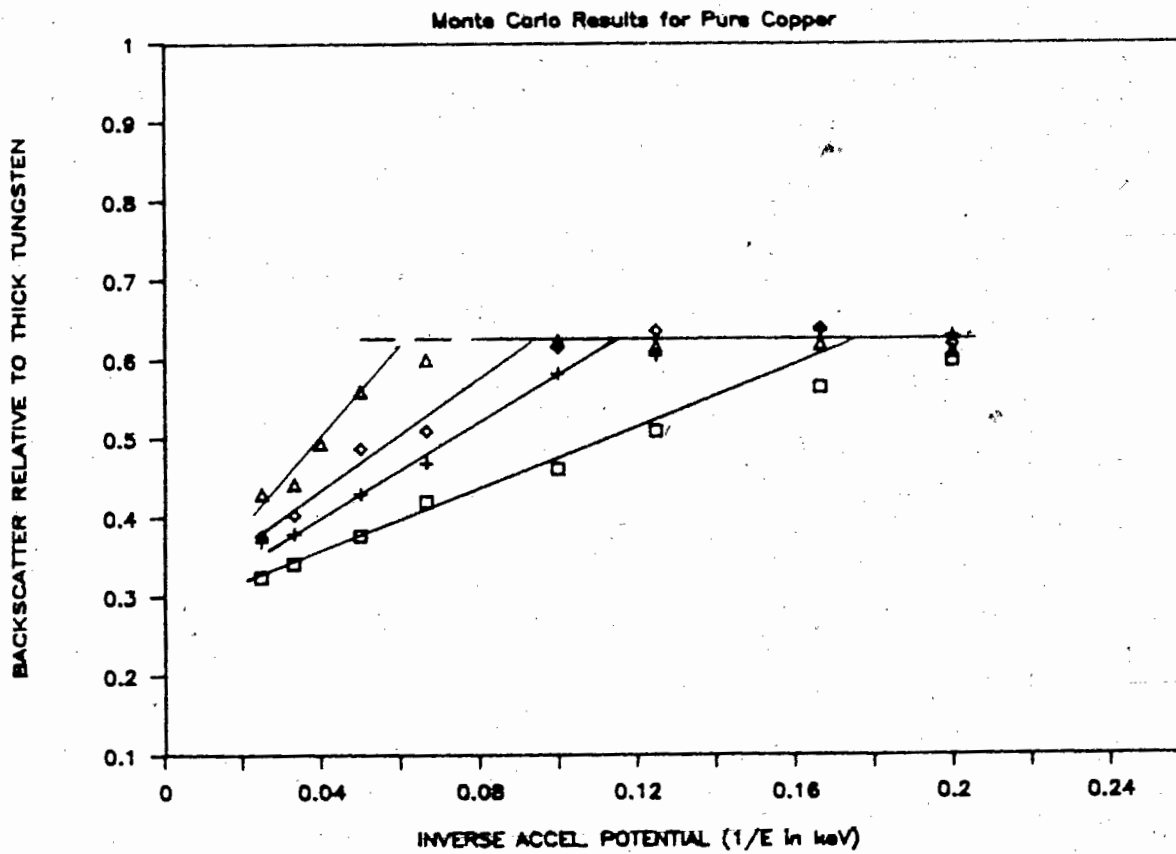
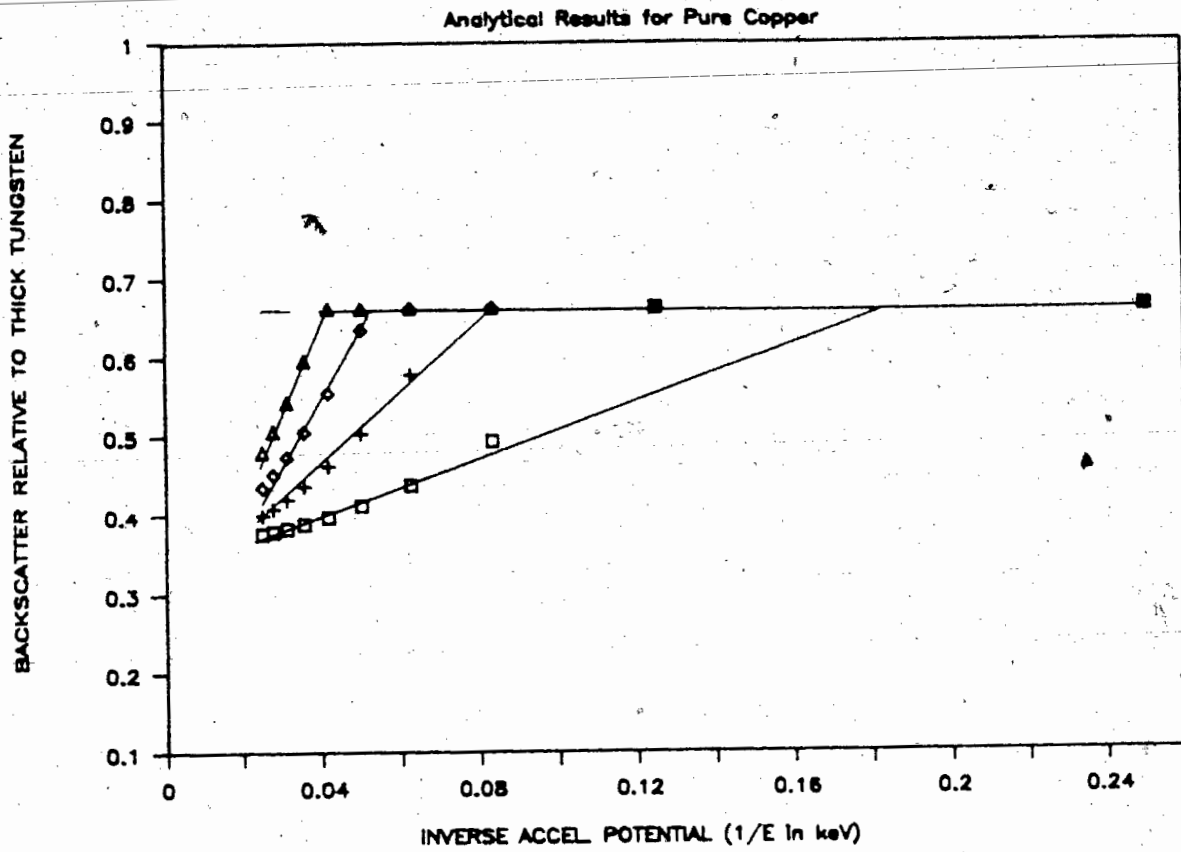


Figure 5. Theoretical Results for Pure Copper

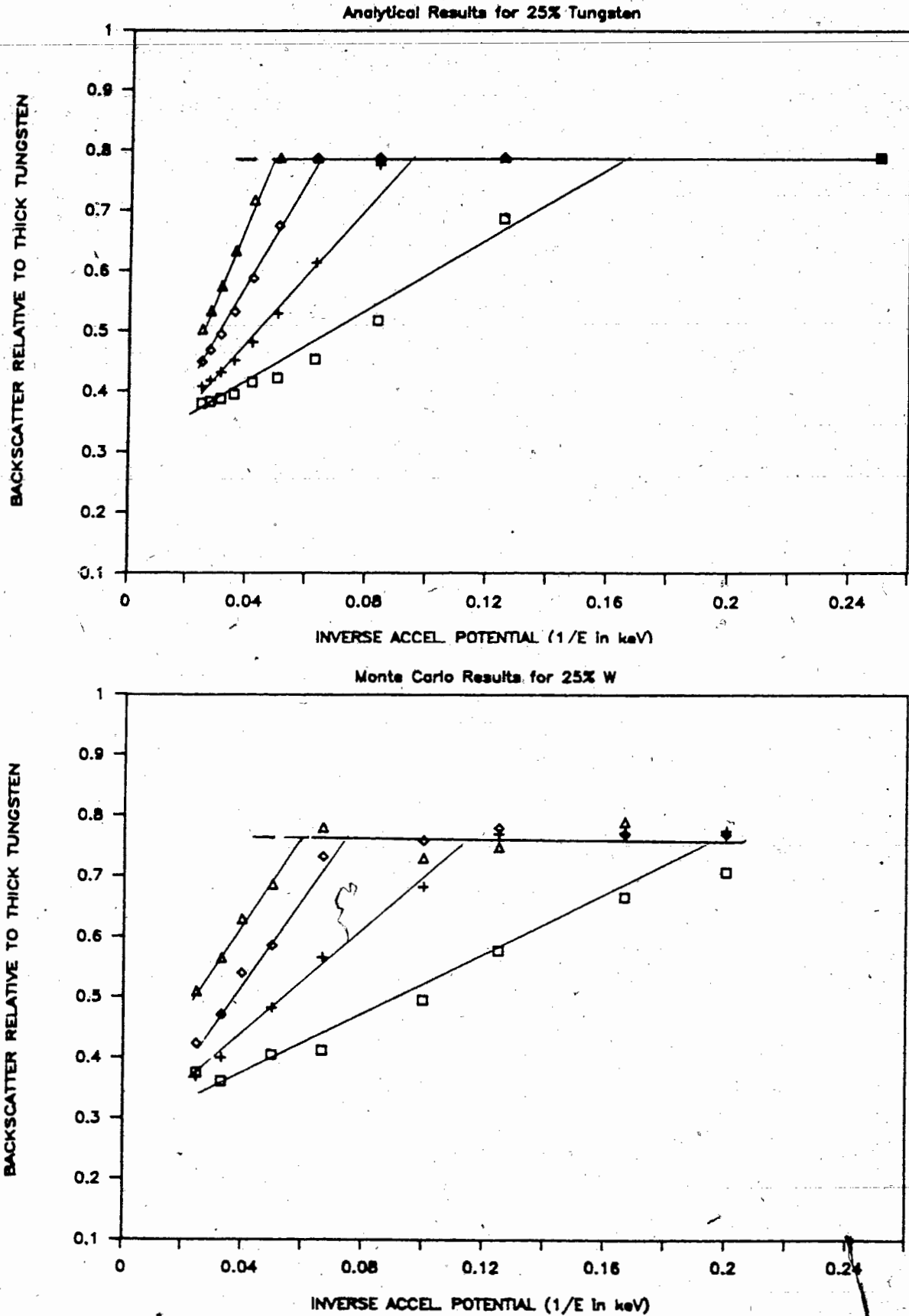


Figure 6. Theoretical Results for 25% Tungsten, 75% Copper

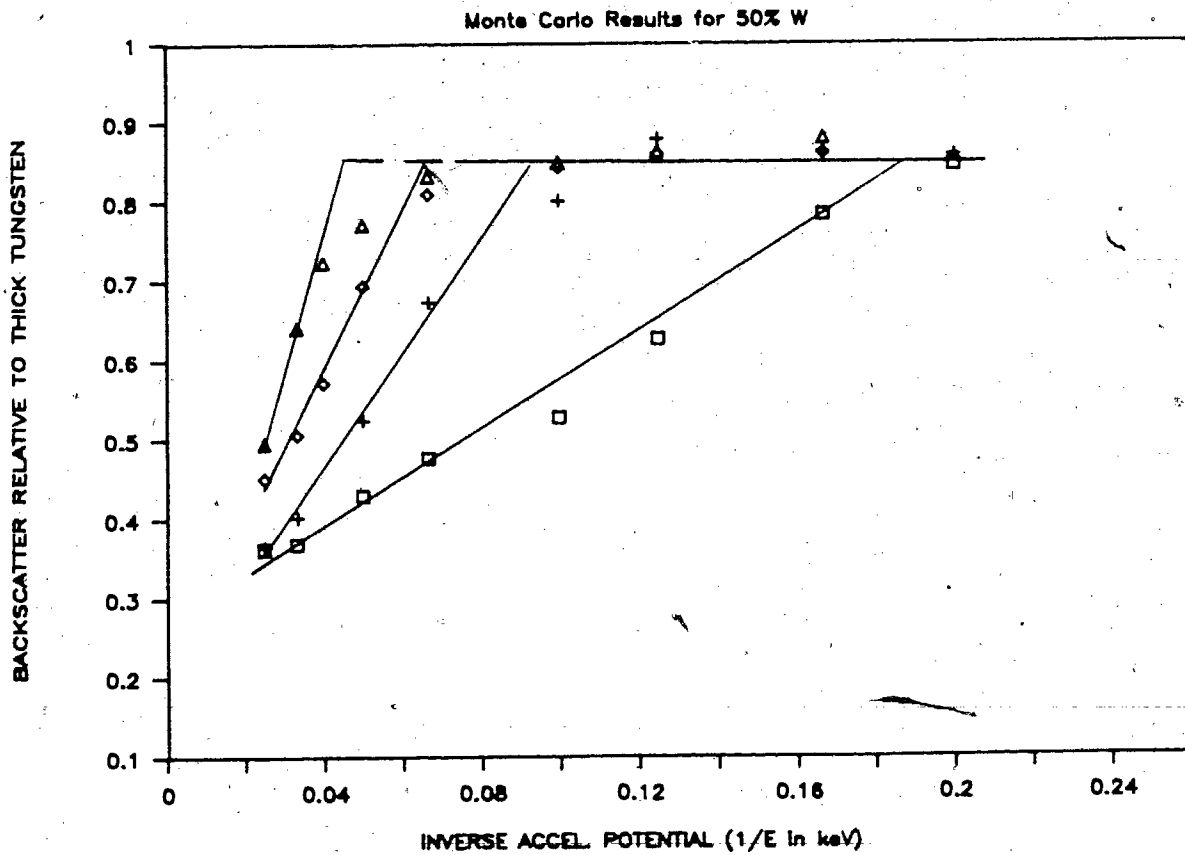
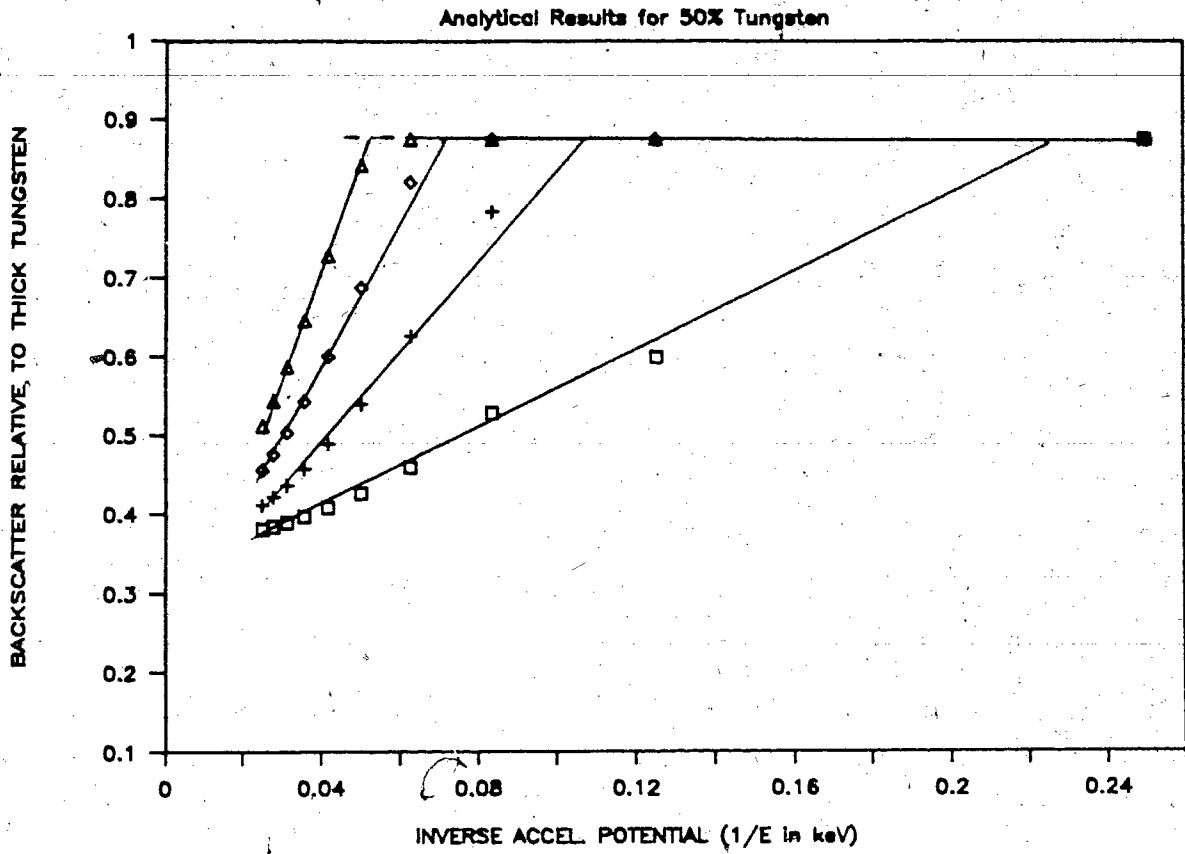


Figure 7. Theoretical Results for 50% Tungsten, 50% Copper

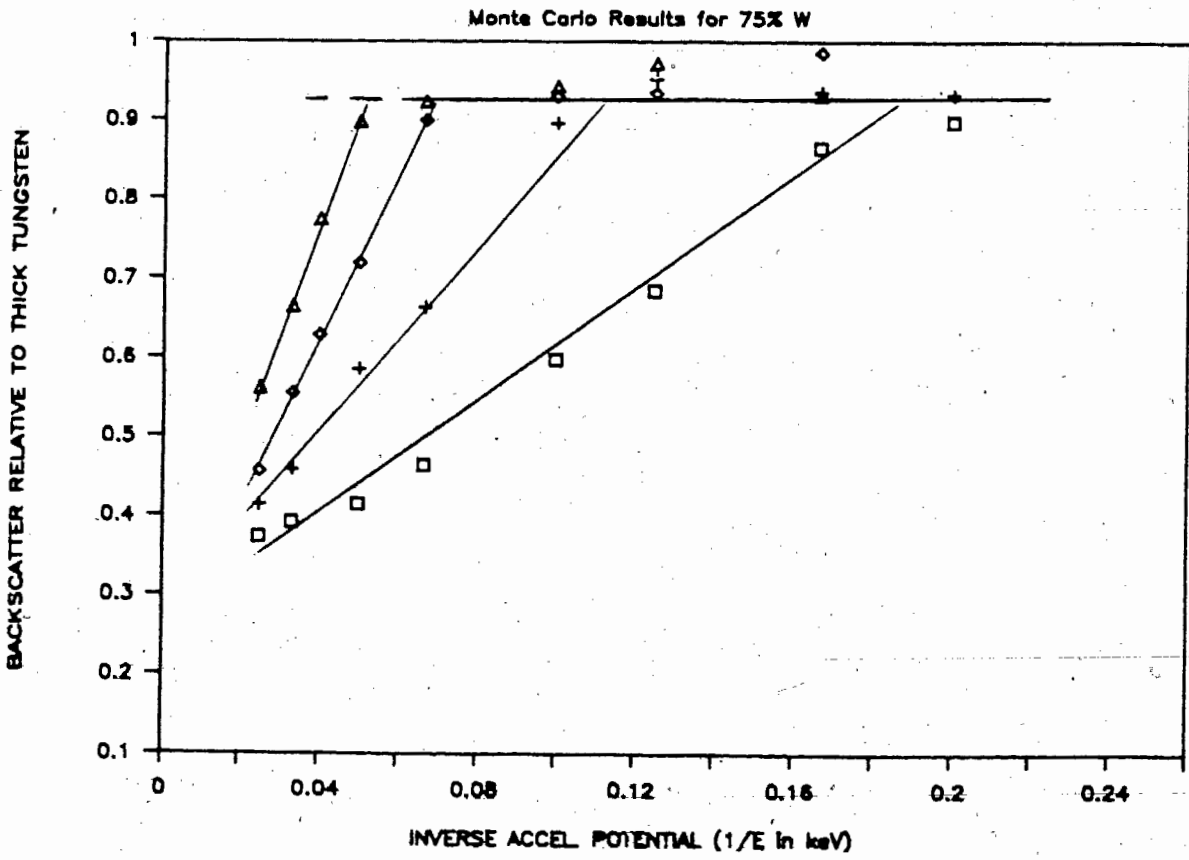
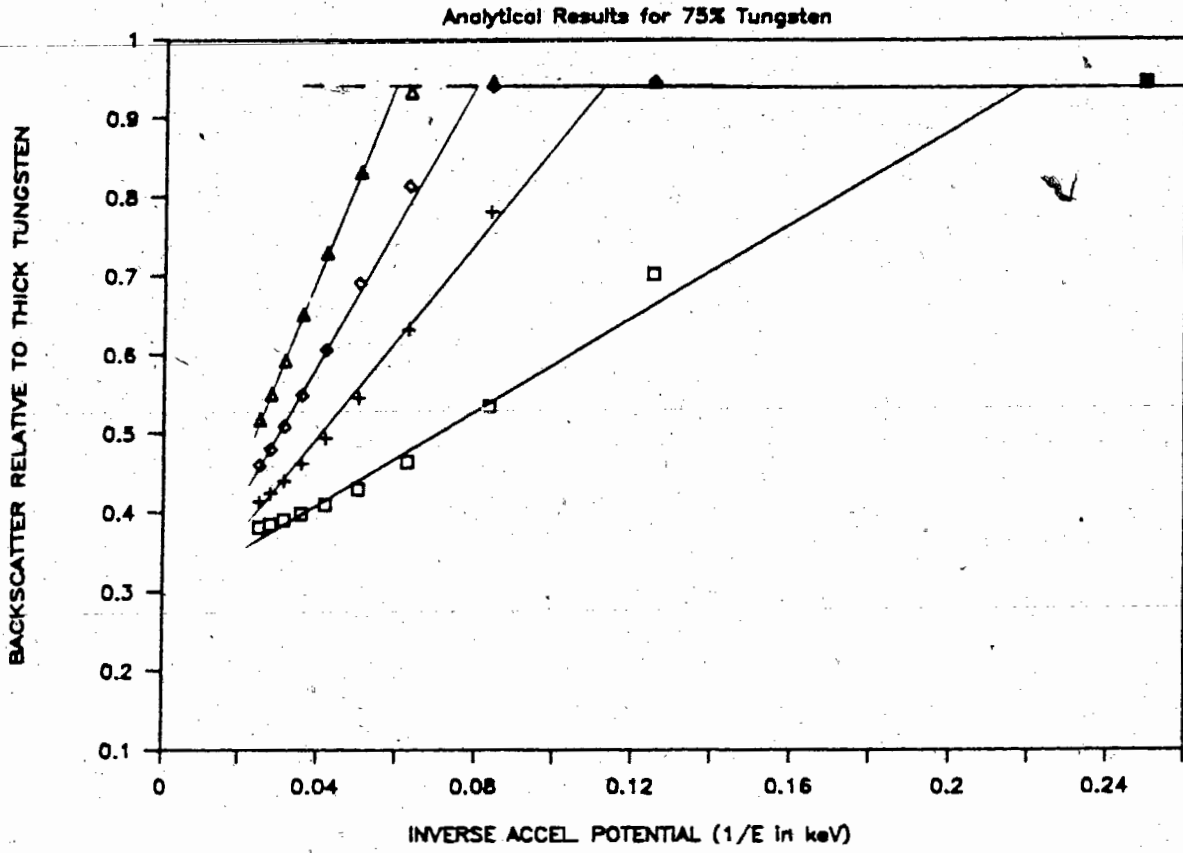


Figure 8. Theoretical Results for 75% Tungsten, 25% Copper

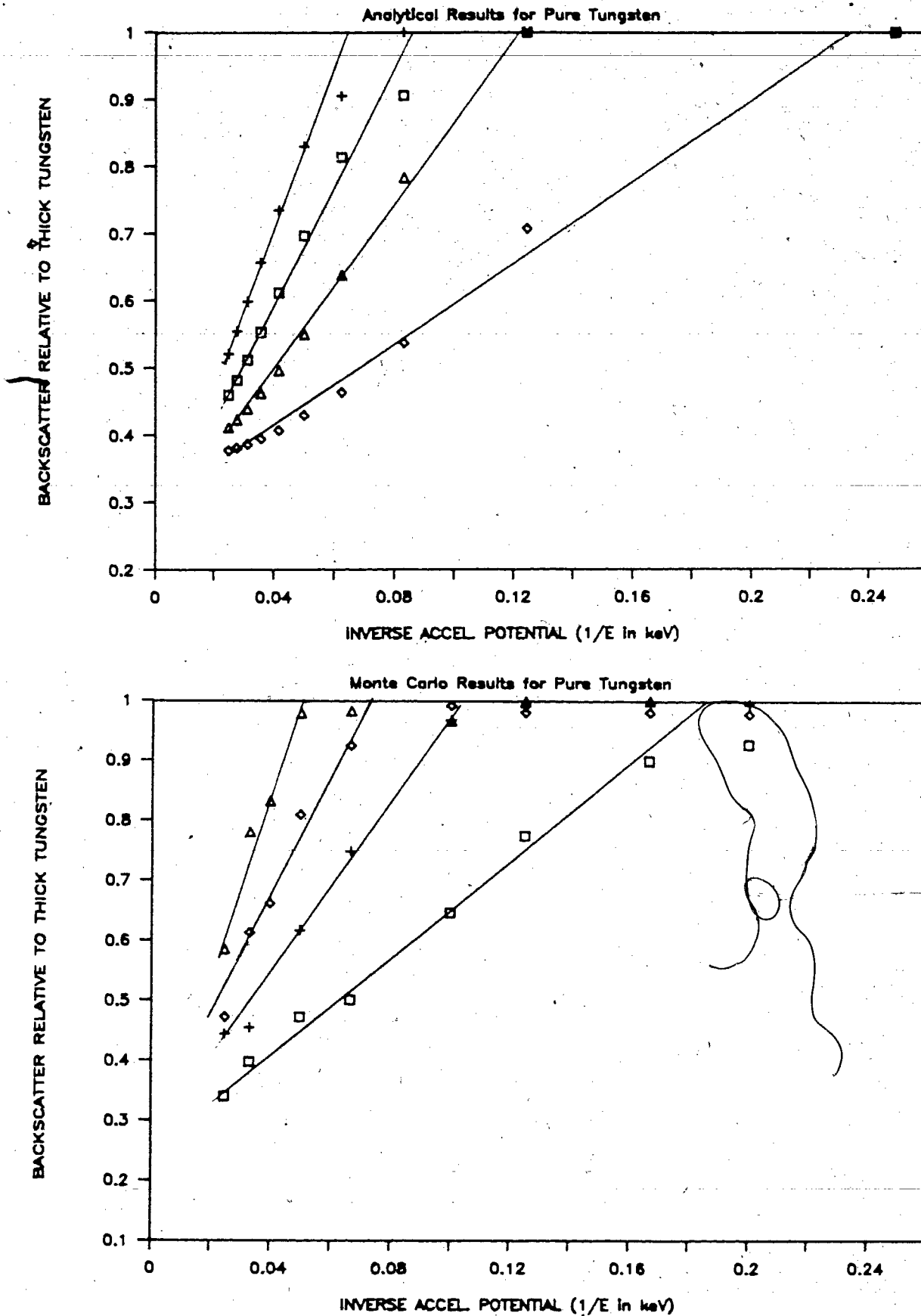


Figure 9. Theoretical Results for Pure Tungsten

Thus the value of η_w must be accurately known for all energies in the experimental range. It was a straightforward matter to calculate the tungsten η_{bulk} for the analytical model, as η_{bulk} values are independent of electron incident energy. In the Monte Carlo simulations, the results from bulk tungsten for all voltages needed careful simulation, as the functional relationships between η_{bulk} and incident beam energy were not as straightforward.

Values of η_{bulk} obtained in the simulation of bulk tungsten, copper, and silicon all show a slight downward trend of η_{bulk} with increasing voltage, as shown in figure 10. Published experimental evidence (see for example [41]) indicates a flat or slightly upward trend for thick W and Cu, but this should have minimal effect on the accuracy of the simulation, as the slopes of all three lines are approximately equal and all values were divided by the tungsten values at each value of the energy.

When comparing the slopes of the inclined portions of the results, the slopes for the analytical model are both steeper for thick samples and less steep for thin samples. The parameter $1/E_i$, which is the inverse energy at which the sloped and horizontal lines intersect, shows these differences clearly. For thick films, $1/E_i$ increases with increasing tungsten content in the analytical model, a trend which is not observed either in Monte Carlo results or the experimental results of section 4.

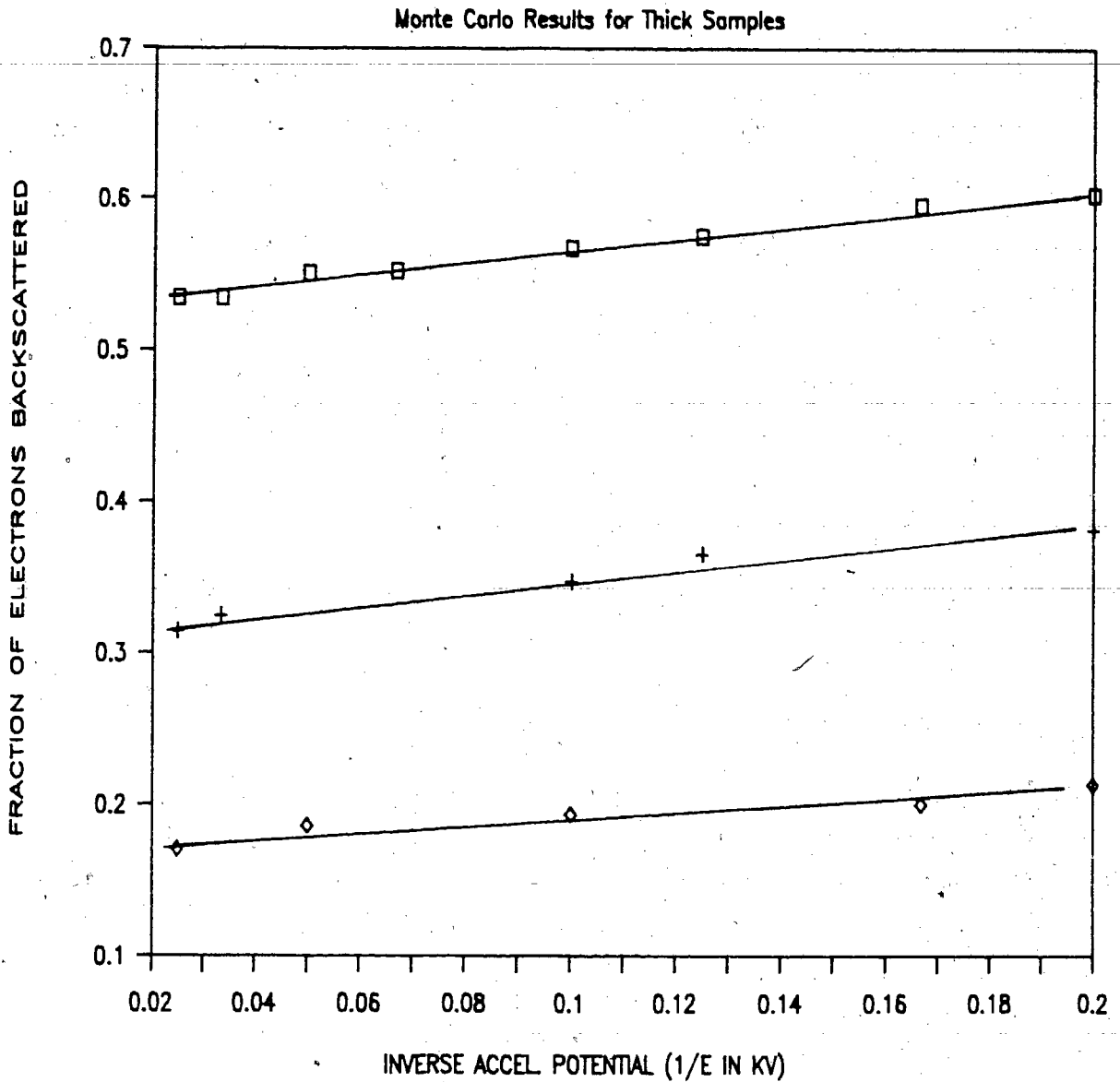


Figure 10. Monte Carlo Results for Thick Samples. The fraction of simulated electrons backscattered by thick targets of tungsten (square symbols), copper (cross symbols), and silicon (diamond symbols) has been plotted as a function of inverse incident beam energy. 5000 electrons were simulated for each point to cover the range of incident beam energies used in the experiment. The slopes of the lines all fall within uncertainty of one another.

It is interesting to note that experimental values of η_b for copper and tungsten obtained from the literature are within uncertainty of those from the analytical model, but are 5-10% lower than those of the Monte Carlo simulation. Fortunately this effect is minimized in these experiments by the comparative nature of the measurements. Thus the Monte Carlo results of figures 5-9 show very good correlation to the experimental results and are within the statistical uncertainties (which will be discussed in section 3.3.3).

3.3.2 Differences in Both Models From the Experiment

Implicit in the analytical and Monte Carlo models presented is that electrons backscattered from the surface are collected over a full 2π str. solid angle. But as noted previously, the detector used in this experiment has a considerably more complex geometry, whose character is shown in figure 3. The models have the potential for simulating more restrictive collection solid angles, but this would require further work, and the 2π results have the advantage of being comparable to the results of others.

Simulation results of the angular backscatter distributions for the extreme cases of pure bulk copper and tungsten are plotted in figure 11. Although these show a negligible difference, Hohn [28] has shown experimentally that the tungsten distribution is wider angle in general. This could produce a systematic error in that proportionally more electrons from the tungsten surface will miss detection by the Robinson detector.

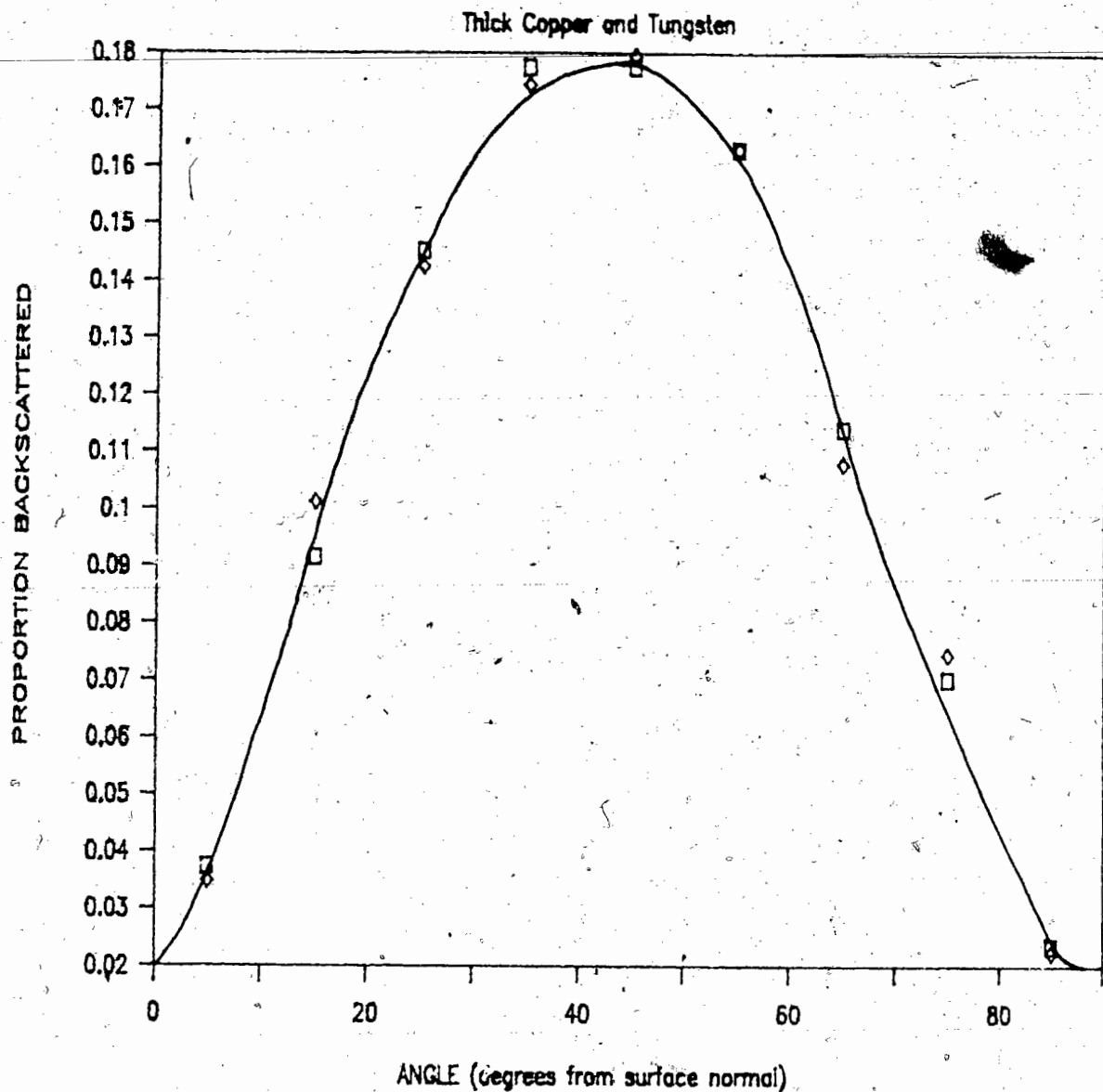


Figure 11. The Angular Distribution of Backscattered Electrons. Statistics were compiled on the angular distribution of the electrons which were backscattered in the Monte Carlo simulations. The angle at which a simulated electron leaves the surface of a target was divided into 10 degree intervals. The number of electrons backscattered into each 10 degree interval was divided by the total number of electrons backscattered before being plotted, so that the curves for both bulk tungsten (square symbols) and copper (diamond symbols) are normalized.

But this is countered by the non-negligible solid angle of the aperture in the Robinson detector for which a proportionally larger number of electrons from copper are not detected.

Total systematic error due to geometric considerations is not expected to exceed 2%, in part because of the cancelling nature of the aperture and other shape corrections. The actual systematic error due each geometrical consideration is hard to estimate, because the real distributions of scattering angles have not been measured here (though there are some citations in the literature for copper and gold).

Another possible difference between experimental results and the Monte Carlo simulations is due to the response of the detector to electrons of different energies. In general scintillation detectors have threshold energies in the kilovolt range, below which they do not detect the incoming particle. For the detector used in this experiment very little below 3 kV is detected with useful signals occurring at 4 kV and above. Thus the Monte Carlo program was modified to print out the energy distribution which the backscattered electrons have, as shown in figure 12 for the case of bulk copper and tungsten.

This effect appears to be significant, with systematic differences between experiment and Monte Carlo simulation expected to be on the order of 2-10%. The effect is minimized for thin film measurements at higher energies as the back-

Thick Copper and Tungsten

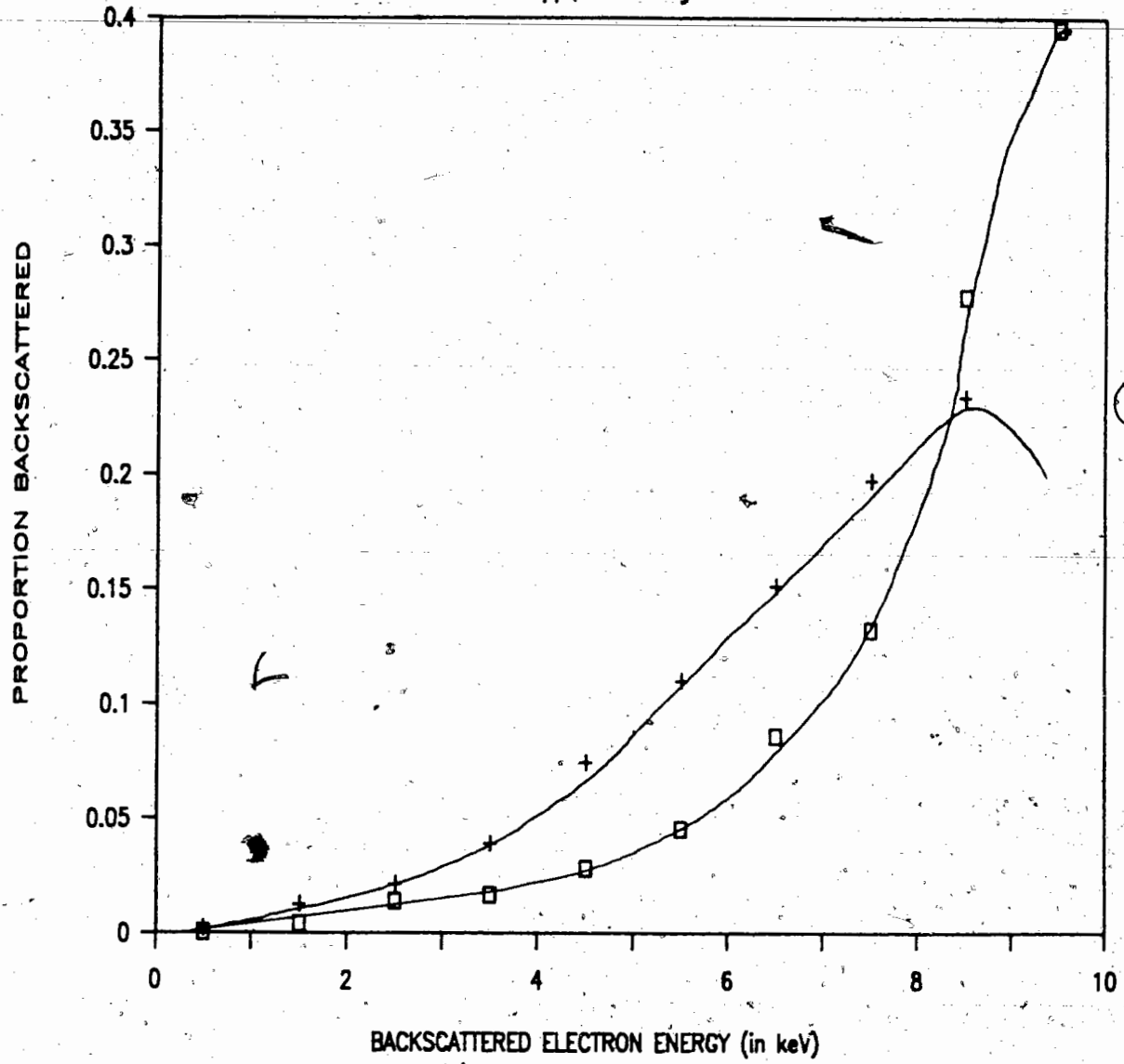


Figure 12. The Energy Distribution of Backscattered Electrons. Statistics were compiled on the energy distribution of back-scattered electrons in the Monte Carlo simulations. The incident beam energy used was 10 kV, and the range of energies for back-scattered electrons was divided into 10, 1 kV intervals. Curves were normalized as in figure 11, and the results for tungsten are plotted as crosses, while squares were used for copper.

scattered electron energy distribution of the substrate becomes dominant, but for the bulk measurements to be discussed in section 4.3 this effect is more likely to cause a difference between the experimental values of this work and those of others (on which the analytical model is based). Once again, there is very little data in the literature on actual backscattered electron energy distributions for thin films on substrates, so the above effect would be difficult to correct for. The effect does not affect the overall accuracy of the thickness determination method derived in this thesis, so corrections were not attempted.

The final discrepancy between Monte Carlo simulations and the actual experiment is differences in densities of the experimentally realizable thin films compared to the bulk density values assumed for the Monte Carlo work. The effects of error in density were tested by running simulations of bulk tungsten, changing the density value over a factor of four without changing the other parameters (for a semi-infinitely thick case). Values are shown in table II for the 10 keV accelerating potential case.

TABLE II

Density in gm/cm ³	Portion Backscattered	Uncertainty
19.3	.5675	± .0075
25.7	.5760	± .0107
12.9	.5690	± .0107
6.43	.5812	± .0108

All values are within random uncertainty of one another and no systematic trends can be noted. Thus thin film density errors can be neglected in Monte Carlo simulations for constant mass thickness.

4 EXPERIMENTAL RESULTS

Results from independent measurements of the samples are summarized in section 4.1. ZAF x-ray fluorescence measurements were conducted on samples from each sputter run, and these results along with other composition determinations are summarized in sections 4.1.1 and 4.1.2. Results from the differential weighing and quartz oscillator thickness measurements are discussed in section 4.1.3. Sections 4.2.1 and 4.2.2 discuss results from the contrast determinations and how they compare with results from the theoretical section.

The accuracy and applicability of the thickness measurement method presented here is mainly dependent on the accuracy of the contrast measurements. Sections 4.2.3 and 4.2.4 are studies of possible systematic errors in contrast measurements and the random error associated with them. Methods for calculation of the composition and thickness from these results are derived in sections 4.3.1 and 4.4.1, with their accuracies estimated in sections 4.3.2 and 4.4.2. Finally, section 4.5 covers the applicability of this new method of thickness determination with regard to ease of use and which samples can be measured.

4.1 Results From the Independent Characterization of Samples

4.1.1 Composition Determinations

Results of the ZAF x-ray fluorescence analyses done for each sputter run used in this experiment are summarized in table III.

TABLE III

Sputter Run	% Tungsten and Copper		No. Analyses
9	0.0	100.0	2
11	100.0	0.0	3
15	28.0	31.6	2
22	68.4	72.0	2
24	18.6	81.4	2
26	100.0	0.0	1

The rationale behind the sputter run numbering is as follows: To obtain the five desired compositions of samples, 26 different runs of sputtering were done, as mentioned in section 2.2. Early sputter run samples (sputter runs 1-14) of Cu-W had deteriorated before the final thickness measuring method had been established. The pure copper run number 9 and pure tungsten run number 11 did not deteriorate so were used in the final analysis. Other reasons for the need for so many runs include the trial and error composition control and some equipment failures (sputter runs 19-21). Sputter run 17 was used for the thin free standing film experiment and sputter run 23 was used in a sample deterioration experiment described below.

The internal consistency of the ZAF measurements was checked by doing the same sample several times and at different accelerating potentials. Variations on the order of 2%-3% relative were observed, and averaged together to obtain the final values listed. Analyses were done under nearly ideal conditions for analyses of this kind, so accuracy of the ZAF corrections is expected to be 1-2% relative, as shown by Yakowitz [50]. This indicated that samples were not ideal, either because of non-homogeneities or non-ideal sample-detector geometry. Though analysis routines of this type are based on empirical formulae and are prone to long term drifts in measuring parameters, our system is checked regularly for accuracy using stoichiometric compounds.

Results from the thin free standing film ZAF analyses discribed in section 2.2.3 are given in table IV.

TABLE IV

Sample	Composition	Thickness
supported film	31.6% Cu 27.1	~650 nm. ~240 nm.
Thin free film different spot	29.1 30.7	~20 nm. ~20 nm.

Results from the compositional analysis of free standing films prepared in sputter run 17 was in good agreement with

results from regular ZAF analysis. As noted previously, the x-ray analysis of freestanding films is expected to be much more accurate, to the order of .5% [51], so this provided a good verification of the composition values obtained in table III even though deposition was on a different type of substrate.

4.1.2 Thickness Determinations

Results of the differential microbalance weighing have been plotted against the change in frequency of the quartz oscillator for all sputter runs. A sample plot is given in figure 13 with the slope equal to the experimental value of c_s (after the masses of the films had been converted to mass per unit area as described below). Values of c_s and standard deviations for each of the six sputtering runs used in the final analysis are in table V.

TABLE V

Sputter Run Number	Calibration Constant	Uncertainty
9	1.97	$\pm .07$
11	2.8	$\pm .2$
15	2.32	$\pm .15$
22	6.8	$\pm .3$
24	3.16	$\pm .15$
26	2.56	$\pm .05$

Masses were converted to mass per unit area measurements by dividing each sample mass by individual substrate sizes and correcting for partial coating of the sides of the substrates.

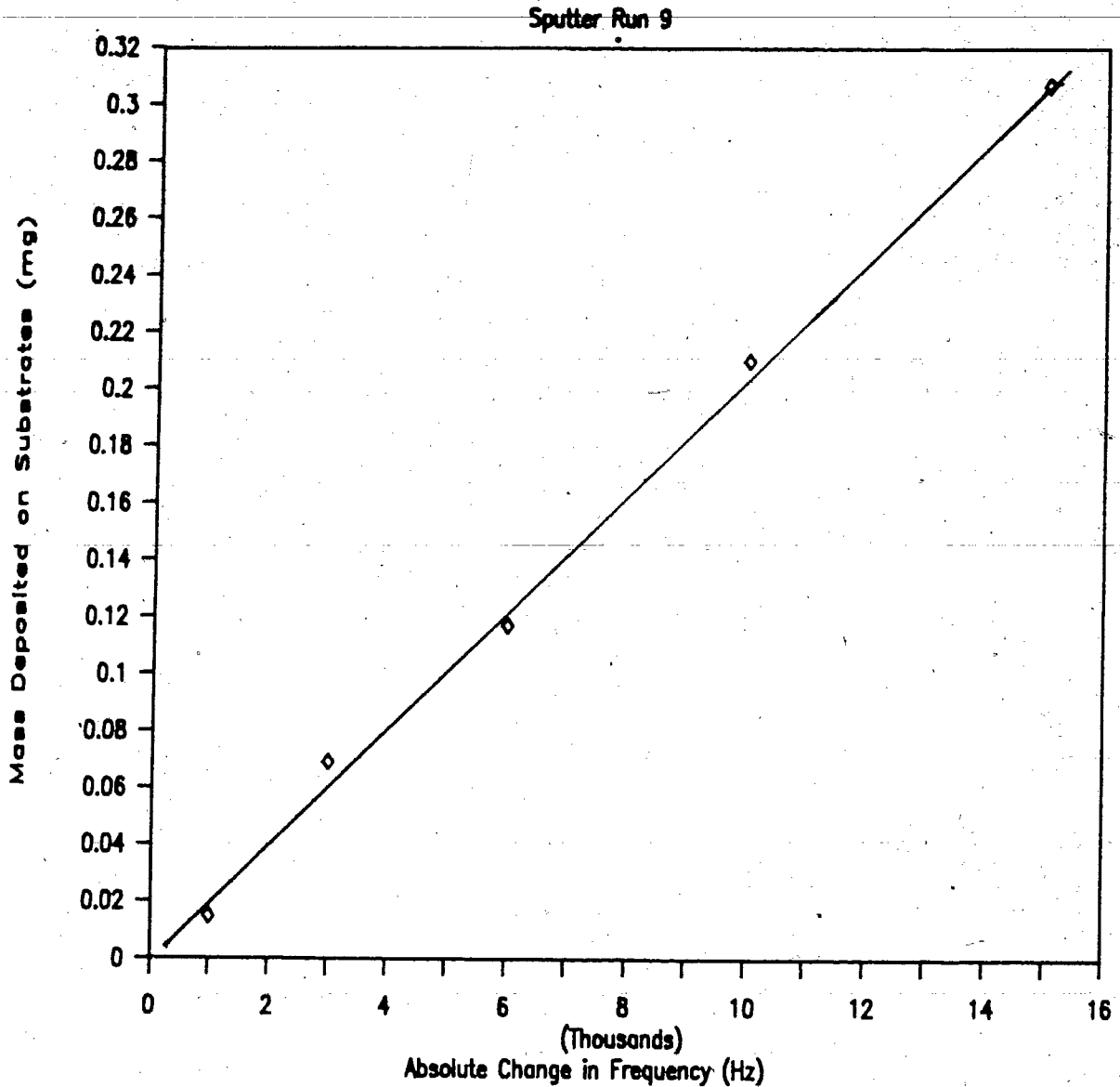


Figure 13. Calibration Graph for the Thickness Monitor. The frequency readouts of the Sloan vibrating crystal thickness monitor were correlated with mass measurements of the sample substrates (mounted adjacent to the vibrating crystal) each time the monitor was used. The slope of the resulting curve gives the calibration factor c_s . Shown here is the curve for sputter run 9, after masses have been corrected for variations in substrate size and coating of the sides of the substrates.

All substrates were found to be within 2% of the 1.00 cm² nominal area. The area of the sides of the substrates was approximately .15 cm² in total. Estimation of the total coverage of these sides was made difficult by their irregular texture, but thickness of the coatings on the sides were estimated from backscattered electron measurements in the SEM. Thickness appeared to be 1/2 to 4/5 of the front surface coverage and extremely non-uniform. Thus corrections of 5% to 12% were applied to the total masses to obtain the mass per unit area.

Estimating the surface area and coverage of the sides of the substrates was a major source of uncertainty in c_s . This was included in the standard deviation of the calibration constants listed above. Other uncertainties (including the uncertainty in frequency readings and vernier caliper readings for the dimensions of coated substrates) were less than ±1% relative, so were not significant.

As mentioned in section 2.2, the calibration constant was a function of the sputtering parameters, in general increasing c_s was observed for increased argon gas pressure while sputtering. This variation in c_s was tested in sputter run 23. The argon pressure was changed from the lowest practical value (for which the plasma remained excited) for sample 23.1 to the highest practical value (after which other parts of the sputtering chamber give spurious glow discharges) in sample 23.2. Though

both were nominally 3000 Hz depositions, the mass of the high pressure deposit was four times greater. Changing sputtering parameters changes the substrate heating and angle of incidence of the impinging tungsten and copper atoms, and both of these effects were felt to play a role.

4.2 Contrast Results from the SEM

4.2.1 Contrast Results for Samples

The results given in figures 14-18, consist of 5 graphs of 4 or 5 samples each with contrast relative to bulk tungsten plotted as a function of impinging electron beam energy. Data was taken with both on-screen and computer methods as these agreed to within 2-3% in all cases. Accelerating voltages were chosen for simplicity as well as accuracy and with the inverse energy scale in mind. However, there is capability on our SEM to make measurements at 1 kV intervals if desired. The lower limit of 5 kV was chosen as signals from the 4 kV measurements were very noisy, and the upper limit of 40 kV was the maximum accelerating voltage obtainable with the ISI DS 130 SEM used.

As mentioned previously, all plotting of data was done on an inverse energy scale as this gave the best correspondence to straight lines for the higher energy regime. The use of an inverse scale also enhances the division between the horizontal

Sputter run 9, Pure Copper

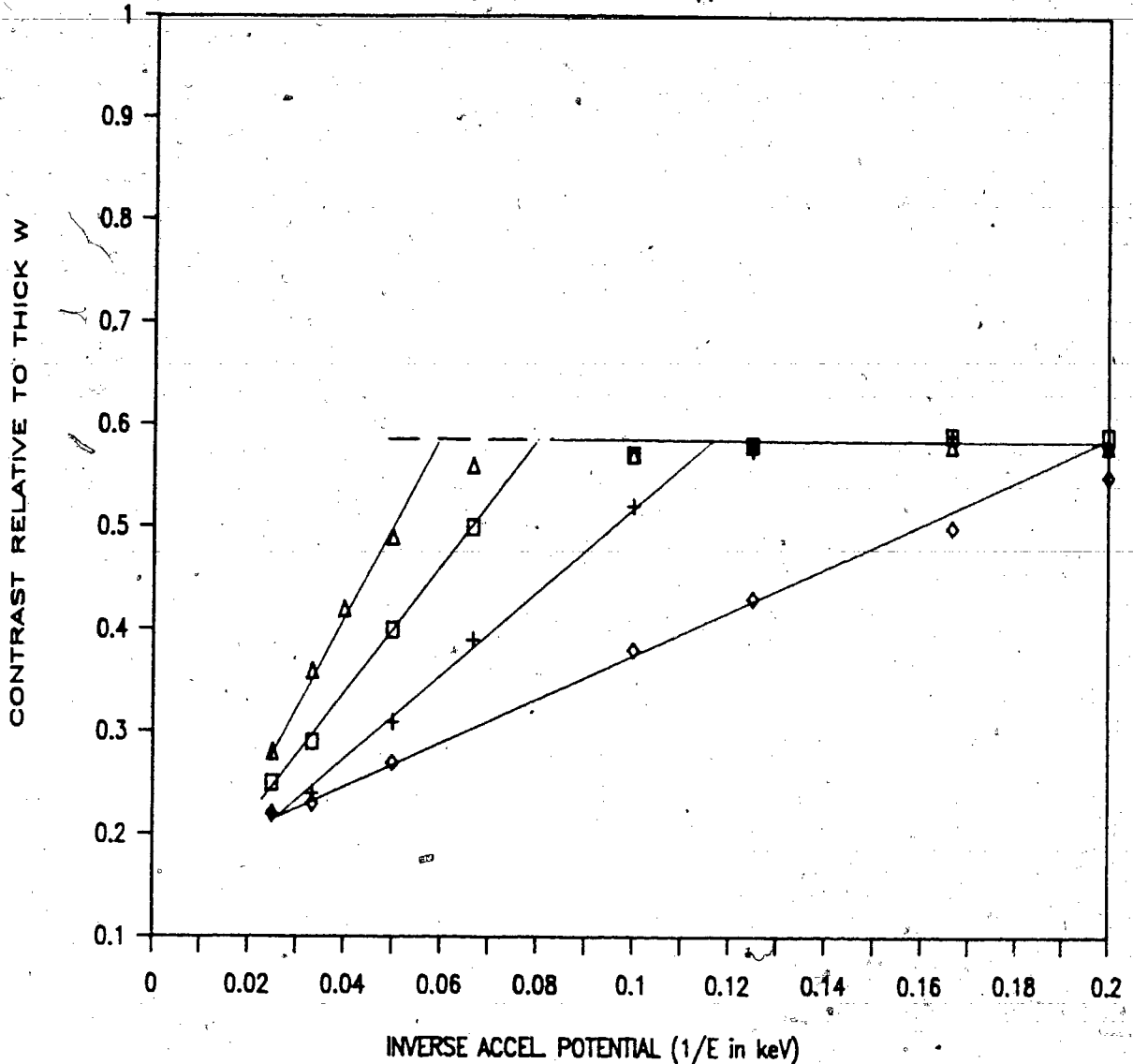


Figure 14. Experimental Contrast Results for Sputter Run 9. A pure copper target was used for this sputter run. Sample thicknesses of .020, .060, .120, and .200 mg/cm² were deposited, and results from these have been plotted as diamonds, crosses, squares, and triangles respectively. All values were obtained using the procedures outlined in section 2.3, which give a value for the contrast between the backscatter coefficient of the sample, and that for thick tungsten.

Sputter run 24, 19% Tungsten

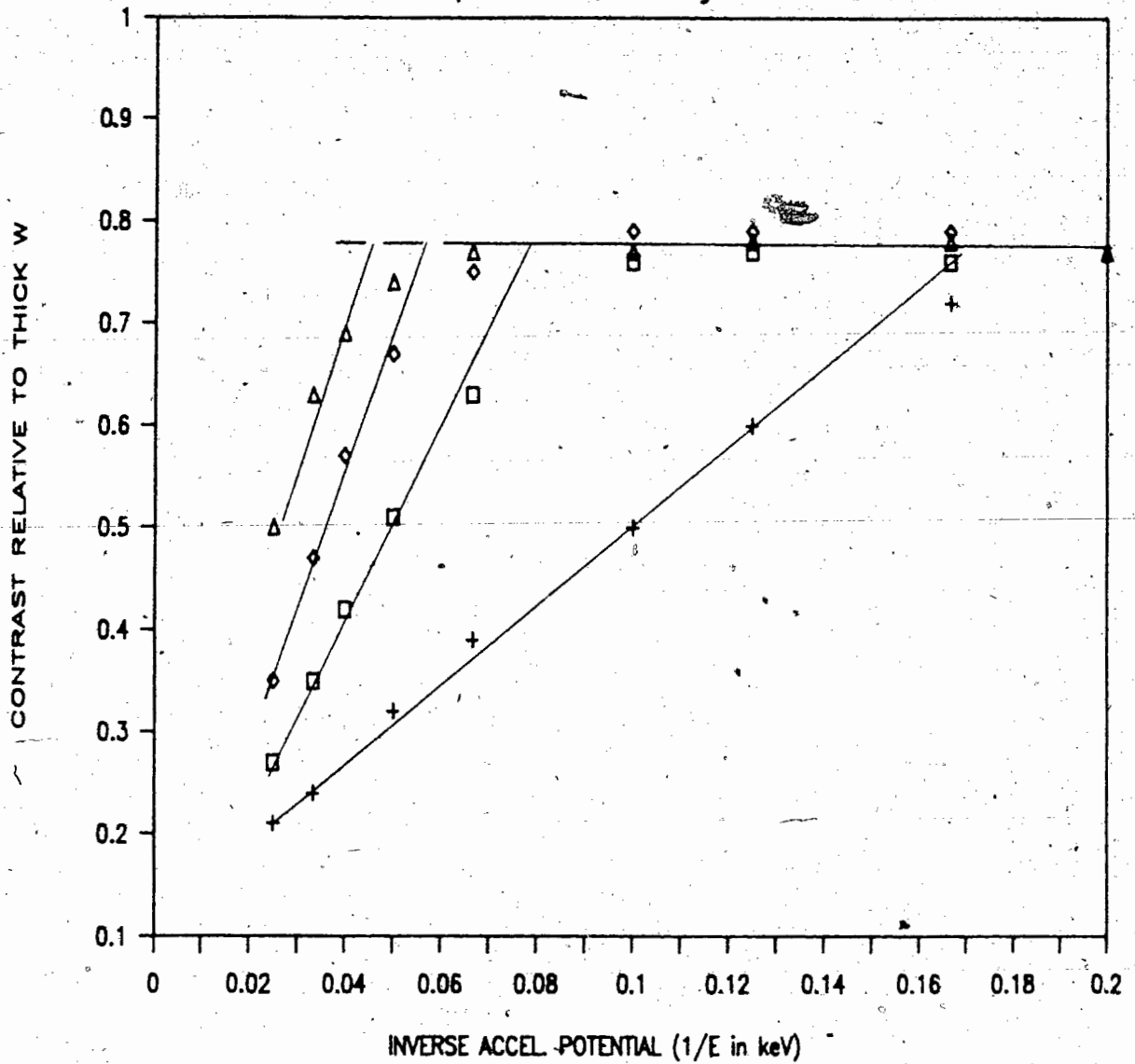


Figure 15. Experimental Contrast Results for Sputter Run 24. Sputter run 24 gave a ZAF composition analysis of approximately 19 atomic percent W, 81 atomic percent Cu. Sample thicknesses of .032, .095, .190, and .310 mg/cm² were deposited, and results from these have been plotted as crosses, squares, diamonds, and triangles respectively. All values were obtained using the procedures outlined in section 2.3, as in figure 14.

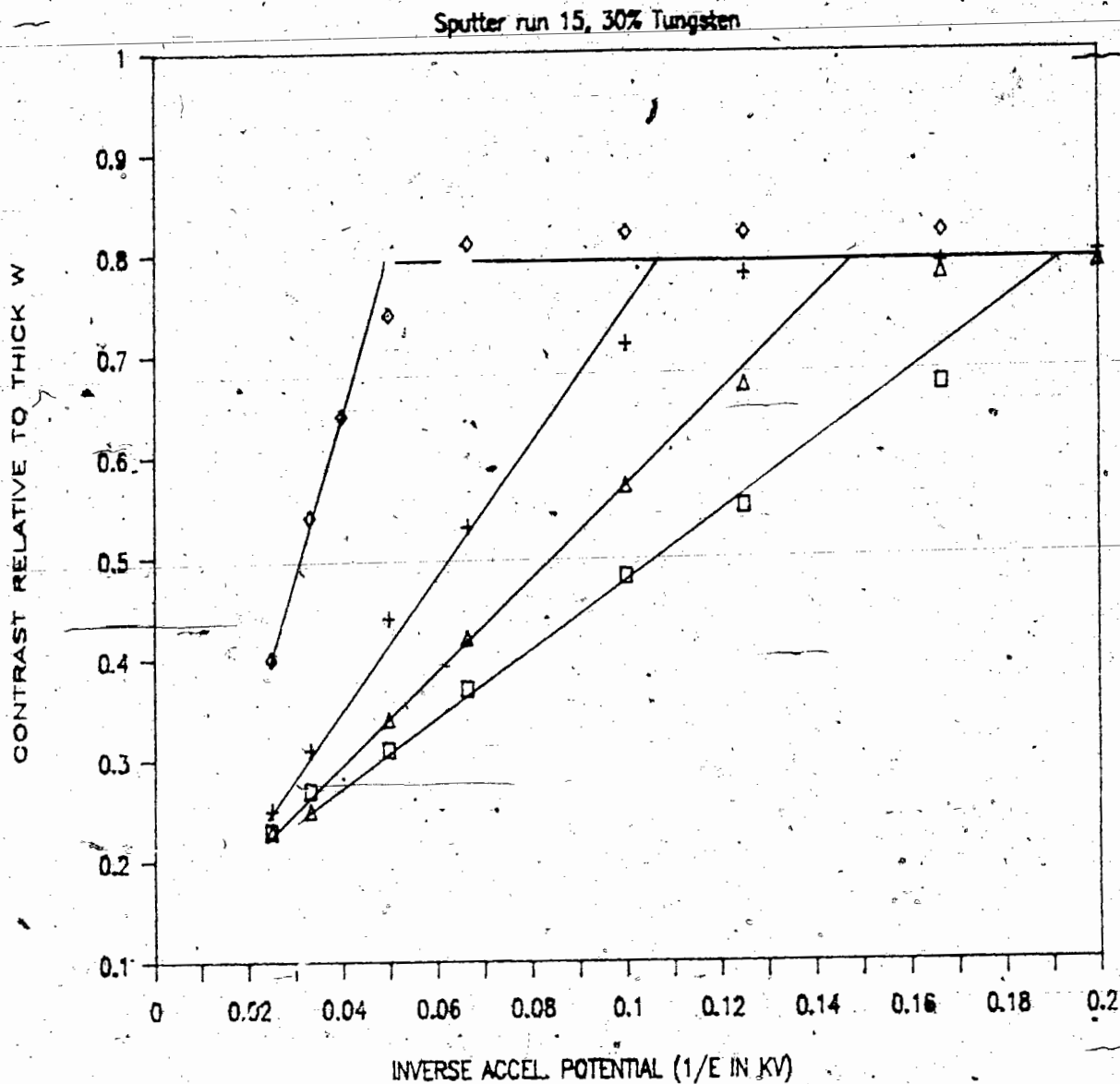


Figure 16. Experimental Contrast Results for Sputter Run 15. Sputter run 15 gave a ZAF composition analysis of approximately 30 atomic percent W, 70 atomic percent Cu. Sample thicknesses of .023, .070, .140, and .232 mg/cm² were deposited in this sputter run. Contrast results from these have been plotted as squares, triangles, crosses, and diamonds respectively. All values were obtained using the procedures outlined in section 2.3, as in figure 14.

Sputter run 22, 68% Tungsten

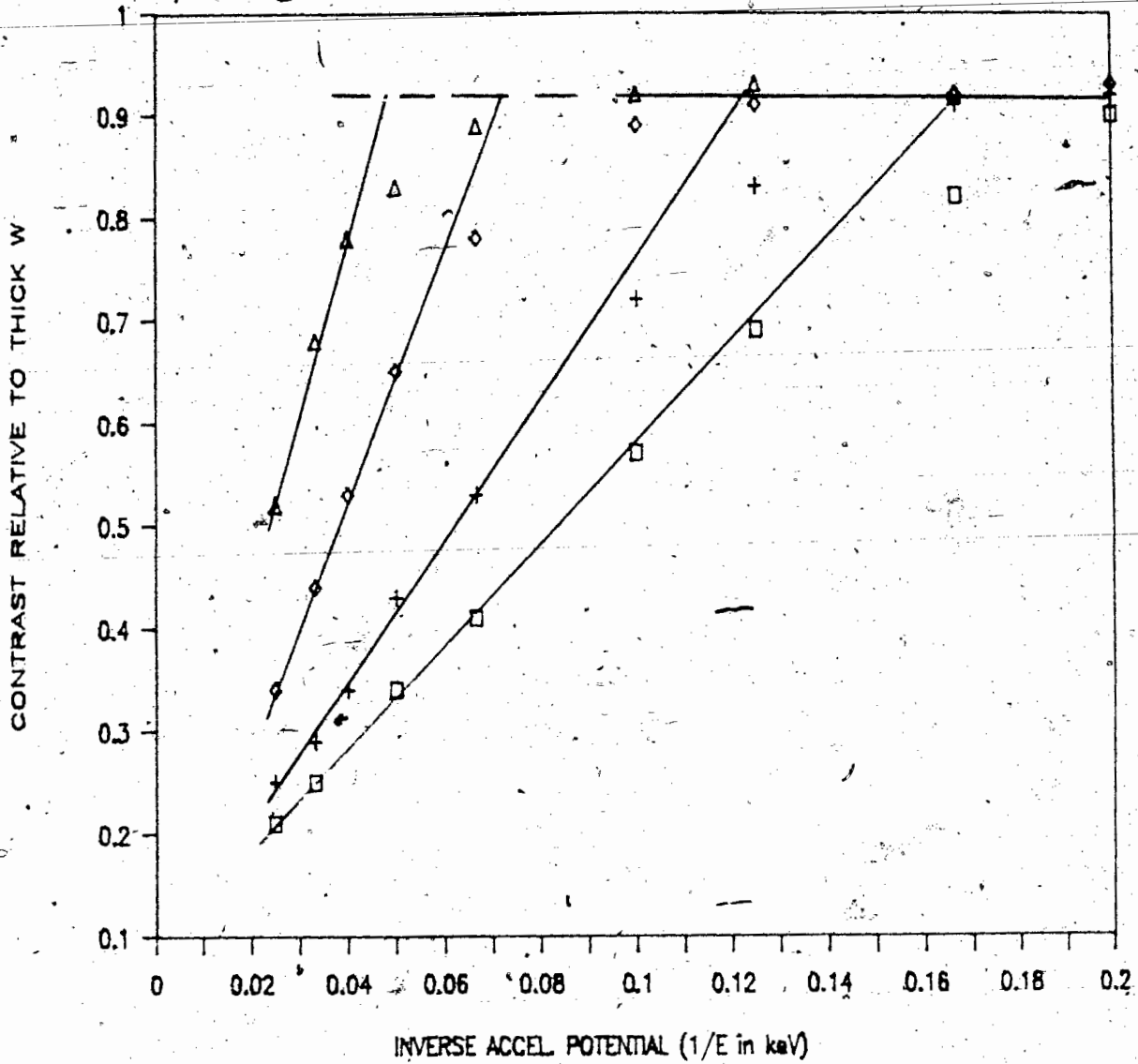


Figure 17: Experimental Contrast Results for Sputter Run 22. Sputter run 22 gave a ZAF composition analysis of approximately 68 atomic percent W, 32 atomic percent Cu. Sample thicknesses of .034, .068, .140, and .210 mg/cm² were deposited in this sputter run. Contrast results from these have been plotted as squares, crosses, diamonds, and triangles respectively. All values were obtained using the procedures outlined in section 2.3, as in figure 14.

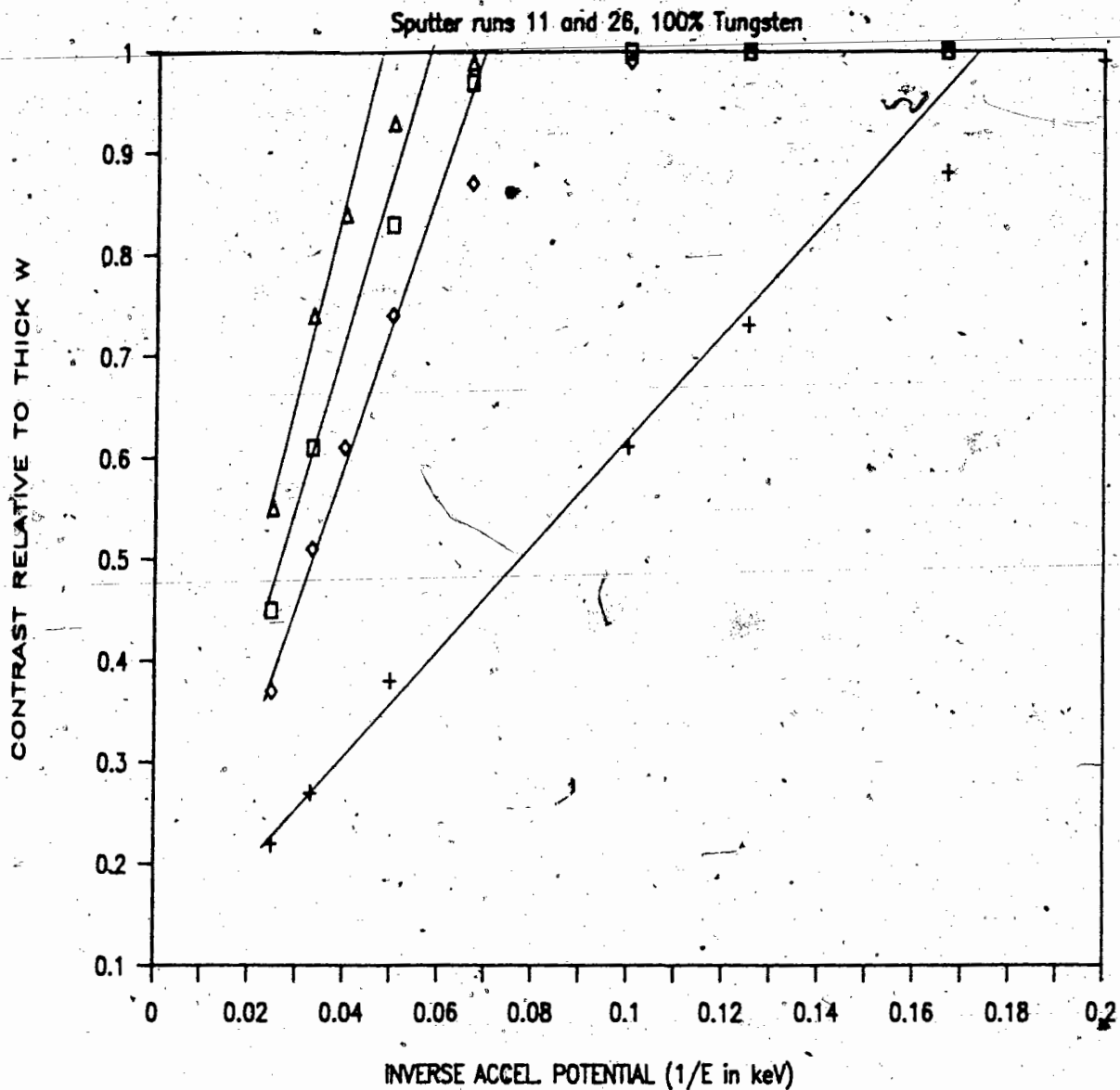


Figure 18. Experimental Contrast Results for Sputter Runs 11 and 26. Sputter runs 11 and 26 were both pure tungsten runs. Sample thicknesses of .026 and .170 mg/cm² were obtained from sputter run 26, and thicknesses of .220 and .280 mg/cm² were deposited in sputter run 11. Contrast results from these have been plotted as crosses and diamonds for the sputter run 26 samples, and as squares and triangles for sputter run 11 samples.

section of a given graph where the electron beam no longer penetrates the film and the 'linear region' in which the beam readily penetrates. Thus the information of film thickness can be separated from the information about composition in a natural way simply by dividing the plot into two portions and doing linear extrapolation on each. Methods for finding composition from the horizontal, low energy portion of the plot are discussed further below as are methods for thickness determination.

4.2.2 Comparison with Theoretical Results

The shapes of the curves in the Monte Carlo and analytical results show good agreement with experimental curves. However, in point by point comparison of theoretical results with the experimental results, small differences in the lower energy results and significant departures from experimental results at 30 and 40 keV are noticeable. Agreement is better for samples of compositions near tungsten as this is the internal standard for the experimental and theoretical results.

Two trends in the experimental data are not well modelled theoretically. The slopes of the inclined portions of the curves were different, leading to different intercepts of the sloped and horizontal sections of the results, and linearity of the graph of the backscatter contrast η_r versus inverse energy at higher energies was not modelled in the analytical results alone. In both of these trends the Monte Carlo simulation did better than the analytical model, but neither was sufficiently

accurate to be used in thickness determinations of unknown samples. The accuracies for composition determinations were better, as discussed in section 4.3.

4.2.3 Accuracy of Contrast Measurements

The overall accuracy of each measurement was dependent on a number of parameters, some of which have been outlined in section 2.4 already. These parameters can be divided into two groups, systematic errors, and random measurement uncertainties. Several sources of possible systematic error were investigated and these will be discussed in this section, while discussion of random uncertainties has been reserved for the next section. Possible causes of systematic error amenable to study included charging effects, sample non-homogeneity, surface texture effects, and surface contamination due to the electron beam. Errors arising from the microscope itself and other surface contaminants are also discussed but in more general terms due to their natures.

Charging of a sample under the electron beam occurs whenever the sample has electrical insulating properties or is not properly grounded. Charging can be either positive or negative (but is usually negative), and will change the backscattered electron intensity downward or upward accordingly. Charging can be detected directly in two ways, it has the effect of blurring any high magnification images in the SEM, and it can cause time dependent deflection of the electron beam, with the

result that the image on the screen appears to wander.

Charging was first noted in sputter run 6, which gave thin film backscatter values higher than those of pure tungsten. It was also found that the backscatter coefficient did not flatten out at low incident beam energies as it should, but had a rising value. This was thought to be due to the sample charging to a constant potential (say 1 kV) which only became apparent as it reached a significant proportion of the incident beam energy. As expected, the high magnification image showed charging effects as well.

Sputter run 6 was analysed to be pure tungsten, which does not charge, neither should tungsten with a thin layer of tungsten oxide on tungsten, so the most probable cause of the charging was partially oxidized tungsten mixed throughout the tungsten films. Suspicions that this was the cause were strengthened by the facts that tungsten ions are a strong getter for any residual oxygen in a vacuum system, and tungsten oxide forms smooth films of metallic appearance. Other sputter runs also showed charging effects, and at 5-6 keV incident energies, errors in η_r of 5-10% were noted. This error was the major source of inaccuracy in the determination of film composition from backscatter coefficients.

Sample inhomogeneity was discussed somewhat in section 2.2. Copper and tungsten are immiscible, thus separation of the

elements could occur in the metastable sputtered Cu-W alloys. The effects on η_r of the separation and migration of copper to the surface of the films was that η_r appeared to decrease as separation continued. Also, η_r decreased at low incident energies rather than flattening out as is the case for homogeneous samples. This was because a greater proportion of copper was near the surface and copper has a lower η_0 than tungsten. At lower beam energies the beam does not penetrate as far into the sample, thus the backscatter production volume will be closer to the surface, where the concentration of tungsten is lower, then the apparent average atomic number will be lower, resulting in a lower value for η_r . Structural changes were also expected to accompany component separation, thus a study was conducted to systematically determine sample inhomogeneity effects.

The heating of a sample can increase the rate of component separation dramatically. Heating occurs in varying amounts at the time of deposition depending on sputtering parameters. So to simulate this, two samples of sputter run 23, one with anomalously high η_r , the other with anomalously low η_r , of the same thickness were heated in a vacuum system with a partial pressure of argon at approximately 10 millitorr. Both samples had dramatic surface feature changes with very little heating, and the sample with anomalously high η_r now gave anomalously low η_r readings, while the other went observably lower.

Upon inspection at higher magnification (approximately 10,000 times) the surface of both samples had changed from smooth and continuous to being covered with fairly uniform circular spots of approximately .1 to .5 microns in radius. X-ray fluorescence analyses were done on some of the circular spots. Results of the analyses showed that the spots were quite obviously copper rich, while the remaining film in the background went from approximately 80% Cu to 50% Cu (the remainder being W, of course). This appears to be strong evidence for phase separation causing the anomalously low values of η_r .

Summarizing, sample inhomogeneity led to two effects:

i) the decrease of η_r as the incident beam energy decreased and
ii) structural changes visible at high magnification. Either or both of these effects could be used to test for component separation. In practice the constancy of η_r at low beam voltages was used to establish sample homogeneity for films over $40 \mu\text{g}/\text{cm}^2$ thick. For films thinner than this, high magnification observations were used to check that the structures associated with separation had not developed.

Surface roughness effects were investigated by preparing four extra samples in sputter run 8. Standard silicon substrates were roughened with 400 grit emery cloth and 80 grit sandpaper to give them a variety of surface textures. They were then coated in two thicknesses of W-Cu film, one each of approximately $70 \mu\text{g}/\text{cm}^2$ and $220 \mu\text{g}/\text{cm}^2$ thickness. Deposition

was done using the same sputtering parameters as for the smooth samples of sputter run 8.

As shown in table VI, surface roughness did not have a strong effect on η_r at normal incidence, while at high angles all rough samples were significantly brighter than smooth samples of equal thickness. All roughened samples responded with similar results. Samples were measured at 10, 20, and 30 keV with relative results almost equal in each case, so only the 20 keV results of the fine sanded substrate coated with a $70 \mu\text{g}/\text{cm}^2$ thick film are shown for the sake of clarity.

TABLE VI

Sample	Angle	Contrast
$93 \mu\text{g}/\text{cm}^2$ smooth	0 degrees	.7972
$93 \mu\text{g}/\text{cm}^2$ rough	0	.7941
smooth	75	.8788
rough	70	.9309

All values for roughened and smooth samples were equal within uncertainty for angles between 0 and 50 degrees (measured in 10 degree intervals). This is probably due to the wide solid angle of the Robinson detector which tends to 'flatten out', or minimize surface feature effects on the image obtained. This, along with the very good spatial resolution capable with this

thickness measurement method, makes it an excellent candidate for a rough film measuring technique. A more thorough survey of different surface textures (especially finer ones) needs to be done in this area, as discussed in section 5.2.

Effects of sample contamination by the electron beam were measured by allowing the beam to traverse the same line for an extended period to see if a change in backscatter contrast would be noted. Although a line of carbonaceous contamination became apparent under the secondary electron imaging mode after about 10 minutes, no change in the image was seen in BSE imaging mode even after an hour. A normal measuring process for a variety of energies typically took about 20 minutes, so this contamination was not expected to be a problem.

Other possible sources of systematic error could be samples not perpendicular to the beam or not coplanar, calibration of the accelerating voltage (or energy) of the electron beam, charging of the scintillation plastic if not grounded properly, and dirt or grease contamination of the samples. All of these errors are avoidable by using careful technique and well maintained equipment, but could contribute significant errors to the experimental results if not avoided.

4.2.4 Sources of Random Uncertainties

Sources of random uncertainties can be divided into basically two categories; screen or computer reading

uncertainty, and, random fluctuations or noise caused by accelerating voltage fluctuations, electron beam current fluctuations, and electronic noise inherent in the detector and amplifiers.

Uncertainties in 'on screen' readings come from parallax in lining up the ruler with the screen, the finite linewidth of the screen trace, and in the case of noisy (typical lower energy readings) signals, the determination of the average level by estimation. Computer readings are much less subject to these considerations, but the computer will average over an image with specks of dust or pinholes in the film which can lead to a small random uncertainty, especially in tilted or noisy images.

Fluctuations in voltage, current, intensity or brightness due to amplifier noise, photomultiplier signal and all the other noise and interference can be expected in a system of this complexity and power output. However, the modern SEM is designed to minimize such fluctuations. Statistical noise can not be avoided is a major portion of the reading uncertainties of both image analysis techniques mentioned earlier, so constitutes the largest source of random uncertainty.

Total uncertainties in these two methods have been estimated by repeated measurements of the same samples on different days. Signal noise was a function of the incident beam accelerating potential so estimates ranged for 'on screen

measurements' from ± 0.01 (where contrast is normalized to a zero to one scale) at 40 kV to ± 0.03 at 5 kV. Similarly for computer aided measurements the range was from 0.002 to 0.005.

4.3 Composition Determination

4.3.1 Composition Determination Method

The horizontal contrast levels to which the low energy values have been extrapolated to in figures 14 to 18 have been plotted in figure 19 as a function of composition. Also plotted are analytical results from the Niedrig equation and the Monte Carlo simulation results, both using the simple average atomic number as outlined in equations 4a and 4b on page 51. The correspondence between all three is good except for the copper value of η_r for which there is a .03 to .07 difference. This difference is significant, so for best accuracy a calibration curve of backscatter versus atomic number Z is necessary.

Excellent agreement with experimental results was obtained using an empirical relation derived for pure elements by Herrmann and Reimer [23] and using the rms values for Z_{off} for alloys. This agreement is demonstrated in table VII;

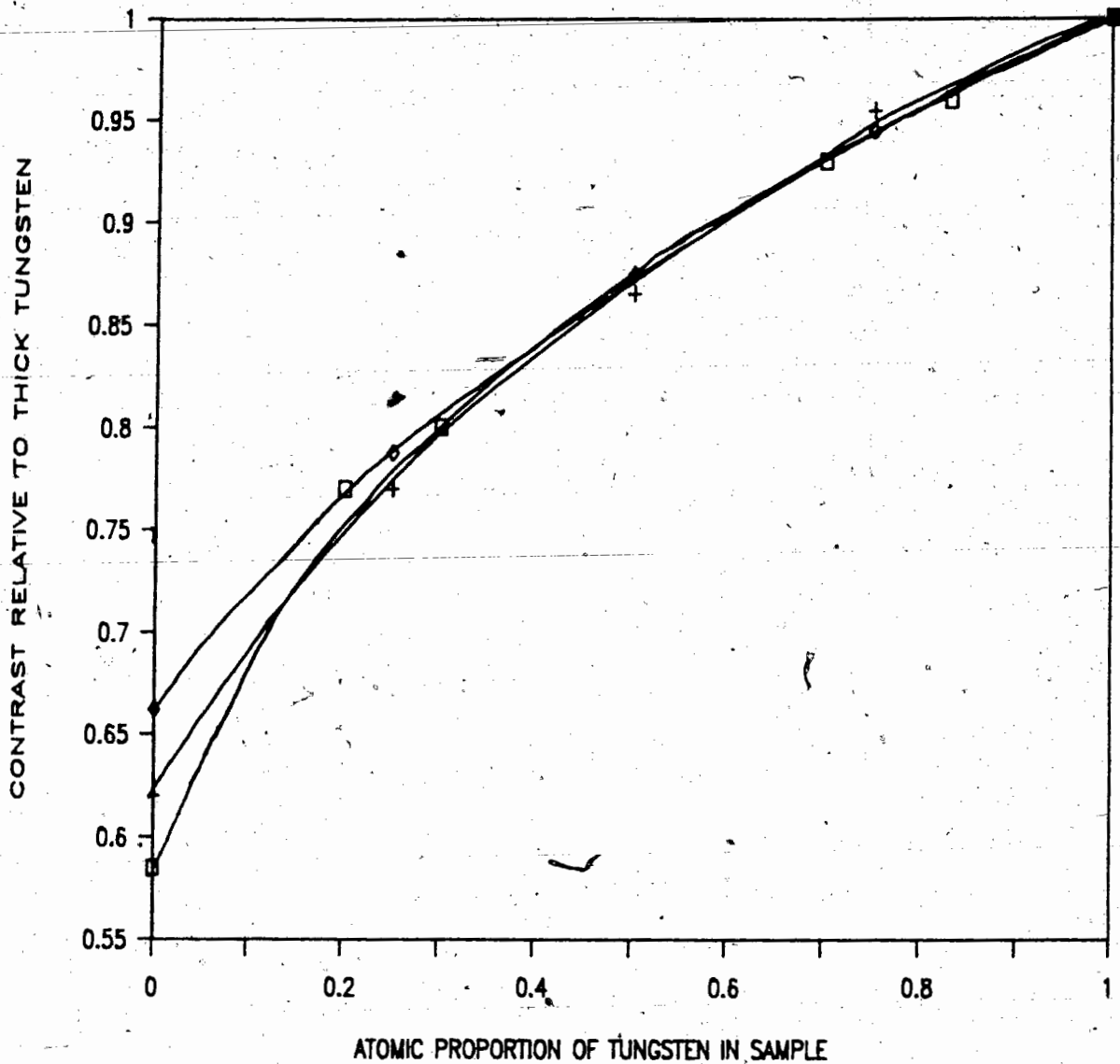


Figure 19. Calibration Curve for Compositions. The extrapolated horizontal segments of the experimental curves in figures 14-18 have been plotted as a function of composition using the square symbols. Similar results from the analytical model and Monte Carlo simulation graphs of figures 5-9 have been plotted as diamonds and crosses. Compositions for the theoretical results were obtained from the simple averages of atomic numbers used in these calculations.

TABLE VII

Percent Tungsten	Experimental value of η	Herrmann and Reimer model
0.0%	.59 ± .01	.594
18.6 ± .5%	.77	.757
28.0	.80	.810
68.4	.93	.944
100.0	1.0	1.000

The agreement of Herrmann and Reimer's model with experimental data was felt due to its more accurate modelling of the high η_b range, especially the value for tungsten. This agreement gives a simple and well established method for determining the average atomic number of any sample being measured, and hence a composition in the case of a binary alloy whose two constituents are known. Further possible applications include compounds and mixtures of stoichiometric compounds such as minerals, provided the effects of charging of the samples can be avoided.

4.3.2 Accuracy of Composition Determinations

The accuracy of this method for the determination of composition is mainly controlled by the accuracy of the determination of η_r for the material being measured. However, for highly accurate measurements on clean, homogeneous, conducting films the accuracy is also affected by the choice of calibration curve (e.g. using Herrmann and Reimers' or one derived for a specific measuring apparatus) and by the accelerating voltage used to make the measurement.

Some variations were noted in the level of η , extrapolated for the members of a single sputtering run. These appear to arise from variations in the composition of the samples themselves. Though sputtering in general gives consistent compositions, several possible causes for a 2%-3% variation in a given sputter run have already been discussed in section 2.3. These variations of composition could not usually be tested explicitly due to the difficulties in quantitative x-ray analyses of thin supported films noted earlier. However, qualitatively the x-ray analyses follow the trends of composition variation displayed by the backscattered electron method and do show its sensitivity to composition variation. The variations encountered fall mostly into the cumulative uncertainties in the experiment, however, so it was not felt important to pursue this further or draw any conclusions from it.

The fact that Herrmann and Reimer's empirical curve fit the data of this experiment within uncertainties does not mean that it will fit data taken with other detectors under other conditions. The scatter in published results over the last 30 years proves this. Thus a calibration curve measured using the experimental apparatus is the most accurate. The agreement with empirical and theoretical curves does indicate that a single calibration curve will be reasonably accurate for all binary alloys.

Finally, this composition determination method is dependent on the fact that relative backscatter coefficients for different materials are relatively constant over the range of accelerating potentials used. Though these coefficients have been shown to vary only slowly with energy, there is some variation. The variation was noticeable in measurements of bulk silicon η , versus energy as shown in figure 20. Fortunately, materials of $Z \geq 30$ all vary in a similar manner, so in a comparative experiment like this the effect goes unnoticed. However, for experimental systems of lower Z , a systematic correction factor would need to be introduced. These correction factors could be derived quite simply using bulk pure element samples, as is discussed further in section 5.2.

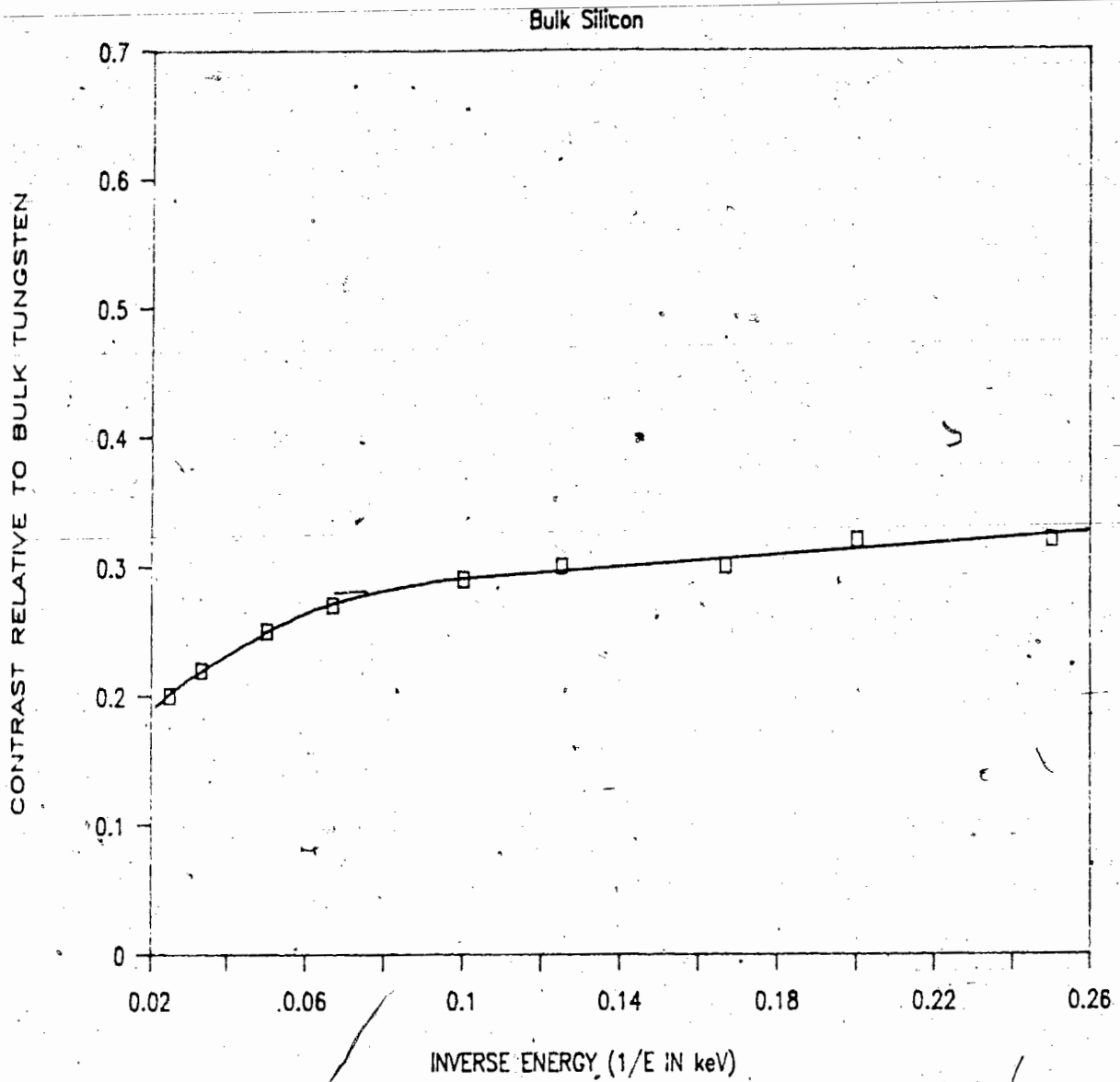


Figure 20. Experimental Contrast Results for Bulk Silicon. The results in this figure were taken using an uncoated silicon substrate for a sample. Measurements and the plotting of the results were done in the same manner as for figures 14-18.

4.4 BSE Contrast Thickness Determination

4.4.1 Intercept Method

Of utmost importance to the usefulness of this thickness determination method is the applicability of the calibration curve derived here to experimental systems of other elements. As backscattering of electrons is mainly dependent upon the incident electron's interaction with charges in the target, the backscatter coefficients should be a function of 'charge thickness' for all materials rather than mass thickness. Charge thickness can be found from mass thickness according to;

$$T_{ch} = T_M \times Z_{eff} N_a / A_{eff} \quad (7)$$

where Z_{eff} and A_{eff} are the effective atomic number and atomic mass as defined in equations 4a and 4b on page 51. N_a is Avogadro's number, which can be excluded if T_{ch} is to be given in moles of electrons rather than in absolute numbers.

In figures 14-18, an inclined straight line for each thickness of sample intersects the horizontal 'low energy' line at a particular value $1/E_i$, where E_i will be called the intercept energy. When E_i is plotted as a function of charge thickness as in figure 21 it is found that all results follow a single curve within uncertainty. The curve on the log-log graph is almost a straight line, and can be approximated by one for quick thickness estimates. The slope is approximately 1.6,

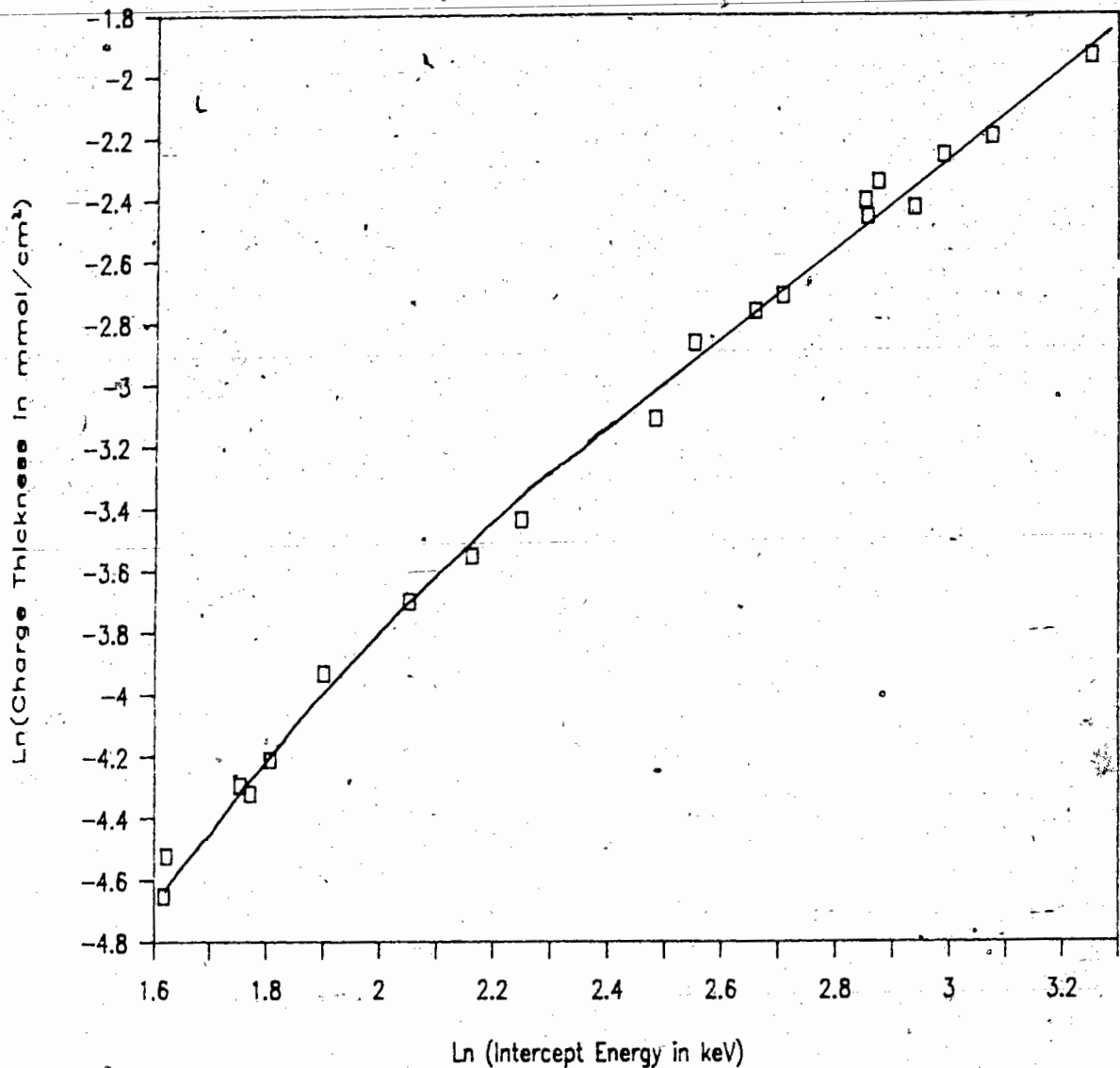


Figure 21. Experimental Thickness Calibration Curve. The data for this curve was taken from the extrapolated intercept energies E_i of figures 14-18 for all of the samples. These were plotted against the samples' charge thicknesses. The scatter of the points falls within the uncertainties in the thickness and no significant differences between different sputter run results were noted.

giving a relationship for the charge thickness T_{ch} of;

$$T_{ch} = \alpha E_i^{1.6} \quad (8)$$

where α is a proportionality constant equal to $7.6 \times 10^{-4} \pm .5 \times 10^{-4}$ if E_i is in keV and T_{ch} is in moles/cm².

The thickness of a given sample can thus be obtained by determining its value of E_i and interpolating its charge thickness from the graph in figure 21, or the straight line approximation to that graph. This thickness determination method is dependent on the observation that E_i is independent of the composition of a sample for a given charge thickness. This observation can be explained by the fact that E_i is a measure of the incident beam energy at which a significant number of electrons penetrate the film and travel into the substrate. The electrons most likely to penetrate the film are those which have undergone small angle, inelastic scattering events with atomic electrons rather than elastic collisions with the nuclei of the sample. Thus the composition of the nuclei has little effect on E_i , while the charge thickness (which refers to the thickness of atomic electrons passed through) is the relevant parameter.

To convert a derived charge thickness to mass thickness, most authors approximate the Z/A ratio as 1/2, however there is a 12% difference between the Z/A ratio of copper and tungsten. Because of the logarithmic nature of the graphs, corrections of

this magnitude appear smaller than they are, though for a sample whose Z/A ratio is not well known, an intermediate value based on the simple compositional analysis of section 4.3 should lead to errors of less than 2%.

4.4.2 Accuracy of This Method

Thus from these straight line approximation to the charge thickness log-log curve the thickness of films can be determined, probably to a relative accuracy of $\pm 10\%$ typically, without the need for further calculations or thin film standards. Extrapolating charge thicknesses directly from the graph in figure 21 can be much more accurate, giving an accuracy of under $\pm 3\%$ or $\pm 1 \mu\text{g}/\text{cm}^2$ for films of $40 \mu\text{g}/\text{cm}^2$ thickness.

Extreme care must be taken in the graphical determination of the intercept energy E_i , as the sloped portion of the results is not truly straight. Consistent results were obtained in this experiment by taking the four experimental points of the highest energy for each sample and interpolating. Interpolation of the resulting value of E_i on the charge thickness calibration curve must also be done with great care, as relative errors in E_i are increased by the 1:6 exponential factor.

The intercept method of thickness determination is extremely sensitive to differences in thickness between samples of the same composition. A difference in thickness of less than 1% was detected in sputter run 25 for two thin films of the same.

composition though this difference was within the measuring uncertainty of the weighing thickness determinations.

4.5 Applicability of the Method

An important and underlying consideration in any method developed for determining thicknesses is its inherent practicality and ease of use. Monte Carlo calculations so far do show that the method developed here may be transferrable to other systems of elements under certain restrictions in their atomic number combinations.

An implicit assumption in the thickness determination portion of the method is that the substrate atomic number is either lower than or higher than both atomic numbers of the constituents of the deposited film. If its atomic number were to be between, slope determinations for films of average atomic number near that of the substrates would be very inaccurate. If the film and substrate had the same effective atomic number, the film would appear to have zero thickness, independent of its actual thickness.

With regard to the use of contrast to determine composition it is evident from figure 19 that the two components of the film must have reasonably different Z values. When the difference is large the slope of the curve is correspondingly large and hence it is possible to determine the composition with reasonable

accuracy. If thickness alone is being measured the composition does not play an important role because it only affects the interpolated value of Z/A used to convert charge thickness to mass thickness.

In spite of the limitations discussed above this method for measuring thickness and composition is applicable to a wide range of systems and is at least as rapid as other methods with similar capabilities. The time taken for an average thickness measurement was about 30 minutes including pump down of the SEM and full computer data acquisition (on screen data acquisition was considerably quicker, shaving 10-15 minutes off this time). Graphical data analysis was also estimated to take 30 minutes at the outside, and this is considerably better than x-ray fluorescence methods, most of which rely on hours of Monte Carlo simulations (which need to be run overnight in batch jobs at our facility).

The necessary equipment and standards for the practical employ of this method include an SEM with BSE detector and provision for linescan mode, a sample holder capable of holding the sample and reference coplanar to one another and normal to the beam. Standard reference materials are simply pure metal foils (preferably well polished) with atomic numbers near the atomic number of the lowest or highest of those in the binary alloy to be measured. While this latter constraint is not strictly necessary it will improve accuracy somewhat and is

simple to achieve in practice. Computer processing of the image and or data is optional, but desirable because it increases accuracy, as noted earlier in the section on random uncertainty 4.3.

5 CONCLUSIONS

5.1 Summary of the Experiment

A method for determining thin film thickness has been developed from the Curzon-Rajora method and has been tested on binary alloys of copper-tungsten on silicon substrates. Calibration curves were derived to enable the composition and thickness of an unknown sample to be determined. Theoretical calculations done by a Monte Carlo method indicate that these calibration curves would be useful for any samples of elemental compositions with atomic numbers between 29 and 74 (those of copper and tungsten) and that the method should be expandable to include samples of all atomic numbers.

Composition can be determined to between 3% and 6% depending on the slope of the curve of contrast versus composition in the region of actual sample. Similarly, the total uncertainty in thickness determination is between 3% and 10%, depending both on the thickness and analysis method chosen. The accuracy of the thickness determination was only weakly related to the accuracy of the composition determination, such that an error of 10% in composition would lead to an error of less than 1% in mass thickness.

Applicability of the new method has been shown to be much wider than the copper-tungsten system studied in this

experiment. Constraints on the applicability of the method include;

- 1) that the substrate atomic number is either lower than or higher than both atomic numbers of the constituents of the deposited film,
- 2) that the substrate or film may not charge significantly under the electron beam,
- 3) that the films be between 40 and 300 $\mu\text{g}/\text{cm}^2$ thick (for an SEM of 40 kV maximum accelerating potential).

The method shows promise of overcoming some of these limitations, as discussed in the next section.

Practicality and ease of use of the new method have been shown to be better or equivalent to other nondestructive post-deposition method, requiring under an hour per measurement for an experienced operator. All equipment and standards needed are commercially available and are becoming more readily available as the SEM becomes a more popular research and analytical tool.

5.2 Topics for Further Work

Many topics for further work have been discovered in doing this experiment. Some of these, such as the variation in backscatter coefficient with incident angle and collection angle, have fundamental scientific interest. Others, such as improvements in theoretical models have mixed scientific and practical applications, while efforts to increase the electron

beam intensity and studies to expand the applicability of this method have mainly practical interest only. Each topic mentioned elsewhere in this thesis is discussed briefly in sections 5.2.1 to 5.2.6.

5.2.1 Variation of Incident Beam and Detector Angles

As mentioned in the introduction, work in both of these topics has been done before, with results of fundamental scientific interest. It is of fundamental interest to see how η_r varies with energy at an 'off normal' incident beam angle for bulk and thin film samples, or to measure how the distribution of backscattered electrons varies with incident energy. Evidence collected so far in this experiment indicates that η_r varies slowly as a function of both of these parameters, so careful measurements would need to be made to be of fundamental interest.

5.2.2 Improvements in Theoretical Models

The analytical model discussed in section 3.1 showed qualitative agreement with experimental data but deviated from that data and the Monte Carlo simulations in both linearity of the graphs and invariance of intercept energy E_i with composition for a given charge thickness. These shortcomings preclude its use as a model for this thickness determination method.

The assumptions made in the model were very simple and designed to enhance its agreement with experimental bulk data

for η_b as published in the literature. Changing some of these assumptions (such as the energy dependence on the electron range in the sample) could improve the model to the point where its quantitative results agree to within uncertainty of experimental results. An effort was made in the theory to stay away from an empirical formulation, but removing this restriction for practical purposes should also yield more accurate results.

5.2.3 Increasing Signal Current

Noise is especially apparent in the low signal-high amplification situations of low beam energy. Dramatic improvements can be obtained by withdrawing the final aperture from the objective polepiece of the SEM. This allows many more electrons through, but the resulting loss in resolution due to the broadening of the beam spot made focussing difficult and any high resolution work (e.g. checking for charging effects in the sample, as in section 4.3) impossible.

Further investigation into the effects of using a defocussed beam on measured values of η are needed to ensure that this method yields similar values as any charging effects are magnified by the increased current. The computer accumulation of data gives the option of counting data extremely slowly. This may also improve the signal to noise ratio but needs to be studied for beam contamination effects.

5.2.4 Measurement of Very Thin Films

Sheng et al. [52] have shown that the Curzon-Rajora thickness method can determine the thickness of very thin films (from 0 to 40 $\mu\text{g}/\text{cm}^2$) very accurately using calibration curves. Because these films are too thin to determine the energy intercept E_i , calibration curves would also be needed for the method of this thesis.

Such calibration curves could use a slope-point determination, as the slope and a single point (preferably near the 5 keV region) would uniquely identify the composition and thickness of a film. This can be seen by referring to the Monte Carlo results in figs. 5-9. For a given thickness, (say 28 $\mu\text{g}/\text{cm}^2$) the slope of the data increases slowly and monotonically with increasing tungsten concentration. Also the value of η_r at 5 keV increases dramatically with increasing tungsten concentration. So the combination of these two values should yield a unique composition and thickness value.

5.2.5 Thickness Determination for Rough Films

As discussed in section 4.2, the measurements of η_r were quite insensitive to surface textures in the films or substrates. A quantitative survey of the effects of different textures and roughnesses could provide the necessary correction factors to give good accuracy for rough film thickness measurement. The meaning of thickness is less well defined on rough substrates and this too would require further investigation.

The systematic nature of roughness effects at high angles could be minimized by having the reference substrate or material of similar roughness as the film to be measured, but a decrease in accuracy is felt to be inevitable in extremely rough films as the overall thickness is no longer so clearly defined, and neither is the incident angle of the electron beam (especially if the backscatter production volume is of similar dimensions as the texture of film and substrate).

5.2.6 Measurement of Films of Arbitrary Composition

The charge thickness determination technique presented in this thesis has proven to be independent of composition for the materials tested. With more experimental data the method could prove to be independent of composition for films of arbitrary number of components. The Z/A conversion factor to change charge thickness into mass thickness could be graphically interpolated from the periodic table but experiments need to be done to examine the amount of error introduced. Thus this method shows promise of being much more widely applicable than has been explored by this experiment.

APPENDIX A

This appendix describes the image processing done using the EE&G Ortec EEDS II computer and its associated hardware and software. The EEDS II system is run by a Digital Systems Corp. PDP 11 computer running the RT 11 system software. EE&G have provided a programming language derived from BASIC incorporating commands and features specific to the EEDS II hardware configuration. The authors of this programming language added several image processing commands and deleted the more structured control statements of BASIC, naming the resulting language ORACL.

An image processing program called LSCANR was written using ORACL to compare the signal level of two segments of a linescan image which had been previously stored in the computer (using the method described in section 2.2 of this thesis). The predefined functions and subroutines in ORACL were each stored separately on the 8 inch floppy program disk so only the necessary ones were called to reside in the computer's software memory, as shown in lines 60-110 of the program.

Each linescan image is held in two consecutive of the eight 1024 channel memories which have been given the addresses A through H. In lines 160 to 240 the program interacts with the operator to obtain the addresses of the linescan image and background image (an image of counts obtained when the electron

beam is turned off) which are given as double letters, eg. the default values BC and DE. The SELMEM function in line 210 selects (for the program) which of the firmware memories subsequent functions in the program are to act upon, returning an error message in variables ER and J if incorrect addresses are input.

The program has an option to set the portions of the line-scan whose levels are to be compared (or ROI's, standing for Regions Of Interest) automatically or to allow an image to have its ROI's set manually. Manual setting of ROI's is usually done when the image is complicated by scratches or unusual geometries which the automatic ROI's do not cover properly. The EEDS II system has been designed for straightforward manual setting of ROI's whenever an image is being accumulated or accessed. The computer's automatic graph generation routine provides a cursor superimposed on the image which can be positioned by the joystick built into the EEDS II. Using this cursor and special function keys for ROI setting, any region of an image can be marked as an ROI in any of 14 colours labelled from A to N.

The program has been set up to search for one ROI marked line segment (usually the one on the left) in colour A (red) and the second line segment in colour B (green). This search is done by the GETROI function in lines 240 and 280. GETROI returns the channel numbers of the left and right extremes of the ROI, and returns zero values if an ROI in the colour

searched for is not found. If not found, the program transfers control to the error handling section of the program.

If the program sets the ROI's automatically, it marks them on the image using the SETROI command in lines 631 to 650. The modified image is then displayed using the GODSP command. GODSP runs the computer's automatic graph generation routine to display the memory selected by the DSPMEM command. To get back to the interactive terminal mode of the computer once it is in display mode, the "Terminal" special function key is pressed (as suggested by the program in line 632).

In either automatic or manual modes, the program then sums the values (which represent signal strength and hence proportion of backscattered electrons from the sample) from the whole ROI using the SUMMEM command. When divided by the number of channels summed over, the result gives an average value of the relative intensity of backscattered electrons detected for the portion of the linescan covered by the ROI. However, this division was not done as all operations could be carried out using the sums and using sums gave better precision (smaller round off error) in the computer.

The program presents the operator with the option to correct for slope in manual mode but slope is corrected for automatically in automatic mode. In both modes the procedure for slope correction is the same. Small ROI's are set up on

either side of the red and green ROI's. Colour M ROI's (medium blue) bracket the red ROI and colour N (black) is used for the other. Each of these smaller ROI's (they are typically 10 to 20 channels wide) are summed over and divided by their number of channels to obtain the average number of counts in the middle of the ROI. A slope is calculated from each of the blue and black ROI's by taking the difference in the height of the right hand ROI from the left, and dividing by the difference of their centre channels. In the automatic mode this is quite simple as the channel numbers are all preset. Once the two slopes are calculated, they are printed out by line 370.

Generally it was found that the two slopes were approximately equal, indicating that the effect was in fact one slope affecting the entire image. To correct for this single slope the number of counts under each ROI due to the slope was calculated by a simple geometrical formula. To derive this formula, the inherent slope of the image is given to an imaginary line through the origin (taken to mean zero counts in channel zero in this case) of the image, as shown in figure A1. The equation of the line is then;

$$f(x) = m x \quad (A1)$$

Where m is the slope and x is the channel number. The number of counts contributed to each ROI can then be calculated by integrating the area under this line between the minimum and maximum channel numbers of each ROI.

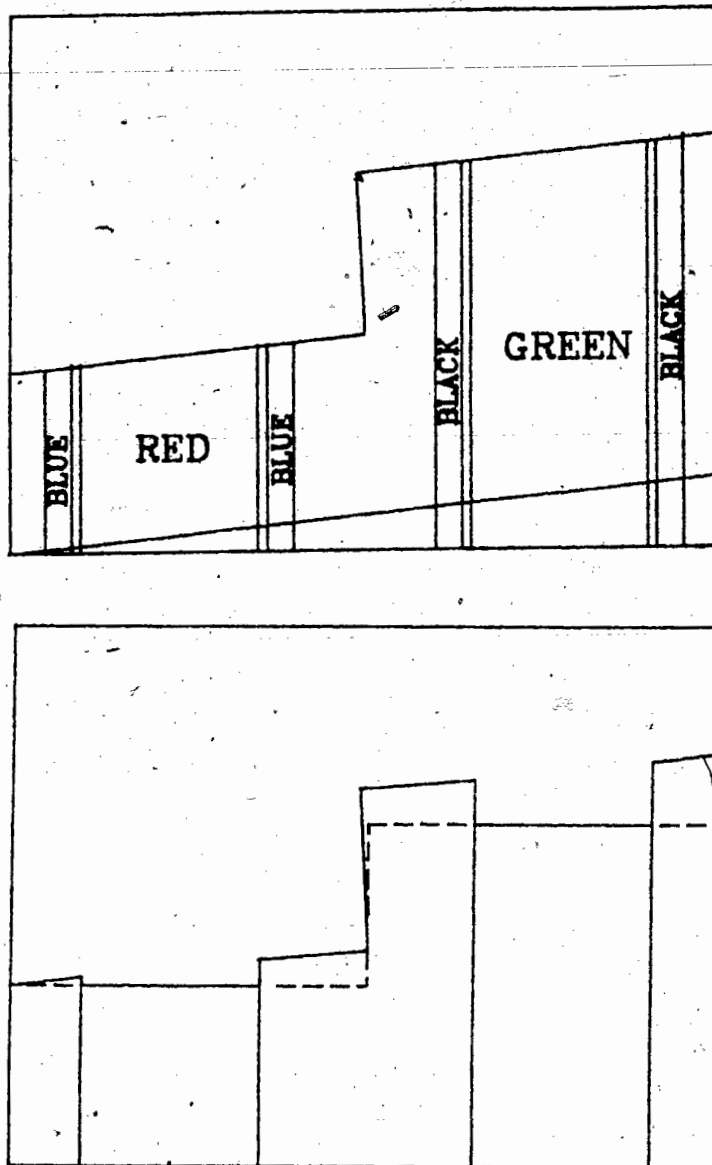


Figure A1. Computer Correction of Slopes in Linescan Images. The upper drawing shows a typical linescan image as recorded by the computer, (with exaggerated slope for clarity). The regions used for calculating a correction for the intrinsic slope (shown here at the bottom of the image) are super-imposed by the computer in the blue and black colours. The lower drawing shows the result of the corrections on the two areas, red and green, which are to be compared for a contrast measurement. The dashed line shows what the image would look like without slope.

$$\text{Area} = \int_{\text{min}}^{\text{max}} m \times dx \quad (\text{A2a})$$

$$\text{Area} = \frac{m}{2} ((\text{max})^2 - (\text{min})^2) \quad (\text{A2b})$$

where 'min' and 'max' are the minimum and maximum channel numbers of a given ROI. When these areas are subtracted off of the image the remainder appears flat, as shown in figure A1.

The final correction to the image needed is the subtraction of the background level of counts. The background count level was found by taking an additional image of the number of counts obtained when the electron beam was turned off. Background images were found to be very flat and of a level adjustable by adjusting the amplifier settings of the detector, so were attributed to electronic DC level offset. Corrections are done simply by subtracting the relevant areas of the background image, defined by the min and max channel numbers of the ROI's, from the image being processed. This correction is done in lines 400 to 480 of the program using the same image processing functions described previously.

The computer finally divides the sums from the two corrected ROI's (red and green) and prints out the ratio, the

desired result and its inverse for convenience. Experience showed that the contrast uncorrected for slope effects was also of interest for comparison, so this is also printed out. There is a final option for another run or the program transfers control to the main menu of the computer in lines 530 to 545.

The main menu of the program disk was modified to include running LSCANR as an option. The resulting program package was designed to be operated by a non-expert, with appropriate prompts and several options for image processing available automatically. This increases the time needed to run the program to over a minute, but the increased flexibility and ease of use saved many hours of time re-measuring samples.

```
10 !PROGRAM TO TAKE ROIS OF
20 !A LINESCAN IMAGE, SUB.
30 !BACKGROUND AND INTEGRATE
40 !TO DETERMINE CONTRAST
50 !
51 INTEGER TRUSUM, CHANS, TRU2, CHANS2
55 INTEGER SUM1, SUM2, B, SUMB, SUMB2
60 CALL SETROI
64 CALL GODSP
66 CALL DSPMEM
70 CALL SELMEM
74 INTEGER ER, ERR, ERRR, ERRRR
76 INTEGER AR, ARR, ARRR, ARRRR, RAR
80 INTEGER MIN, MAX, MIN2, MAX2
90 CALL GETROI
100 INTEGER I, J, K, L, M, N, O, P, Q
102 STRING BAC(3), MEM(3), MEM2(3)
104 STRING DAT(3), TILT(3), ANOT(3)
110 CALL SUMMEM
130 INTEGER C, D, E, F, G, H
144 INTEGER X1, X2, X3, X4, X5, X6, X7, X8
150 !
152 ! PROGRAM ASKS FOR DATA LOCATIONS IN MEMORY
160 !
165 DAT="BC "
170 ASK "MEMORY LOCATION OF DATA IMAGE? ", DAT
180 BAC="DE "
190 ASK "LOCATION OF BACKGROUND IMAGE? ", BAC
200 !
204 ! NOW SELECT THE SOFTWARE MEMORY FOR MANIPULATION
205 ! BY THE SELMEM FN.
206 !
210 J=SELMEM(DAT, ER)
211 IF (J).EQ.(-1) GOTO 605
212 ASK !, !, "SET ROI'S AUTOMATICALLY?", TILT
214 IF (TILT).EQ.("Y"); GOTO 632
220 !
230 ! NOW GET CHAN. NOS. FOR THE REGIONS OF INTEREST (ROI'S)
235 ! WITH REGIONS A & B (RED AND GREEN) ON LEFT & RIGHT RESPECT.
240 K=GETROI(1, 1, 1, MIN, MAX, ERR)
242 IF (MAX).EQ.(0) GOTO 625
244 !
250 SUM1=SUMMEM(MIN, MAX)
270 IF (SUM1).EQ.(-1); GOTO 955
280 L=GETROI(2048, -1, 2, MIN2, MAX2, ERRR)
290 SUM2=SUMMEM(MIN2, MAX2)
294 !
296 ! FINDING ROI'S M AND N FOR SLOPE CORRECTION
300 !
301 COR1=0
302 COR2=0
304 ASK !, "SLOPE CORRECTION? (Y)", MEM2
306 IF (MEM2).EQ.("N"); GOTO 400
```



```
310 M=GETROI(1,1,13,X1,X2,ERRR)
320 AVG1=SUMMEM(X1,X2)/(X2-X1+1)
330 O=GETROI(X2+1,1,13,X3,X4,ERRR)
334 AVG2=SUMMEM(X3,X4)/(X4-X3+1)
336 !
340 SLOPE1=(AVG2-AVG1)/((X3+(X4-X3)/2)-(X1+(X2-X1)/2))
344 !
350 F=GETROI(2048,-1,14,X7,X8,ERRR)
355 AVG4=SUMMEM(X7,X8)/(X8-X7+1)
360 Q=GETROI(1,1,14,X5,X6,ERRR)
365 AVG3=SUMMEM(X5,X6)/(X6-X5+1)
368 SLOPE2=(AVG4-AVG3)/((X7+(X8-X7)/2)-(X5+(X6-X5)/2))
370 TYPE !,"SLOPES 1 AND 2 CALCULATED TO BE:",SLOPE1,SLOPE2
372 SLP AVG=(SLOPE1+SLOPE2)/2
374 ! SLOPE CORRECTION -----
375 MIN=MIN-1
377 MIN2=MIN2-1
380 COR1=SLP AVG*(MAX*MAX-MIN*MIN)/2
385 COR2=SLP AVG*(MAX2*MAX2-MIN2*MIN2)/2
390 MIN=MIN+1
395 MIN2=MIN2+1
397 ! BACKGROUND CORRECTION !-----
400 N=SELMEM(BAC,ARR)
410 SUMB=SUMMEM(MIN,MAX)
420 !
430 SUMB2=SUMMEM(MIN2,MAX2)
450 !
460 ! SUBTRACT BACKGROUNDS AND TAKE RATIO, FINAL PRINTOUT ----
470 !-----
472 CHANS=MAX-MIN+1
474 CHANS2=MAX2-MIN2+1
476 SIZFAC=CHANS2/CHANS
480 SUM1=SUM1-SUMB
484 SUM2=SUM2-SUMB
486 UNCOR=SIZFAC*SUM1/SUM2
488 TYPE !,"UNCORRECTED LEFT SIDE OVER RIGHT IS:",UNCOR
490 TRUSUM=SUM1-COR1
492 !
494 TRU2=SUM2-COR2
500 RATIO=SIZFAC*TRUSUM/TRU2
505 TYPE !,"RATIO (L.H.S. OVER R.H.S. IS:",RATIO
507 RATIO2=1/RATIO
510 TYPE !," IT'S INVERSE IS:",RATIO2
520 !
530 ASK !,!,!, "WOULD YOU LIKE ANOTHER RUN?",ANOT
535 IF (ANOT).EQ.("Y"); GOTO 152
540 TYPE !,"GOOD BYE THEN"
545 *CEXIT "RUN MENU MAIN"
547 STOP
549 !
550 ! THIS ENDS THE MAIN BODY OF THE PROGRAM, BUT THERE ARE THE
560 ! ERROR HANDLING SUBROUTINES AS WELL.
570 !-----
605 TYPE !,"PROBLEM WITH SELECTING MEMORY, TRY AGAIN"
607 ASK !,"DO YOU WANT TO TRY AGAIN? (Y OR N) ",MEM.
```

```
609 IF (MEM).EQ.("N"); GOTO 617
615 GOTO 160 !BACK TO THE BEGINNING
617 TYPE !,"WELL, BYE THEN"
619 STOP
625 ASK !,"ROIS NOT FOUND, WOULD YOU LIKE TO SET SOME?",MEM
627 IF (MEM).EQ.("N"); GOTO 633
629 ASK !," TYPE Y WHEN READY ",MEM2
630 GOTO 240
631 ! ROI AUTO SET ROUTINE-----
632 TYPE !,!, "HIT TERMINAL BUTTON TO CONTINUE"
633 D=SETROI(1,20,13)
634 E=SETROI(801,820,13)
635 I=SETROI(21,800,1)
636 F=SETROI(1201,1220,14)
637 K=SETROI(1221,2000,2)
638 G=SETROI(2001,2020,14)
639 ER=DSPMEM(DAT)
640 GDSPF
642 MEM2="Y "
644 ASK !,"OK? (DEFAULT YES)",MEM2
648 !
650 IF (MEM2).EQ.("N");GOTO 607
750 !
760 !TILT CORRECTION USING PRESET ROI'S
770 ! -----
772 MIN=21
774 MAX=800
776 MIN2=1221
778 MAX2=2000
780 AVG1=SUMMEM(1,20)/20
790 AVG2=SUMMEM(801,820)/20
800 AVG3=SUMMEM(1201,1220)/20
810 AVG4=SUMMEM(2001,2020)/20
815 ! SLOPE CALC. 2 ///////////////////////////////////////////////////
820 SLOPE1=(AVG2-AVG1)/800
824 SUM1=SUMMEM(21,800)
826 SUM2=SUMMEM(1221,2000)
830 SLOPE2=(AVG4-AVG3)/800
840 GOTO 370 ! BACK TO CORRECTION FACTOR CALC.
955 TYPE !,"SOME PROBLEM OBTAINING DATA"
965 STOP
```

APPENDIX B

This appendix is a summary of the mathematics used by the Niedrig model for calculating the electron backscattering from solids. As the Niedrig model is a combination of two previous theories developed by Everhart [34] and Thummel [35], each of these theories has been summarized as well. All the theories presented here have been reviewed in detail in Niedrig's paper [37], so these summaries, while necessary in explaining the computer programs written for this thesis, will be kept as brief as possible.

The analytical model of Everhart was derived by assuming that all backscattered electrons travel straight into a target and undergo one elastic collision according to the Rutherford atomic scattering formula before escaping the surface. The number of electrons scattered into a conical solid angle $2\pi \sin\theta d\theta$ from an incremental volume of solid Sdx by atoms of charge Ze is given by;

$$dn_0(x, \theta) = \frac{e^4 Z^2 n_0(x) dx}{(4\pi\epsilon_0)^2 16 S E^2} \frac{N_A \rho}{A} \frac{2\pi \sin\theta d\theta}{(\sin^4 \theta/2)} \quad (B1)$$

E is the kinetic energy of the electron ($E=mv^2/2$) and n_0 is the electron density per square centimeter at the depth x in the solid. N_A is Avogadro's number, and ϵ_0 is the permittivity of free space. ρ is the material's density, and A is the atomic weight of the atoms in the solid.

Typically in theories of this kind the distance travelled through the solid by an incident electron is written in terms of the dimensionless parameter $y=x/R$. Where R is the total range of the electron in the solid. Everhart (and Niedrig) used the Thomson-Widdington formulation of continuous energy loss in solids to calculate this range. This law gives the energy of an electron having passed a distance x through a solid as;

$$E^2 = E_0^2 - 1/4 m_0^2 c_T^2 \rho x \quad (B2)$$

where E_0 is the initial electron energy, and c_T is Terrill's constant as measured by Terrill in 1923 [53]. The electron range can be calculated by setting E equal to zero. This gives;

$$R = 4E_0^2 / m_0^2 c_T^2 \rho \quad (B3)$$

Also the substitution of $\theta = \pi - \vartheta$ is a more convenient parameter, as shown in figure B1. Substituting the relationships for x , θ , and R into the probability B1 gives the relationship;

$$dn_0(y, \theta) = \frac{a n_0(y) dy}{2(1-y)} \frac{\sin(\theta) d\theta}{\cos^4(\theta/2)} \quad (B4)$$

where a is usually referred to as Everhart's constant;

$$a = \frac{\pi Z^2 e^4 N}{(4\pi\epsilon_0) m_0^2 c_T^2 A} = 0.024 Z^2 / A \quad (B5)$$

The equation B3 can be solved for $n_0(y)$ by integrating over θ and y using the assumption that electrons scattered less than 90 degrees are not scattered at all. Thus θ goes from 0 to $\pi/2$

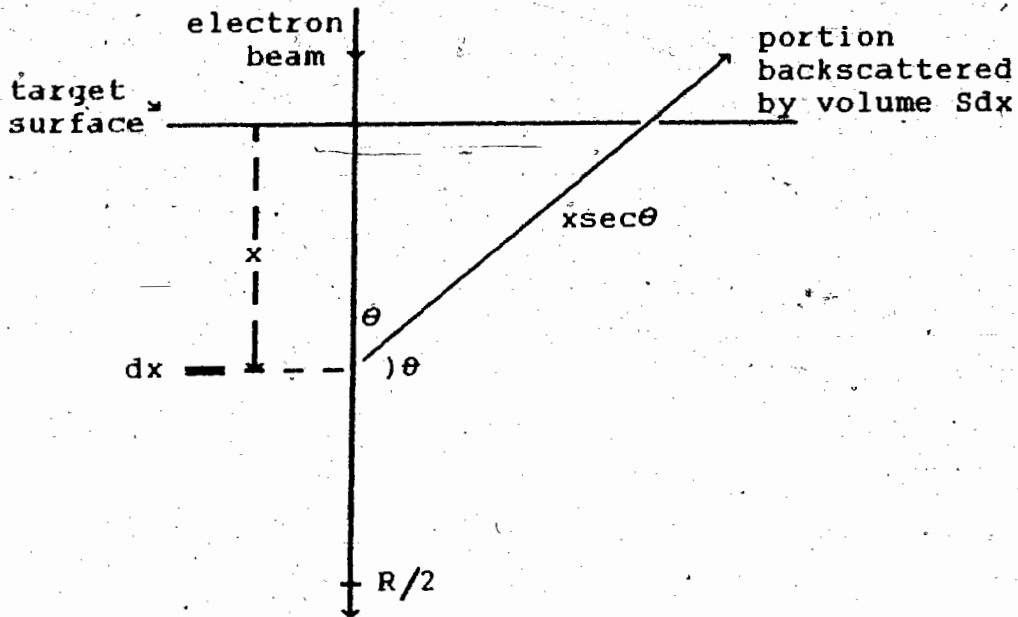


Figure B1. Idealized Electron Beam Path in the Everhart Model.

The variables indicated on the diagram are discussed in the text. The model is symmetrical about the vertical axis described by the incident beam path.

and y is left as an indefinite integral. When this is done the integrals are solvable and result in;

$$n(y) = n (1-y)^{\alpha} \tag{B6}$$

To solve for the number of electrons backscattered, equation B6 can be substituted back into B4 and the resulting equation integrated using the boundary condition that only electrons with sufficient energy to reach the surface will be counted. Mathematically, the condition becomes that $y + y \sec \theta \leq 1$ (see figure B1). The maximum angle θ_0 for which electrons

can still escape from a given depth y thus becomes one of the boundaries of the integration, while y is integrated from 0 to $1/2$ ($x=R/2$), as beyond this depth no electrons have sufficient energy to return to the surface. For a more complete derivation and explanation see [34].

The resulting equation for the backscatter coefficient is;

$$\eta = \frac{a-1+(0.5)^a}{a+1} \quad (B7)$$

This result is extendable to the thin film case (where the film's thickness $D < R/2$) by integrating y from 0 to $y=D/R$. This gives;

$$\eta_T(y) = \frac{a-1}{a+1} \left[1 - \left[1 - \frac{2a}{a-1} y \right] (1-y)^a \right] \quad (B8)$$

with $y=D/R$.

The Thummel continuous diffusion model has a similar derivation but with different scattering assumptions. The beam is assumed to travel straight into the target before scattering at a depth x_D which has a probability distribution $\Phi(x_D)$ associated with it. This is rather like the Everhart formulation, but once scattered the electrons travel in all directions isotropically such that their total distance travelled is equal to their range R . The total range of electrons in the solid has been calculated in the same manner as

In the Everhart model. Thus the proportion of electrons which are backscattered is calculated quite easily by considering the range of the electrons around the scattering depth to be a scattering sphere. The backscattered portion is just that portion in the solid angle of the scattering sphere subtended by the surface of the solid. As the scattering is isotropic, the number scattered into that solid angle is proportional to the solid angle divided by the total solid angle 4π . This gives;

$$d\eta_D = \frac{1}{2} \frac{1-2y_D}{1-y_D} \Phi(y_D) dy_D \quad (B9)$$

in cartesian coordinates. $\Phi(y_D)$ is the probability distribution for the diffusion depth y_D . This equation can be integrated in a similar manner to the Everhart model to give the total backscatter ratio η . Results depend largely on the form of the probability distribution Φ assumed.

The Niedrig model uses the function;

$$\Phi(y) = k(1-y)^{\alpha+k-1} \quad (B10)$$

where k is a constant to be determined. This function was chosen to make the Thummel model mathematically analogous to the Everhart model such that their differential forms could be added together and integrated together. Substituting B10 into B9 and adding B4 gives;

$$dn(y, \theta) = \frac{a}{2} \frac{n(y)dy}{(1-y)} \frac{\sin \theta d\theta}{\cos^4(\theta/2)} + k \frac{n(y)dy}{(1-y)} \sin \theta d\theta \quad (B11)$$

This formula can be integrated in the same fashion as the Everhart model, to give for thick samples;

$$\eta = a \left[\frac{a+k-1+(0.5)^{a+k}}{(a+k)(a+k+1)} \right] + k \left[\frac{a+k-2+(0.5)^{a+k-1}}{(a+k)(a+k-1)} \right] \quad (B12)$$

and for thin films;

$$\eta_t = a \frac{a+k-1}{(a+k)(a+k+1)} \left[1 - \left(1 - 2 \frac{a+k}{a+k-1} y \right) (1-y)^{a+k} \right] + k \frac{a+k-2}{(a+k)(a+k-1)} \left[1 - \left(1 - 2 \frac{a+k-1}{a+k-2} y \right) (1-y)^{a+k-1} \right] \quad (B13)$$

The diffusion constant k was solved for by setting the single scatter constant a to zero and equating the result with the results of a Thummel type model which uses a more realistic function for $\Phi(u)$. Neidrig used the function;

$$\Phi_N(u) = \frac{2.4}{\pi} \frac{u^2}{(0.6^2 + u^2)^2} \quad (B14)$$

Using this function the Thummel model gives the result of;

$$\eta_N = \frac{1.2y_D}{\pi(1+0.36y_D^2)^2} \left[\frac{1+1.8y_D^2+0.259y_D^4}{1.2y_D} \arctan\left(\frac{1}{1.2y_D}\right) - \ln\left(\frac{(1+1.44y_D^2)^{1/2}}{0.6y_D}\right) - \frac{1+0.36y_D^2}{2} \right] \quad (B15)$$

The value of the mean diffusion depth y_D was calculated from a formula derived by Archard;

$$y_D = \frac{40}{7Z} \quad (B16)$$

where Z is the atomic number of the target material.

The diffusion constant k could then be calculated iteratively from the formula (setting $a=0$ in equation B12);

$$\eta_N(y_D) = \frac{k(Z)-2+(0.5)^{k(Z)-1}}{k(Z) - 1} \quad (B17)$$

where the dependence of k on Z has been shown explicitly here.

The computer program KZCALC shown below was written in the BASIC programming language to calculate k for each value of Z of interest (value of Z for alloys were calculated according to equation 4 in section 3.1 of the text). Line 160 corresponds to equation B16 and uses the value of Z obtained from the programmer by line 140. Lines 180-220 correspond to equation B14 and the resulting value of DIFETA (η_N) is printed by line 240.

Equation B17 was algebraically manipulated to bring all terms to the right hand side and was then set equal to ZEROW, as shown in line 320. A trial value of k was input and the result checked to see if ZEROW was higher than or lower than zero. It was found that if the actual value of k is lower than 1, a positive result for ZEROW indicated that the trial value of k was too high. However if the actual value for k was greater than 1 (k was found to vary between 0 and 1.3 for atomic numbers between 0 and 85) the the indication meant that the seed value of k was too low. This fact is reflected in line 370, which checks estimated k values for values greater than 1. Line 390 takes the difference between the trial value of k and the previous one (or a second seed value in the first iteration), divides by two, and either adds or subtracts the result to give the trial value of k to get a new trial value. Line 440 checks to see if the iterations have converged to the point where equation 320 (B16) is satisfied. If not, the program tries again until it is.

The program usually converged in seven to ten iterations as long as both of the seed values for k were either under 1 or over 1, and on the same side of 1 as the actual value of k. Because of the iteration scheme employed, the seed values given the program must also bracket the actual value of k. This requires a certain amount of trial and error (errors are detected readily when the program either fails to converge or converges to 1) as the actual value of k is not known. k is a

smooth function of Z so seed values were not too difficult to estimate.

The value of k thus obtained provides one of the input parameters for the program ETACALC, also written in BASIC. This program was written to calculate the backscatter ratio for thin films of copper-tungsten alloy on silicon substrates. It uses equations B3, B5, B12, B13, and equation 6 of the main text. The backscatter ratio is calculated for 10 different values of incident beam energy between 4 and 40 keV and results are divided by the result for bulk tungsten to simulate the experimental conditions of section 2 of this thesis.

ETACALC calculates average values of atomic number Z , atomic mass A , and estimated density ρ from the fraction of tungsten in the target solid in lines 150-190. The dimensional thickness D of the thin film is used in equation B13, so this is calculated from the mass thickness (the relevant parameter in this thesis) in line 200. Line 240 calculates Everhart's coefficient according to equation B5. Lines 280-400 are needed to calculate bulk backscatter coefficients according to equation B12 for the target thin film material and the silicon substrate material (for which $k=0.3665$ in line 290).

The range of the electrons in the target R is calculated in line 460 according to equation B5 and, as the thin film equations are only valid if $D < R/2$, line 480 defaults the value

of η calculated to the bulk value if R is too small (i.e. the incident beam energy E is too low). Lines 495-540 are devoted to calculating the thin film value of η according to equation B13, and the value of η for the thin film and substrate system is calculated in line 570 according to equation 6. The final printout in line 600 outputs to the line printer the value of η from line 570 divided by the value for bulk tungsten (0.4677699) as calculated by equation B12.

```

10 ' Program to calculate the diffusion constant for electrons in solids.
20 ' This program uses equations formulated by H. Niedrig in Proc. of
30 ' SEM 1981 I, pp. 29-45. It uses eqns. (39),(44), (45), where;
40 '
50 ' DIFETA = the backscatter coefficient (eta) for the pure
60 ' diffusion model, using Niedrig's form of continuous
70 ' scattering prob. with depth of beam in the sample.
80 '
90 ' Z1 = The atomic number of the sample.
100 '
110 ' WHYD = The reduced total diffusion depth of electrons in the
120 ' sample from Archard (J. Appl. Phys. 32, 1961, pp. 1505)
130 '
140 ' INPUT "AVG. /Z, and two seed values bracketing actual";Z1,KNEW,KZ
150 '
155 '
160 ' WHYD=40/7/Z1
180 ' DIFETA1=1.2*WHYD/3.1416/(1+.35*WHYD^2)^2 'four portions of eqn.
190 ' DIFETA2=(1+1.8*WHYD^2+(.259*WHYD^4))/1.2/WHYD*ATN(1/1.2/WHYD)
194 '
200 '
210 ' DIFETA3=LOG((1+1.44*WHYD^2)^.5/.6/WHYD)+(1+.36*WHYD^2)/2
220 ' DIFETA = DIFETA1*(DIFETA2-DIFETA3)
230 '
240 ' PRINT "CALCULATED DIFFUSION CONST. IS;";DIFETA
250 '

```

```
260 , ..... START OF ITERATION LOOP
270 ,
280 ,
290 , KOLD=KZ
300 , KZ=KNEW
310 ,
320 , ZERO = (.5)^(KZ-1) + KZ*(1-DIFETA) - 2 + DIFETA 'iteration eqn.
330 ,
340 , CHECK=ABS(ZEROW)
350 , PRINT CHECK
360 ,
370 , IF KOLD>1 THEN ZERO=-ZERO 'change direction of iteration
380 , 'according to value > 1 or not
390 , IF ZERO>0 THEN KNEW=KZ+ABS(KZ-KOLD)/2 ELSE KNEW=KZ-ABS(KZ-KOLD)/2
400 ,
410 , This 'IF' statement decides if ZERO is high or low and adjusts
420 , KZ accordingly
430 ,
440 , IF CHECK>.000001 THEN GOTO 270 ' check if convergence is good enough
450 ,
460 , PRINT "DIFFUSION CONSTANT K IS;" ;KNEW;" FOR ELEMENT Z OF;" ;Z1
470 , END
```

```

10 , This program calculates backscatter coefficient eta as a fn.
20 , of energy for thin films of thickness D using the Niedrig
30 , formulation as discussed in J. Appl. Phys. 53(4), April 1982
40 , pp.R15-R49
50 , This model uses a combination of single scattering and diffusion
60 , scattering with original single scattering formulation by
70 , Everhart in J. Appl. Phys. 31, pp. 1483-1490
80 ,
90 ,
100 ,
110 , INPUT "MASS THICKNESS , FRACTION OF W, AND K FACTOR";MASST,N1,K
120 ,
130 , INITIALIZE
140 , .....
150 , N2=1-N1
160 , Z1=74*N1+(29*N2)
170 , M1=183.8*N1+(63.5*N2) , GM/MOLE
180 ,
190 , RHO=19.3*N1+(8.8999999*N2) , GM/CUBIC CM
200 , D=MASST/RHO , MASS THICKNESS
210 ,
220 , LPRINT "ANALYTICAL RESULTS FOR";N1*100; "% TUNGSTEN, WITH THICKNESS";D; "NM"
230 ,
240 , A#=.024*Z1*M1 , SCATTERING COEFFICIENT
250 ,
260 ,
270 , DEFINE SUBSTRATE K AND A COEFFICIENTS
    FOR SILICON
280 , KF#=K
290 , KS#=.3665
300 , A3#=.012*14
310 , F1#=A#+KF#
320 , S1#=A3#+KS#
330 , S2#=S1#-1
340 , F2#=F1#-1

```

```

350
360
370
380
390
400
410
420
430
440
450
460
470
480
490
495
500
510
520
530
540
550
560
570
580
590
600
610
620
630
640

```

CALCULATE BACKSCATTER COEFFICIENTS FOR SEMI-INFINITELY THICK FILM MATERIAL AND SUBSTRATE MATERIAL
 $ETAF\# = (A\# * (F2\# + (.5)^{F1\#}) / (F1\# * (F1\# + 1))) + KF\# * (F1\# - 2 + (.5)^{(F2\#)}) / (F1\# * F2\#)$
 $ETAS\# = A3\# * (S2\# + (.5)^{S1\#}) / (S1\# * (S1\# + 1)) + KS\# * (S1\# - 2 + (.5)^{(S2\#)}) / (S1\# * S2\#)$
FOR I=1 TO 10 ' LOOP TO CALCULATE ETA FOR DIFFERENT ENERGIES
E= I*4
R#= (E^2)*24.5/RHO ' WHERE E IS IN KV, RHO IS IN GM/CM
IF D>R#/2 THEN ETATRU#=ETAF#: GOTO 590 ELSE GOTO 490
FACTOR2#=ABS(1-D/R#)
ETSEC#= 1-(2*F1#*D/F2#/R#)
ETHALF# =A#*F2#/(F1#*(F1#+1))*(1-ETSEC#)*(FACTOR2#^F1#)
ETFOR#= 1-(2*F2#*D/(F2#-1)/R#)
ETOTHER#=KF#*(F2#-1)/(F1#*F2#)*(1-ETFOR#)*(FACTOR2#^F2#)
ETATHN#=ETHALF#+ETOTHER#
ETATRU#= ETAS#+ETATHN#*(1-ETAS#/ETAF#)
PRINT "TRUE FINAL ETA IS";ETATRU#
LPRINT "TRUE FINAL ETA FOR ENERGY";E
LPRINT "RELATIVE TO SOLID W IS";ETATRU#/.4677639 'ACCORDING TO THIS MODEL
LPRINT " " "
NEXT I
END



APPENDIX C

The most important assumption in the N.B.S. Monte Carlo program used in this study is the 'elastic scattering only' assumption. Once this has been assumed all interactions of the electron being modelled with the solid can be described by the Rutherford elastic scattering formula modified to simulate atomic screening and relativistic effects;

$$\sigma_E = 5.21 \times 10^{-24} \frac{Z^2}{E^2} \frac{4\pi}{\alpha(1+\alpha)} \left[\frac{E + m_0 c^2}{E + 2m_0 c^2} \right]^2 \quad (C1a)$$

Or in differential form;

$$\frac{\delta\sigma}{\delta\Omega} = 5.21 \times 10^{-24} \frac{Z^2}{E^2} \left[\frac{E + m_0 c^2}{E + 2m_0 c^2} \right]^2 \frac{1}{(\sin^2 \Phi/2 + \alpha)^2} \quad (C1b)$$

here Φ is the elastic scattering angle to be integrated over. σ_E is the total collision cross-section in the solid, Z is the atomic number, E is the electron beam kinetic energy (in keV), and m_0 is the electron rest mass. c is the speed of light, ($m_0 c^2 \cong 511$ keV) and α is the screening factor [41]:

$$\alpha = 3.4 \times 10^{-9} \frac{Z^{2/3}}{E} \quad (C2)$$

The Rutherford scattering cross-section can be integrated to give a probability distribution function for the angle ϕ an electron would be scattered into. If the probability is given a

random number R , the functional form is;

$$\cos\phi = 1 - \left[\frac{2\alpha R}{1+\alpha-R} \right] \quad (C3)$$

The distance travelled by an electron between collisions can also be calculated from the Rutherford collision cross-section. The path length between collisions s can be derived from the formula:

$$s = \frac{A}{N_{\alpha} \rho \sigma_E} \quad (C4)$$

In this simulation the path length between collisions has been randomized to avoid the somewhat unrealistic pattern of energy loss and collisions occurring at extremely regular intervals. The random number generator used was resident in the version of the VS version of FORTRAN used on the mainframe computer. Randomization was done by:

$$s_R = -s \log |R| \quad (C5)$$

A simulated electron thus has a collision path length which is a function of its energy through the energy relationship in σ_E . In the simulation of an electron passing through a solid, the energy is assumed to change continuously, thus the path length needed to be recalculated at every collision.

To determine the electron's change in kinetic energy as it passes through a solid, a continuous energy loss approximation is necessary, as the Rutherford scattering formula is for elastic scattering only (no energy loss). A formula which works well in practice is the Bethe continuous energy loss formula;

$$\frac{\delta E}{\delta s} = \frac{2ce^4 \eta Z}{E} \left[\frac{1.166E}{J} \right] \quad (C6)$$

where E is the energy (in eV) of the electron, s is the distance travelled through the solid, and J is the mean ionization potential for the solid [50].

The mean ionization potential formula was obtained from:

$$J = 9.76 \times 10^{-8} A + \left[\frac{5.85 \times 10^{-2}}{A^{0.12}} \right] \quad (C7)$$

this equation is an empirical fit to experimental data taken from neutron scattering, but as most measurements of this parameter are indirect, this is the best that could be obtained.

The program listed below has been organized into a series of subroutines. The main program, MONTE3, acts in a supervisory role to acquire the necessary parameters and print out results. It transfers control to subroutine MONTE when the parameters are obtained. Subroutine MONTE controls the actual simulation of each electron, with the main loop which goes from 1 to the

number of electrons to be simulated (this number is also one of the input parameters). MONTE then goes into a second loop, in which each iteration is one scatter event for a simulated electron. MONTE calls a subroutine to determine what direction the electron is scattered into, the new coordinates of the electron after scattering, and the parameters of the material at these new coordinates necessary to start a new scatter calculation.

The subroutine FINDZS was written to simulate targets with surface features, and will find the z coordinate of the surface at a given x and y coordinate. Targets in the simulations for this work were flat, so this subroutine was not used. PARA was written to output suitably randomized values for the azimuthal scattering angle, the cosine of the elastic scattering angle, and the path length of a given step between collisions. Subroutine MOVE calculates the new coordinates of a simulated electron given the old coordinates, the scattering angles, and the path length. The final subroutine is TARGET, which returns values for the average atomic number, atomic mass, and density at the input coordinates.

The subroutine TARGET includes the mathematical description of the structure and materials in the target. In this simulation thin films of a variety of materials were deposited on the flat surface of bulk silicon, so the mathematics of the structure are simple relations of the normal to the surface z.

The parameters for the thin film material of atomic number, mass, and density of the were also passed to this subroutine, as these were changed frequently. The subroutine returns the values -1 if the electron is out of the solid.

When the value of -1 is returned by subroutine TARGET, or the simulated electron's energy falls below a predetermined limit, the subroutine MONTE starts a new electron at the surface of the target. Electrons which reach the surface are counted and their final energy and scattering angle is noted as falling into one of ten categories to compile statistics on them. The statistics printed out by the supervisory program MONTE3 are the number of electrons backscattered over the total number simulated, the number backscattered in each of ten 1 kV energy categories, and the number scattered into each ten degree angle category. These categorized results provided the data for the figures 11 and 12 in the main text.

MONTE CARLO ELECTRON TRAJECTORY SIMULATION

This program preforms a Monte Carlo simulation for an electron beam striking a given target. The nature of the target is determined from the subroutine TARGET.

The mainline of this program prompts the user for the required parameters to do the simulation. It then passes these parameters to the subroutine MONTE which does the actual simulation. The subroutine passes back the number of electrons which were backscattered from the target when it has completed the simulation.

Note that all quantities are expressed in cm , keV , g ,and radians.

VARIABLE LIST :

- BSCANG - the max. angle w.r.t. the Z axis at which backscattered electrons can be detected
- ELBSC - the number of backscattered electrons
- ELNO - the number of electron trajectories to be done
- ENBEAM - the electron beam energy
- XSTART, YSTART - the coordinates of the electron beam

```
REAL XSTART, YSTART, ENBEAM, BSCANG
INTEGER ELNO, ELBSC, SEED
DIMENSION BARGPH(0:9), BAR2(0:9)
INTEGER BARGPH, BAR2
COMMON BARGPH, BAR2
DO 15 I = 0,9
  BARGPH(I) = 0
  BAR2(I) = 0
15 CONTINUE
```

```
WRITE (6,10)
10 FORMAT (//15X,'MONTE CARLO ELECTRON TRAJECTORY SIMULATION'
$ /15X,42('=')//)
```

```
XSTART = 0
YSTART = 0
ENBEAM = 10
BSCANG = 1.27
```

```
WRITE (6,50)
50 FORMAT ('Enter the number of electron trajectories to be',
$ ' simulated.')
```

```
READ (5,*) ELNO
```

```
WRITE (6,80)
80 FORMAT (//'WORKING ...')
```

```
CALL MONTE (XSTART, YSTART, ENBEAM, BSCANG, ELNO, ELBSC)
```

```
WRITE (6,90) REAL(ELBSC) / REAL(ELNO) * 100
90 FORMAT (//F7.2, ' % of the electrons were backscattered.')
```

```
DO 95 J = 0,9
  WRITE (6,100) BARGPH(J), J
```

```

100   FORMAT (/ , I4 , ' Electrons in ' , I2 , ' KV energy range' )
95    CONTINUE
      DO 97 K = 0 , 9
        WRITE ( 6 , 105 ) BAR2(K) , K * .10 , K * 10 + 10

```

```

105   FORMAT (/ , I4 , ' Electrons in ' , I2 , I3 , ' degree range' )
97    CONTINUE

```

```

C
C   END

```

```

C
C *****
C

```

SUBROUTINE MONTE (XSTART, YSTART, ENBEAM, BSCANG, ELNO, ELBSC)

The Monte Carlo simulation which this subroutine preforms is taken from the paper "Monte Carlo Electron Trajectory Simulation - An Aid For Particle Analysis" by D.E. Newbury, R.L. Myklebust, K.F.J. Heinrich, and J.A. Small. It is published in the book, "Characterization Of Particles : NSB Spec. Pub. 533", pp 39-62. (located at SFU library under TA 418.78 P378 1978)

VARIABLE LIST :

- ASANG - Azimuthal angle for the electron's deflection
- ATOMNO - Average atomic number of the target material at the present coordinates.
- ATOMWT - Average atomic weight of the target material at the present coordinates.
- BETHE - rate of energy loss per unit path length due to inelastic collisions (Bethe's formula)
- COUNT - the number of electron trajectories performed
- DENSE - the density of the target material at the present coordinates
- ENERGY - the electron's energy
- ESANG - cosine of the elastic scattering angle
- MIONIZ - the mean ionization energy of the target material at the present coordinates
- OLDSTP - length of the electron's last step
- SCRNFT - screening factor (used for Rutherford's screened elastic cross section formula)
- STEP - length of the electron's next step
- TECS - total elastic cross section (from Rutherford's screened elastic cross section formula)
- XSEED - a seed number for the random number generator
- X, Y, Z - Coordinates of the electron's present position relative to the starting coordinates
- XDELTA, YDELTA, ZDELTA - The displacement of the electron's present position from its last position
- XSTART, YSTART, ZSTART - The starting coordinates for each of the electron trajectories

```
C INPUT :
C XSTART, YSTART
C - the coordinates of the electron beam
C ENBEAM - energy of the electron beam
C BSCANG - the max. angle w.r.t the Z axis at which
C backscattering electrons can be detected
C ELNO - the number of electron simulations to be done
C
C OUTPUT :
C ELBSC - the number of backscattering electrons
C
REAL X, Y, Z, XDELTA, YDELTA, ZDELTA, BETHE, XSEED
REAL ENBEAM, BSCANG, ASANG, ESANG, ATOMNO, ATOMWT
REAL DENSE, ENERGY, STEP, OLDSTP, SCRNF, TECS, MIONIZ
REAL ANG
REAL*8 XSTART, YSTART, ZSTART
COMMON BARGPH, BAR2
INTEGER ENRINT, ANGIN, BARGPH(0:9), BAR2(0:9)
INTEGER ELNO, ELBSC, COUNT
C
C CALL FINDZS (XSTART, YSTART, ZSTART)
C ZSTART = 0
ELBSC = 0
CALL G05CCF
C
DO 20 COUNT = 1, ELNO
CALL TARGET (XSTART, YSTART, ZSTART, ATOMNO, ATOMWT, DENSE)
X = 0
Y = 0
Z = 0
XDELTA = 0
YDELTA = 0
ZDELTA = -1
OLDSTP = 1
ENERGY = ENBEAM
C
C SCRNF = 3.4E-3 * ATOMNO ** 0.6667 / ENERGY
C
C TECS = 6.55E-20 * (ATOMNO / ENERGY * (ENERGY + 511) /
C (ENERGY + 1022)) ** 2 / SCRNF / (1 + SCRNF)
C
C STEP = ATOMWT / DENSE / TECS / 6.02E23
C
C CALL PARA (STEP, ASANG, ESANG, SCRNF, XSEED)
C
C MIONIZ = 9.76E-3 * ATOMNO + 5.85E-2 / ATOMNO ** 0.19
C BETHE = -7.85E4 * ATOMNO * DENSE / ATOMWT / ENERGY *
C LOG(1.1658 * ENERGY / MIONIZ)
C ENERGY = ENERGY + BETHE * STEP
C
C CALL MOVE (X, Y, Z, XDELTA, YDELTA, ZDELTA, STEP, OLDSTP,
C ASANG, ESANG)
C
C CALL TARGET (X+XSTART, Y+YSTART, Z+ZSTART, ATOMNO, ATOMWT, DENSE)
```



```

IF (DENSE .LE. 0) THEN
  ENRINT = INT(ENERGY)
  BARGPH(ENRINT) = BARGPH(ENRINT) + 1
  ANG = ARCOS(ZDELTA/STEP)
  ANG = ANG * 5.729
  ANGINT = INT(ANG)
  BAR2(ANGINT) = BAR2(ANGINT) + 1
  ELBSC = ELBSC + 1
  GOTO 20
END IF

```

```

IF (ENERGY .GT. MIONIZ) THEN
  GOTO 10
END IF

```

```

20 CONTINUE
RETURN
END

```

SUBROUTINE FINDZS (XSTART, YSTART, ZSTART)

This subroutine returns the appropriate value for ZSTART so the electrons' trajectories start just inside the target material. The parameter ERROR determines the tolerance with which the electrons' starting position can vary from the surface of the target.

To find the top surface of the target, this subroutine starts looking at Z=0. If there is no material at Z=0, it looks at Z = -ERROR. If there is no material there, it keeps doubling Z until it finds a value of Z for which there is some material. However, if at Z=0 there is some material, it looks at Z = ERROR. If there is some material there, it keeps doubling Z until it find a value of Z for which there is no material. In both these cases, it locates the top of the target within some interval of Z. From then on it keeps bisecting the interval of Z, until it has located the surface within a small enough interval of Z.

VARIABLE LIST :

- ATOMNO - atomic number of the target material
- ATOMWT - atomic weight of the target material
- DELTA - length of the Z interval
- DENSE - density of the target material
- ERROR - error tolerance for the value of ZSTART
- SIGN - set to +1 if ZSTART > 0
set to -1 if ZSTART < 0
- XSTART, YSTART, ZSTART - starting position of the electron trajectories

```
REAL    ATOMNO, ATOMWT, DENSE, SIGN
REAL*8  XSTART, YSTART, ZSTART, ERROR, DELTA
C
C      PARAMETER (ERROR = 1D-9)
C
C      CALL TARGET (XSTART, YSTART, 0, ATOMNO, ATOMWT, DENSE)
C      IF (DENSE .LT. 0) THEN
C          SIGN = -1
C      ELSE
C          SIGN = 1
C      END IF
C      ZSTART = SIGN * ERROR
C
C      CALL TARGET (XSTART, YSTART, ZSTART, ATOMNO, ATOMWT, DENSE)
10     IF (SIGN*DENSE .GT. 0) THEN
C          ZSTART = ZSTART * 2
C          GOTO 10
C      END IF
C
C      DELTA = ZSTART / 4
C
C      CALL TARGET (XSTART, YSTART, ZSTART, ATOMNO, ATOMWT, DENSE)
20     IF (SIGN*DENSE .GT. 0) THEN
C          ZSTART = ZSTART + DELTA
C      ELSE
C          ZSTART = ZSTART - DELTA
C      END IF
C      IF (ABS(DELTA) .GT. ERROR) THEN
C          DELTA = DELTA / 2
C          GOTO 20
C      END IF
C
C      CALL TARGET (XSTART, YSTART, ZSTART, ATOMNO, ATOMWT, DENSE)
C      IF (DENSE .LT. 0) THEN
C          ZSTART = ZSTART - ERROR
C      END IF
C
C      RETURN
C      END
```

SUBROUTINE PARA (STEP, ASANG, ESANG, SCRNF, XSEED)

This subroutine determines the random parameters for the electron's trajectories. To do this it transforms the random numbers generated by the function G05CAF into random numbers from the appropriate distribution for each of the parameters STEP, ASANG, and ESANG. For instance, STEP has a negative exponential distribution, ASANG has a uniform distribution from 0 to 2*pi, and ESANG has its own special distribution.

C OUTPUT :
C STEP - the path length for the electron
C ASANG - azimuthal angle for the electron's deflection
C ESANG - cosine of the elastic scattering angle
C XSEED - a seed number for the random number generator
C
C

REAL STEP, ASANG, ESANG, SCRNF, TEMP, XSEED

STEP = - STEP * LOG(G05CAF(XSEED))

ASANG = 6.283185 * G05CAF(XSEED)

TEMP = G05CAF(XSEED)

ESANG = 1 - 2 * SCRNF * TEMP / (1 + SCRNF - TEMP)

C
C RETURN
C END
C
C

C
C SUBROUTINE MOVE (X,Y,Z,XDELTA,YDELTA,ZDELTA,STEP,OLDSTP,
C \$ ASANG,ESANG)

C This subroutine moves an electron from its coordinates
C to its new coordinates as determined by the parameters
C STEP, ASANG, and ESANG.

C To determine the electron's new position, a temporary
C coordinate system is created with its origin at the
C electron's present position and its Z axis in the
C direction of the electron's present motion. (ie. if the
C electron is not deflected, it will travel in the positive
C Z direction of the temporary coordinate system) The
C directional cosines of each temporary coordinate axis are
C then calculated. From the parameters STEP, ASANG, and
C ESANG, the coordinates of the electron's new position in
C the temporary coordinate system are easily determined.
C From these coordinates and the directional cosines, the
C change in the electron's position in the main coordinate
C system is calculated, and hence the new coordinates are
C found.

C For more information on this, see Appendix A of the
C paper, "NBS Monte Carlo Electron Trajectory Calculation
C Program" by R.L. Myklebust, D.E. Newbury, and H. Yakowitz.
C It is published in the book, "Use Of Monte Carlo
C Calculations In Electron Probe Microanalysis And Scanning
C Electron Microscopy : NBS Spec. Pub. 460", pp 126-128.
C (located at SFU library under QH 212 E4 W677 1975)

```

C  VARIABLE LIST :
C  AX, BX, CX
C      - directional cosines of temporary X axis
C      Note : the temporary coordinated system is
C      chosen so that BX = 0.
C  AY, BY, CY
C      - directional cosines of temporary Y axis
C  AZ, BZ, CZ
C      - directional cosines of temporary Z axis
C  RADIUS - perpendicular distance from the electrons new
C           position to the temporary Z axis
C  TEMP   - a variable use to temporarily store a number
C  XTEMP, YTEMP, ZTEMP
C           - electron's new position in temporary coordinates
C
C  REAL    X, Y, Z, XDELTA, YDELTA, ZDELTA, STEP, OLDSTP, ESANG,
$          ASANG, AX, AY, AZ, BY, BZ, CX, CY, CZ, RADIUS, TEMP,
$          XTEMP, YTEMP, ZTEMP
C
C  AZ = XDELTA / OLDSTP
C  BZ = YDELTA / OLDSTP
C  CZ = ZDELTA / OLDSTP
C
C  TEMP = SQRT(AZ ** 2 + CZ ** 2)
C  IF (TEMP .NE. 0) THEN
C     AX = - CZ / TEMP
C     CX = AZ / TEMP
C  ELSE
C     AX = 1
C     CX = 0
C  END IF
C
C  AY = BZ * CX
C  BY = CZ * AX - CX * AZ
C  CY = -AX * BZ
C
C  RADIUS = STEP * SQRT(ABS(1 - ESANG ** 2))
C  XTEMP = RADIUS * COS(ASANG)
C  YTEMP = RADIUS * SIN(ASANG)
C  ZTEMP = STEP * ESANG
C
C  XDELTA = AX * XTEMP + AY * YTEMP + AZ * ZTEMP
C  YDELTA = BY * YTEMP + BZ * ZTEMP
C  ZDELTA = CX * XTEMP + CY * YTEMP + CZ * ZTEMP
C
C  X = X + XDELTA
C  Y = Y + YDELTA
C  Z = Z + ZDELTA
C  OLDSTP = STEP
C
C  RETURN
C  END

```

SUBROUTINE TARGET (X,Y,Z,ATOMNO,ATOMWT,DENSE)

This subroutine determines the structure of the target through which the electron trajectories take place. To do this, it returns the average atomic number, average atomic weight, and density of the target at the given coordinates. If there is no material at the given coordinates then a negative density such as -1 should be returned.

INPUT:

X, Y, Z

- the coordinates for which the program requires the atomic number, atomic weight, and density of the target

OUTPUT :

ATOMNO - average atomic number

ATOMWT - average atomic weight

DENSE - density (if there is no material then a negative value is returned)

REAL ATOMNO, ATOMWT, DENSE, THIN
REAL*8 X, Y, Z

IF (Z .LE. 0) THEN

ATOMNO = 74

ATOMWT = 183.8

DENSE = 12.86

ELSE

DENSE = -1

END IF

THIN = -4.E-4

IF (Z .LE. THIN) THEN

ATOMNO = 14

ATOMWT = 28.1

DENSE = 2.4

ELSE

DENSITY UNCHANGED IF NOT THROUGH FILM

END IF

RETURN

END

LIST OF REFERENCES

- [1] see for example; Vossen, J.S., Schnable, G.L., and Kern, W.; J. Vac. Sci. Technology No. 11, (1974), pp. 6-11
- [2] Holland, L.; Vacuum Deposition of Thin Films, Chapman and Hall Ltd. London (1970) pp. 232-248
- [3] Pulker, H. K., Benes, E., Hammer, D., and Sollner, E.; Thin Solid Films 32, (1976). pp. 27-33 p. 27-33 p. 27-33
- [4] Dudding, R.W., J. British Instn. Radio Engrs., 11 (1951), pp. 458-463
- [5] Liebhaufsky, H.A., Pfeiffer, H.G., Winslow, E.H., and Zemany, P.D. in; X-Rays, Electrons, and Analytical Chemistry, Wiley-Interscience, New York, 1972
- [6] Yakowitz, H., and Newbury, D.E., Proceeding on Scanning Electron Microscopy 1976, Part I, IITRI. Chicago, pp. 151-160
- [7] Murata, K.; Proceedings on Scanning Electron Microscopy 1973, IITRI Chicago 1973, pp. 268-276
- [8] Kyser, D.F. Electron Beam Interactions with Solids, SEM Inc., AMF O'Hare Ill. 1981, pp.119-135
- [9] Miller, N.C., and Koffman, D.M., in Microbeam Analysis 1979, D. Newbury ed., San Francisco Press, San Francisco 1979, pp.47-50
- [10] Hohn, F.J., and Niedrig, H.; Proceedings of the Fifth European Congress on Electron Microscopy, Manchester 1972, Institute of Physics, London, 1972, pp. 358-360
- [11] Niedrig, H.; Optica Acta vol. 24, No. 6, (1977) pp. 679-691
- [12] Wolf, E.D., and Everhart, T.E.; Proceedings on Scanning Electron Microscopy 1969, IITRI Chicago 1969, pp. 41-44
- [13] Robinson, V.N.E.; J. Phys. E 7 (1975) pp.650-652
- [14] Curzon, A.E. and Rajora, O.S.; Thin Solid Films 123 (1985), pp. 235-238
- [15] Waits, R.K. in; Thin Film Processes, J.L. Vossen and W. Kern eds. Academic Press Inc., Orlando 1978, pp. 131-163
- [16] ibid. [2], pp. 182-198
- [17] Murata, K.; Phys. Status Solidi A 36 (1976), pp. 197-208

- [18] Reimer, L., Popper, W., and Brocker, W.; Proc. on Scanning Electron Microscopy 1978, SEM Inc. AMF O'Hare Illinois 1978, Part I, pp. 705-710
- [19] McAfee, W.S.; J. Appl. Physics 47 (1976), pp. 1179-1184
- [20] Holliday, J.E. and Sternglass, E.J.; J. Appl. Physics 28 (1957), pp. 1189-1193
- [21] Heinrich, K.F.J.; Proceedings of the 4th International Congress on X-Ray Optics and Microanalysis, Paris 1968 Hermann, Paris 1966, pp. 159-167
- [22] see for example; Darlington, E.H., and Cosslett, V.E.; J. Physics D 5 (1972), pp. 1969-1981
- [23] Herrmann, R. and Reimer, L.; Scanning Vol. 6 (1984), pp. 20-29.
- [24] Holliday, J.E. and Sternglass, E.J.; J. Applied Phys. 30 (1959), pp. 1428-1431
- [25] Westwood, W.D.; Progress in Surface Science No. 7, (1976) pp. 71-74
- [26] see for example; Franks, J., Stuart, P.R., and Withers, R.B.; Thin Solid Films 60 (1979), pp. 231-238
- [27] from Wehner, G.K., and others listed in Thin Film Processes, J.L. Vossen, ed., Academic Press, Orlando Fla. 1978, pp. 15-16
- [28] Hohn, F.J.; Optik 47, (1977), pp. 491-494
- [29] Egerton, R.F.; Electron Energy Loss Spectroscopy in the Electron Microscope, Plenum Press, New York 1986
- [30] Thomson, J.J.; The Conduction of Electricity Through Gases, Cambridge University Press, Cambridge 1906
- [31] Rutherford, E., Philos. Mag. 21 (1911), pp. 669-688
- [32] Bethe, H.A., Rose, M.E., and Smith, L.P.; Proc. American Philos. Society 78 (1938), pp. 573-585
- [33] Nakhodkin, N.G., Ostroukhov, A.A., and Romanovskii, V.A.; Sov. Phys. Solid State 4 (1962), pp. 1112-1119
- [34] Everhart, T.E.; J. Appl. Phys. 31 (1960), pp. 1483-1490
- [35] Thummel, H.W.; Durchgang von Elektronen und Beta Strahlung Durch Materie/schichten, Akademie-Verlag, Berlin, GDR, 1974, ch. 9-11
- [36] Archard, G.D.; J. Appl. Phys. 32 (1961), pp. 1505-1509

- [37] Niedrig, H.; Proc. Scanning Electron Microscopy 1981, SEM Inc. AMF O'Hare, Ill. 1981, Part I, pp. 29-45
- [38] Gomoyunova, M.V., and Letunov, N.A.; Sov. Phys. Solid State 7 (1965), pp. 311-315
- [39] DeNee, P.B.; Proc. Scanning Electron Microscopy 1978, SEM Inc. AMF O'Hare, Ill. 1978, Part I, pp. 741-746
- [40] Niedrig, H.; J. Appl. Phys. 53(4), 1982, pp. R15-R49
- [41] Cosslett, V.E. and Thomas, R.N.; British J. Appl. Phys. 16 (1965), pp. 779-796
- [42] Kalef-Ezra, J., Horowitz, Y.S., and Mack, J.M.; Nuclear Inst. and Methods 195 (1982), pp. 587-595
- [43] Bishop, H.E.; British J. Appl. Phys. 18 (1967), pp. 153
- [44] Shimizu, R., and Murata, K., J. Applied Phys. 42, No.1 (1971), pp. 387-394
- [45] Kyser, D.F. and Murata, K.; IBM J. Research and Develop. July 1974, pp. 352-363
- [46] Shimizu, R., Kataoka, Y., Ituka, T., Koshikawa, T., and Hashimoto, H.; J. Phys. D 9 (1976), pp. 101-114
- [47] Newbury, D.E., Myklebust, R.L., Heinrich, K.F.J., and Small, J.A.; in N.B.S. Special Publication 533, K.F.J. Heinrich ed., U.S. Govt. Printing Office, Wash. 1980, pp. 39-62
- [48] Bishop, H.E. in; N.B.S. Special Publication 406, U.S. Govt. Printing Office, Wash. 1976, pp 5-14
- [49] Newbury, D.E. and Myklebust, S.; Electron Beam Interactions with Solids, SEM Inc. IITRI Chicago 1983, pp.153-163
- [50] Yakowitz, H. in; Practical Scanning Electron Microscopy, J.I. Goldstein and H. Yakowitz eds., Plenum Press, New York 1975, chs. 9-10
- [51] Bolen, R.B., Lifshin, E., and Ciccarelli, M.F. in; ibid. [50], ch. 8
- [52] Sheng, Y.Q., Munz, P., Shultheiss, R., and Bucher, E.; Thin Solid Films 131 (1985), pp. 131-138
- [53] Terrill, H.M.; Phys. Rev. 27 (1923), pp. 101-108